Synthesis, Structure, and Photophysical Properties of Poly(dibenzofulvene) and Its Derivative

(ポリ(ジベンゾフルベン)およびその誘導体の合成、構造、および光物理学的性質)

Dissertation

Tohru Yade

矢出　亨

2006

Graduate School of Materials Science,
Nara Institute of Science and Technology (NAIST)

Table of Contents

General Introduction

The conformation of macromolecules often has a significant influence on properties and functions of polymeric materials, and its control is an important goal in synthetic polymer chemistry. From such a view, various polymers having a stable, specific conformation have been designed and synthesized. Most of such polymers have a regulated helical conformation; some of them show a practical function such as chiral recognition ability.[1,2]

Apart from helical structures, a type of specific conformation available for a linear polymeric chain may be characterized by regularly stacked π-electron systems ("π-stacked structure").[3] A π-stacked structure is known for the DNA double strand where the paired bases inside the double helical complex closely stack on top of each other.[4] DNA's π-stacked structure mediates charge transport which has been proposed to be responsible for the gene mutation.[5] Efforts also have been reported to use DNAs as a semiconducting material.[6]

As for synthetic polymers, π-stacked structure has been evidenced only for poly(phenyleneethylnylene)s,[7] oligomers consisting of alternating donor and acceptor monomeric units,[8] and oligomers having perylene moieties in the main chain[9] except for polydibenzofulvenes[10-17] which this thesis deals with. Although a syndiotactic vinyl polymer with aromatic side groups such as polystyrene may take a π-stacked structure as a possible geometry, a fast conformational dynamics would not allow a stable, specific conformation for such polymers.

In this thesis work, dibenzofulvene (DBF), a fluorene derivative, was found to afford a polymer (poly(DBF)) having a stable π-stacked structure through vinyl polymerization. In poly(DBF), the side-chain aromatic groups are tightly stacked on top of each other along the almost *all-trans* main chain. This is the first example of a vinyl polymer with a stable π-stacked conformation. Because regulated spatial arrangements of chromophores may play an important role in producing organic photophysical/photoelectronic materials with desired properties, poly(DBF) is expected to be practically useful in such fields.

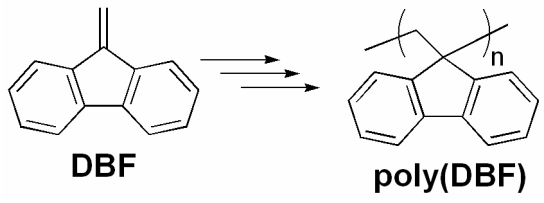

This thesis consisting of four chapters discusses the synthesis, structure, and properties of π-stacked poly(DBF) and its derivatives in detail. Brief contents of the chapters are as follows:

In Chapter 1, full details of the stereostructure of poly(DBF) prepared by anionic polymerization and its photophysical and electrochemical properties are described. Uniform oligomers of DBF with distinct chain lengths were isolated by size-exclusion chromatography (SEC), and the proposed π-stacked structure was unambiguously evidenced by single-crystal X-ray analyses of the uniform oligomers. In addition, a π-stacked structure was also confirmed in solution by ^{1}H NMR analyses combined with theoretical chemical shift calculations. Further, the absorption and emission spectra and cyclic voltammograms were systematically measured for the uniform oligomers and polymers. Through these studies, the effect of the π-stacked structure on the photophysical and electrochemical properties was systematically investigated.

In Chapter 2, the synthesis of poly(DBF) with a π-stacked conformation using free-radical polymerization methods is described. Although free-radical polymerization, which is much less expensive and much more importance in industrial polymer synthesis than anionic polymerization, is generally difficult in controlling polymer stereostructure, it was found to afford a regulated π-stacked conformation of poly(DBF) with a very small amount of structural defect. In addition, the results indicated that the amount of structural defect incorporated into the chain can be controlled by choosing reaction conditions.

In Chapter 3, the charge transfer phenomenon of poly(DBF) though the stacked π-electron systems is discussed. The hole drift mobility of poly(DBF) film was measured by a time-of-flight (TOF) method using a thin film sample. The charge mobility of poly(DBF) film was as high as some main-chain conjugating polymers.

In Chapter 4, the synthesis and anionic polymerization of 2,7-di-*t*-butyldibenzofulvene (tBu_2DBF), a bulky DBF derivative, is discussed. The effect of the side chain *t*-butyl groups on the monomer reactivity and the steteostructure and photophysical properties of the polymerization products was evaluated.

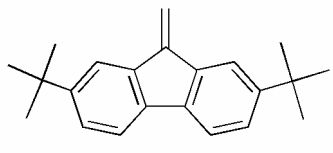

tBu_2DBF

References

(1) Okamoto, Y.; Nakano, T. *Chem. Rev.* **1994**, *94*, 349.

(2) Nakano, T.; Okamoto, Y. *Chem. Rev.* **2001**, 101, 4013.

(3) Nakano, T. In *Bottom-up Nanofabrication ("Synthesis and Properties of Polymers Having a π-Stacked Conformation")*; Ariga K., Nalwa, H. S. Eds.; American Scientific Publications, Stevenson Ranch: in press.

(4) Watson, J. D.; Crick, F. H. C. *Nature* **1953**, *171*, 737.

(5) Bensasson, R. V.; Land, E. J.; Truscott, T. G.; *Excited States and Free Radicals in Biology and Medicine: Contributions from Flash Photolysis and Pulse Radiolysis*; Oxford Press: New York, 1993.

(6) (a) Murphy, C. J.; Arkin, M. R.; Jenkins, Y.; Ghatlia, N, D.; Bossman, S. H.; Turro, N. J.; Barton, J. K. *Science* **1993**, *262*, 1025. (b) Okahata, Y.; Kobayashi, T.; Tanaka, K.; Shimomura, M. *J. Am. Chem. Soc.* **1998**, *120*, 6165. (c) Fink, H.-W.; Schönenberger, C. *Nature* **1999**, *398*, 407. (d) Porath, D.; Bezryadin, A.; de Vries, S.; Dekker, C. *Nature* **2000**, *403*, 635.

(7) Nelson, J. C.; Saven, J. G.; Moore, J. S.; Wolynes, P. G. *Science* **1997**, *277*, 1793.

(8) (a) Lokey, R. S.; Iverson, B. L. *Nature* **1995**, *375*, 303. (b) Nguyen, J. Q.; Iverson, B. L. *J. Am. Chem. Soc.* **1999**, *121*, 2639.

(9) Wang, W.; Li, L.-S.; Helms, G.; Zhou, H.-H.; Li, A. D. Q. *J. Am. Chem. Soc.* **2003**, *125*, 1120. (b) Li, A. D. Q.; Wang, W.; Wang, L.-Q. *Chem.-Eur. J.* **2003**, *9*, 4594. (c) Wang, W.; Han, J. J.; Wang, L.- Q.; Li, L.-S.; Shaw, W. J.; Li, A. D. Q. *Nano Lett.* **2003**, *3*, 455.

(10) Nakano, T.; Takewaki, K.; Yade, T.; Okamoto, Y. *J. Am. Chem. Soc.* **2001**, *123*, 9182.

(11) Nakano, T.; Yade, T. *J. Am. Chem. Soc.* **2003**, *125*, 15474.

(12) Nakano, T.; Yade, T.; Fukuda, Y.; Yamaguchi, T.; Okumura, S. *Macromolecules* **2005**, *38*, 8140.

(13) Nakano, T.; Nakagawa, O.; Yade, T.; Okamoto, Y. *Macromolecules* **2003**, *36*, 1433.

(14) Nakano, T.; Yade, T.; Yokoyama, M.; Nagayama, N. *Chem. Lett.* **2004**, *33*, 296.

(15) Nakano, T.; Nakagawa, O.; Tsuji, M.; Tanikawa, M.; Yade, T.; Okamoto, Y. *Chem. Commun.* **2004**, 144.

(16) Nakano, T.; Yade, T.; Ishizawa, H.; Nakagawa, O.; Okamoto, Y. *ACS Polym. Prepr.* **2002**, *43*, 609.

(17) Yade, T.; Nakano, T. *Polym. Sci. Part A: Polym. Chem.* **2005**, *44*, 561.

Chapter 1
Synthesis, Structure, and Photophysical and Electrochemical Properties of Poly(dibenzofulvene)

1.1 Introduction

The conformation of macromolecules often has significant influence on the properties and functions of polymeric materials. Polymers having a specific conformation, such as a helix, have been synthesized, and their functions have been explored in relation to their structures.[1] A type of unique conformation may be characterized by regularly stacked π-electron systems. Stable and regulated π-stacked structures in polymers are known for DNA,[2] poly(phenyleneethylnylene)s,[3] oligomers consisting of alternating donor and acceptor monomeric units,[4] and oligomers having perylene moieties in the main chain.[5] In the DNA, paired bases are regularly stacked inside the helical strand. In the poly(phenyleneethynylene)s, phenylene groups in the main chain closely overlap due to helical folding of the polymer chain. In oligomers consisting of aromatic donor and acceptor units, the chain folds into a pleated conformation due to a donor-acceptor.

Vinyl polymers with side-chain aromatic groups could also have π-stacked conformations when they have stereoregular main chains. However, most examples of stereoregular synthesis of a side-chain aromatic vinyl polymer involve polystyrene[6] whose conformational dynamics are too fast in solution to maintain a specific conformation. Hence, synthesizing a vinyl polymer that has a stable, regulated π-stacked conformation is a challenging goal. Although a partial π-stacked conformation has been proposed for poly(*N*-vinylcarbazole),[7] the conformation is expected to exist only in relatively short monomeric sequences because the stereoregularity of the polymer is rather low.

In search of novel, functional polymers with specific conformations, our group recently found that dibenzofulvene (DBF) affords a polymer with side-chain fluorene chromophores regularly stacked on top of each other.[8] Despite a structure similar to 1,1-diphenylethylene that does not homopolymerize,[9] DBF readily polymerizes with anionic, cationic, and radical initiators. Because the polymer does not have stereocenters, only conformational isomers are possible as its stereochemical variations. A regular and stable π-stacked structure was indicated for poly(DBF) on the basis of remarkable hypochromism in absorption spectra, exclusive excimer (dimer) emission in fluorescence spectra, and significant upfield shifts of

aromatic proton signals in ^{1}H NMR spectra. The structure was supported by conformational calculations.

This chapter describes the full details of the stereostructure of poly(DBF) prepared by anionic polymerization and its photophysical electrochemical properties. In this study, uniform oligomers of DBF with distinct chain lengths were isolated by size-exclusion chromatography (SEC), and the proposed π-stacked structure was unambiguously evidenced by single-crystal X-ray analyses of the uniform oligomers.[10] In addition, a π-stacked structure was also confirmed in solution by ^{1}H NMR analyses combined with theoretical chemical shift calculations. Further, the absorption and emission spectra and cyclic voltammograms were systematically measured for the uniform oligomers and polymers. Through these studies, the effect of the π-stacked structure on the photophysical and electrochemical properties was systematically investigated.

Stable π-stacked polymers may afford functional electronic materials because stacked π-electron systems can facilitate longrange charge transport, as reported for tetrathiafluvalenetetracyanoquinodimethane and tetramethyltetrasalenafluvalene crystals.[11] Such a charge transfer has been proposed also for DNA,[12a-d] although there is controversy as to whether it is real.[12e-h]

1.2 Synthesis and Isolation of Uniform Oligomers of Oligo(DBF)s

DBF was synthesized according to the literature with modifications.[13] Polymerization of DBF was initiated using an organolithium and was terminated using a protonating or an alkylating reagent (Scheme 1.1). The initiators were 9-fluorenyllithium (FlLi), *n*-BuLi, methyllithium (MeLi), and phenyllithium (PhLi), and the terminating reagents were methanol (MeOH), ethyl iodide (EtI), and benzyl bromide ($PhCH_2Br$). The conditions and results of the reactions with the expected polymer structures are summarized in Table 1.1. In all cases, the DBF monomer was consumed in a high yield. In some cases, the reaction products were partially insoluble in THF or chloroform. The THF-soluble and -insoluble parts indicated very similar IR signals, suggesting that the insoluble parts consist of highermolecular-weight polymers whose chemical structures of repeating units are identical to those of the soluble parts. Highermolecular-weight fractions may tend to become insoluble probably due to the crystallinity of the poly(DBF) chain.

Scheme 1.1 Anionic Polymerization of Dibenzofulvene (DBF)

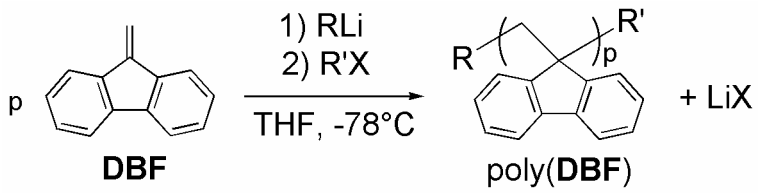

Table 1.1 Anionic Polymerization of Dibenzofulvene (DBF) in THF

entry	polymer structure[a]	DBF (mmol)	initiator (mmol)	terminator (mmol)	temp (°C)	time (hr)	conc (%)	THF-soluble part Yield[c] (%)	THF-soluble part M_n[d]
1	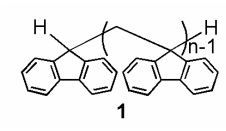 **1**	5.6	9-FlLi (1.1)	MeOH (4.0)	–78	24	>99	>99	860
2		4.6	9-FlLi (9.3)	MeOH (12.1)	0	1	>99	>99	350
3	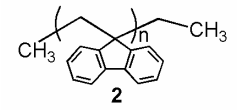 **2**	10.0	MeLi (2.0)	CH_3CH_2I (25.0)	–78	48	84	98	760
4	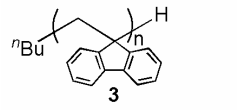 **3**	11.2	*n*-BuLi (2.2)	MeOH (6.2)	–78	24	>99	81	790
5	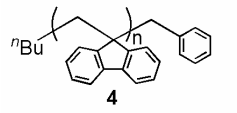 **4**	2.8	*n*-BuLi (0.93)	$PhCH_2Br$ (8.4)	–78	24	>99	99	990[e]
6	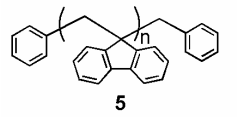 **5**	10.0	PhLi (2.0)	$PhCH_2Br$ (16.8)	–78	48	84	63	950

[a] *n* – 1 and *n* denote of degree of polymerization for entries 1–2 and 3–6, respectively. [b] Determined by ^{1}H NMR analysis of the reaction mixture. [c] THF-soluble part was a mixture of oligomers and unreacted monomer when the monomer conversion was not quantitative. The yield of this part was calculated excluding the weight of the unreacted monomer. [d] Determined by GPC using two OligoPore columns connected in series with oligo(DBF)s as the standard samples (eluent THF). [e] Determined by GPC using two TSKgel G1000H_{HR} columns connected in series with oligo(DBF)s as the standard samples (eluent THF).

The reactions afforded the products (oligomers and polymers) with five terminal-group combinations, **1**–**5**. The efficiency of introducing terminal groups was confirmed by a MALDI-mass spectrum. The observed mass numbers supported the expected polymer structures. The spectra for **1**, **2**, and **5** are shown in Figure 1.1 as examples. Although unintended protonation of the growing anion with protonic contamination could lead to a polymer having hydrogen at the termination end in entries **3**, **5**, and **6** aiming at structures **2**, **4**,

and **5**, respectively, the corresponding spectra in Figure 1.1 showed no clear peaks based on oligomers having hydrogen at the termination end of the chain.

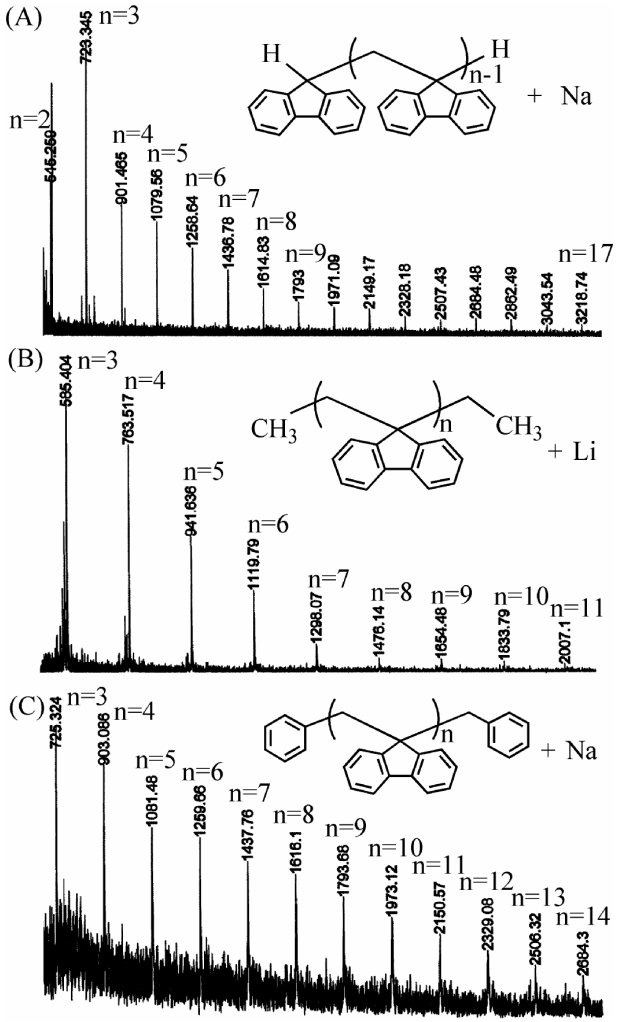

Figure 1.1 MALDI-TOF mass spectra of oligo(DBF)s **1** (Table 1.1, entry 1) (A), **2** (Table 1.1, entry 3) (B), and **5** (Table 1.1, entry 6) (C).

To obtain detailed information on the π-stacked conformation of the DBF polymer and its effect on photophysical and electrochemical properties, THF-soluble products were separated into oligomers that are uniform in terms of the number of fluorene units in a chain (**1**–**5** in Table 1.1; n = 2–8) and polymers ($n \geq 9$, mixture) using a preparative-scale SEC apparatus (Figure 1.2). Chain lengths of the isolated oligomers were determined by MALDI-mass spectra. The purity of the separated oligomers **1** and **2**, which were used for the solution structure and property analyses, was checked by analytical scale SEC. The isolated oligomers contained a small amount of higher- and lower-molecular-weight fractions. The

purity of oligomers **1** (n = 2–8) was in the range of 95–99%, and that of oligomers **2** (n = 2–8) was in the range of 92–99% (Table 1.2).

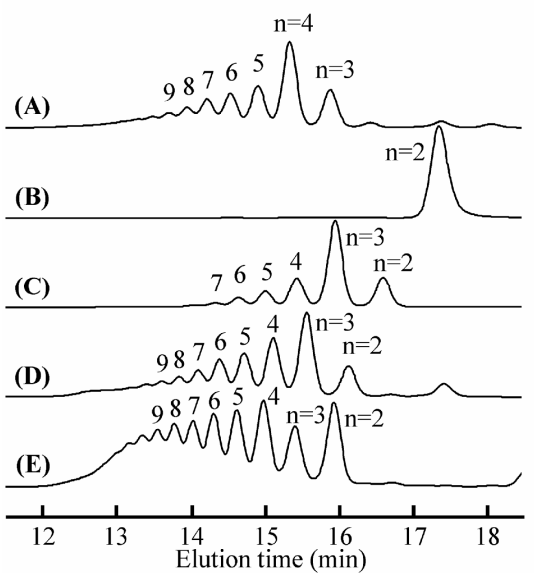

Figure 1.2 SEC curves of oligo(DBF)s **1** (Table 1.1, entry 1) (A), **1** (Table 1.1, entry 2) (B), **2** (Table 1.1, entry 3) (C), **3** (Table 1.1, entry 4) (D), **5** (Table 1.1, entry 6) (E) [column, two PL OligoPore Columns (30 x 0.72 (i.d.) cm) (Polymer Laboratories); eluent, THF; flow rate, 1.0 ml/min].

Table 1.2 Purity of Oligo(DBF)s Isolated by Preparative SEC[a]

	lower-molecular-weight fraction (%)	main fraction (%)	higher-molecular-weight fraction (%)
1 (n=2)	–	>99	–
1 (n=3)	–	95.2	4.8
1 (n=4)	–	>99	–
1 (n=5)	–	>99	–
1 (n=6)	3.1	95.5	0.4
1 (n=7)	–	98.6	1.4
1 (n=8)	0.5	98.1	1.4
2 (n=2)	–	95.1	4.9
2 (n=3)	1.6	97.8	0.6
2 (n=4)	0.8	98.5	0.8
2 (n=5)	3.7	94.9	1.4
2 (n=6)	2.3	96.3	1.4
2 (n=7)	3.3	94.5	2.3
2 (n=8)	2.8	91.8	5.4

[a]Determined by analytical SEC using two OligoPore columns connected in series (eluent THF).

1.3 Crystal Structure Analyses

The oligomers isolated by SEC were subjected to crystallization for X-ray crystal structure analysis. Some of the oligomers led to single crystals suitable for X-ray analyses by recrystallization from a chloroform solution. Crystal structures were solved for **1** (n = 2 and 4), **2** (n = 2 and 6), **3** (n = 3), **4** (n = 4), and **5** (n = 2 and 5). The crystal structures are shown in Figure 1.3, and the crystallographic data are summarized in Table 1.3. The single-crystal structures indicated two conformational characteristics: (1) the in-chain fluorene moieties of oligomers of n = 4–6 are in a π-stacked conformation with the corresponding main-chain carbon-carbon bonds having a slightly twisted trans-trans structure regardless of the terminal groups; and (2) the chain-terminal fluorene moieties are in a π-stacked conformation when the terminal group is ethyl or bulkier, while they are flipped when the terminal group is hydrogen. It is also noteworthy that the π-stacking is not in a perfectly face-to-face manner but the fluorene groups are slightly twisted; the twist takes place in one direction in a π-stacked structure consisting of three or more fluorene units leading to a helical structure. In addition, the stacked fluorene groups are not completely parallel to each other, which is probably due to steric repulsion. The twisted π-stacked structure is most clearly confirmed in **2** (n = 6), the longest molecule for which the crystal structure was solved. This oligomer has a π-stacked conformation throughout the chain and forms a long-pitched, single-handed helical structure where ca. nine monomeric units form one turn as a result of the twisted alignment of the fluorene groups. The conformationally enantiomeric right- and lefthanded helices are paired in the solid state; that is, the crystal formed as a racemic crystal.

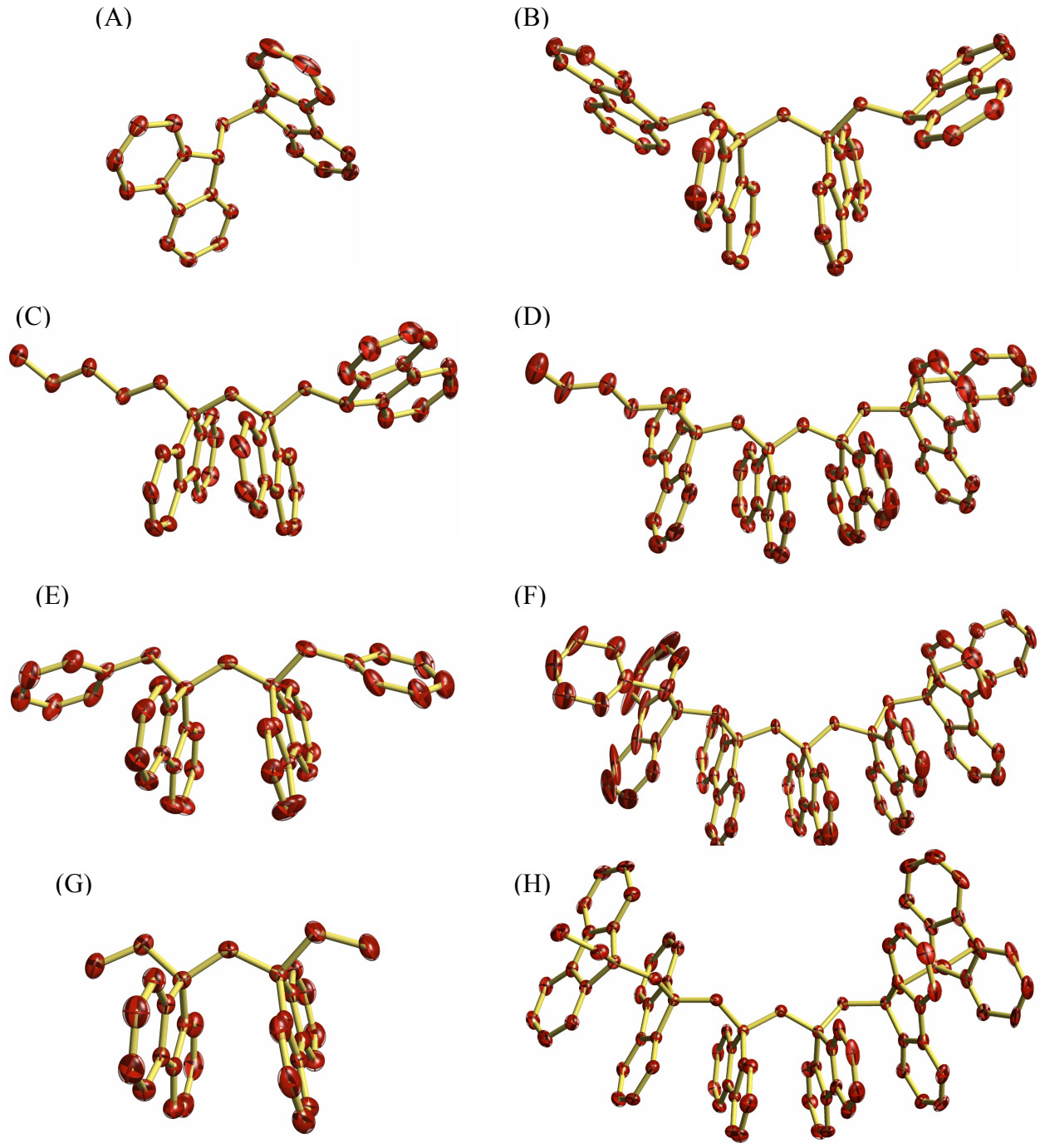

Figure 1.3 Crystal structures of oligo(DBF)s **1** (n = 2 (A) and n = 4 (B)), **3** (n = 3) (C), **4** (n = 4) (D), **5** (n = 2 (E) and n = 5 (F)), and **2** (n = 2 (G) and n = 6 (H)). Hydrogen atoms are omitted for clarity.

Table 1.3 Crystallographic Data of Oligo(DBF)s

property	**1** (n = 2)	**1** (n = 4)	**2** (n = 2)	**2** (n = 6)	**3** (n = 3)	**4** (n = 4)	**5** (n = 2)	**5** (n = 5)
molecular formula	$C_{27}H_{20}$	$C_{55}H_{40}$	$C_{31}H_{28}$	$C_{87}H_{68}$	$C_{46}H_{40}$	$C_{67}H_{56}$	$C_{41}H_{32}$	$C_{41}H_{32}$
fomula weight	344.45	700.92	400.56	1113.49	592.82	861.18	524.70	1059.40
temperature, K	296	296	296	296	296	296	296	296
wavelength, Å	0.71 069	0.71 069	0.71 069	0.71 069	0.71 069	0.71 069	0.71 069	0.71 069
crystal/color	colorless	colorless	colorless	colorless	colorless	colorless	colorless	colorless
crystal system	monoclinic	monoclinic	monoclinic	monoclinic	monoclinic	triclinic	monoclinic	monoclinic
space group	$P2_1/n$	$C2/c$	$C2/c$	$P2_1/n$	$P2_1/c$	$P\bar{1}$	$C2/c$	$P2_1/c$
unit cell dimensions								
a, Å	9.9303(5)	16.3629(9)	12.534(2)	10.4024(5)	13.2214(3)	12.8765(4)	16.6849(5)	11.5072(5)
b, Å	8.5039(4)	15.273(1)	12.674(2)	19.7052(6)	13.3664(2)	15.4623(2)	12.2332(5)	22.102(1)
c, Å	22.030(1)	15.5365(7)	14.546(2)	29.916(1)	19.0154(1)	12.7814(2)	15.4247(5)	27.047(2)
α, deg	90	90	90	90	90	107.723(1)	90	90
β, deg	98.922(2)	103.475(4)	101.975(5)	92.6521(6)	92.523(1)	94.605(2)	110.5185(8)	89.836(1)
γ, deg	90	90	90	90	90	96.765(1)	90	90
volume, Å^3	1837.8(1)	3775.9(3)	2260.4(5)	6125.7(4)	3357.19(7)	2388.91(9)	2948.6(2)	6879.1(5)
Z	4	4	4	4	4	2	4	4
D_{calcd}/g cm^{-3}	1.245	1.232	1.176	1.207	1.173	1.197	1.182	1.023
reflns collected	16 751	7865	8682	42 618	20 119	13 845	14 076	46 223
unique reflns	4192	4328	2543	12 813	7705	10 622	3388	14 864
R_1	0.042	0.042	0.055	0.066	0.053	0.075	0.058	0.143
wR_2	0.090	0.078	0.140	0.145	0.085	0.118	0.140	0.341
GOF	0.96	1.40	1.21	1.31	1.28	2.00	1.23	1.74

1.4 ^{1}H NMR Spectra

^{1}H NMR spectra of the oligomers were measured to confirm the chemical structure and to obtain information on the solution conformation of oligomers **1** and **2** (n = 2–8) and polymers **1** (M_n = 1700, n = 9.6, mixture of $n \geq 9$) and **2** (M_n = 1890, n = 10.4, mixture of $n \geq 9$). Because poly(DBF) has no stereocenter in the main chain, the chemical shift information of a proton signal should only reflect the conformation of the oligomer in its vicinity.

The 1D spectra are shown in Figures 1.4 and 1.5, and the chemical shift values are summarized in Tables 1.4 and 1.5. The peak assignments were performed on the basis of H-H COSY and NOESY spectra[14] (see Experimental Section). The structures of **1** (n = 8) and **2** (n = 8) with the proton numbering system are shown in Scheme 1.2 as generic specimens. The protons showing COSY correlation peaks are marked by blue arrows, and those showing NOESY correlations are marked by red arrows in Scheme 1.2. The same proton-proton correlations were also observed for oligomers of n = 2–7.

As for oligomers **1**, the triplet peaks having an intensity of two protons were first assigned to the terminal methine protons, and the signals due to the methylene protons neighboring the methines were then found by the COSY experiment. In the case of oligomers **2**, the triplet peaks in the highest magnetic-field region were assigned to the terminal methyl protons, and the neighboring methylene signals were identified by the COSY experiment.

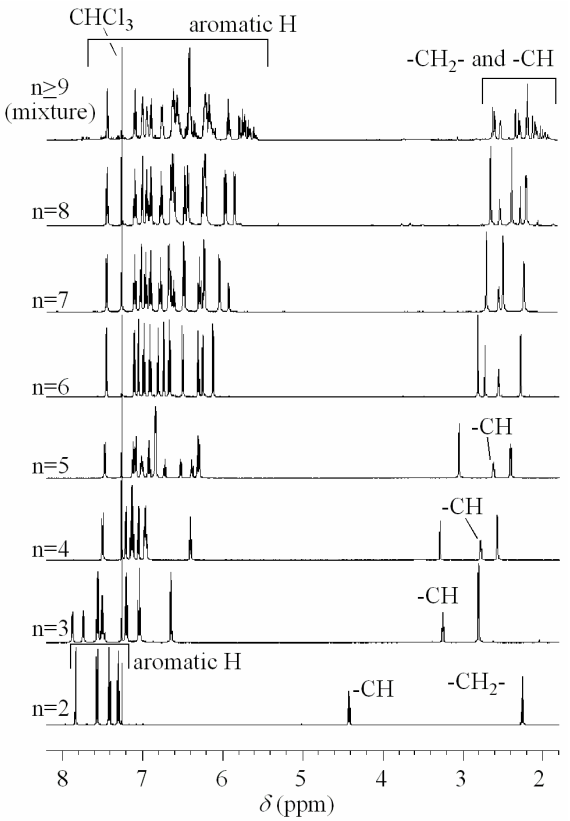

Figure 2.4 ^{1}H NMR spectra of oligo(DBF)s (**1**) (600 MHz, $CDCl_3$, room temperature).

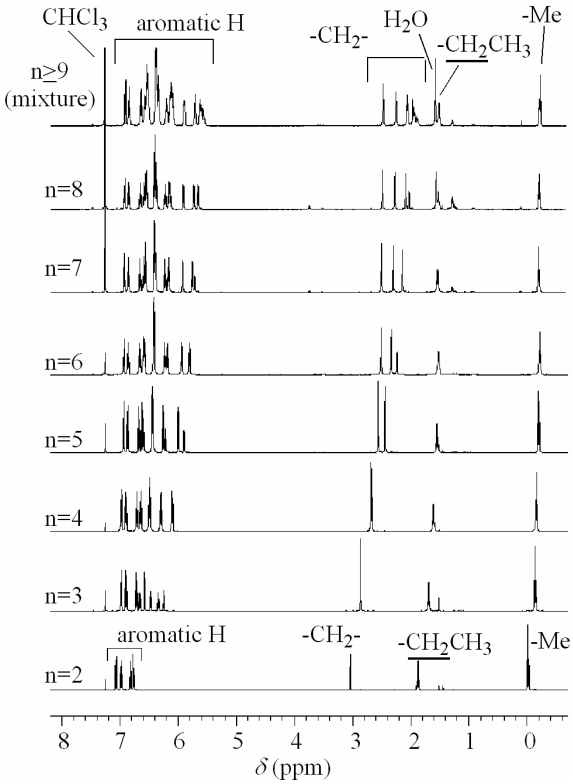

Figure 2.5 ^{1}H NMR spectra of oligo(DBF)s (**2**) (500 MHz, $CDCl_3$, room temperature).

Scheme 1.2 Structures of **1** (n = 8) and **2** (n = 8) with the Proton Numbering Systems[a]

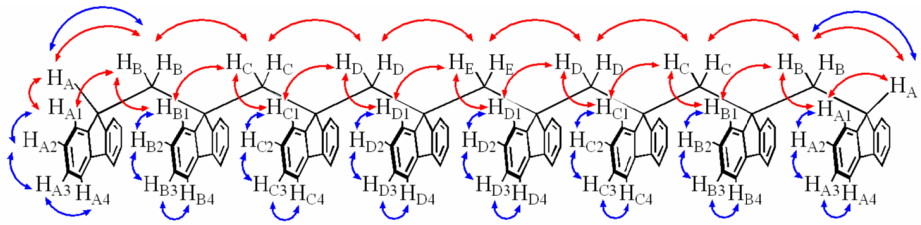

1 (n = 8)

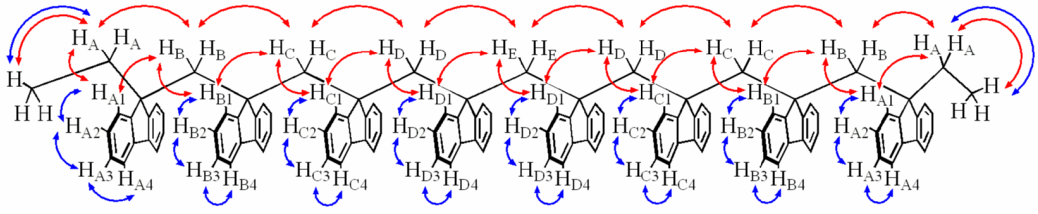

2 (n = 8)

[a]COSY and NOESY correlations were marked by blue and red arrows, respectively. NOESY correlations between aromatic protons are omitted.

Table 1.4 ^{1}H NMR Chemical Shifts (δ, ppm) of Oligo(DBF)s (**1**)

n	2	3	4	5	6	7	8	≥9[b]
H_A	4.42 (t)	3.25 (t)	2.78 (t)	2.64 (t)	2.56 (t)	2.55 (t)	2.53 (t)	2.62–1.88
H_B	2.26 (d)	2.80 (d)	2.57 (d)	2.42 (d)	2.28 (d)	2.23 (d)	2.20 (d)	(methylene
H_C			3.28 (s)	3.06 (s)	2.82 (s)	2.70 (s)	2.64 (s)	protons)
H_D					2.73 (s)	2.49 (s)	2.38 (s)	
H_E							2.27 (s)	
H_{A1}	7.57 (d)	6.64 (d)	6.41 (d)	6.31 (d)†	6.25 (d)	6.23 (d)	6.22 (d)†	5.55–7.44
H_{A2}	7.30 (dd)	7.04 (dd)	6.96 (dd)†	6.93 (dd)	6.91 (dd)	6.91 (dd)	6.90 (dd)	(aromatic
H_{A3}	7.42 (dd)	7.20 (dd)	7.14 (dd)*	7.13 (dd)	7.10 (dd)	7.10 (dd)	7.10 (dd)	protons)
H_{A4}	7.84 (d)	7.56 (d)	7.50 (d)	7.48 (d)	7.46 (d)	7.45 (d)	7.44 (d)	
H_{B1}		7.74 (d)	7.05 (d)	6.85 (d)*	6.74 (d)	6.68 (d)	6.64 (d)	
H_{B2}		7.49 (dd)*	6.97 (dd)†	6.85 (m)*	6.81 (dd)	6.79 (dd)	6.77 (dd)	
H_{B3}		7.51 (dd)*	7.13 (dd)*	7.02 (m)	6.98 (dd)	6.97 (dd)	6.95 (dd)	
H_{B4}		7.88 (d)	7.22 (d)	7.10 (d)	7.06 (d)	7.03 (d)	7.01 (d)	
H_{C1}				6.33 (d)†	6.12 (d)	6.04 (d)	5.96 (d)	
H_{C2}				6.40 (dd)	6.31 (dd)	6.29 (dd)	6.25 (dd)†	
H_{C3}				6.74 (dd)	6.67 (dd)	6.66 (dd)	6.61 (dd)*	
H_{C4}				6.54 (d)	6.50 (d)	6.49 (d)*	6.43 (d)	
H_{D1}						5.93 (d)	5.85 (d)	
H_{D2}						6.24 (dd)	6.22 (dd)†	
H_{D3}						6.62 (dd)	6.61 (dd)*	
H_{D4}						6.50 (d)*	6.47 (d)	

[a] See Scheme 1.2 for proton numbering. Spectra were recorded in $CDCl_3$ at room temperature (600 MHz). Residual $CHCl_3$ signal (7.26 ppm) was used as an internal reference. * and † indicate interchangeable assignments. [b] A polymer (M_n=1700 (vs oligo(DBF)), n=9.6, n≥9 mixture).

Table 1.5 ^{1}H NMR Chemical Shifts (δ, ppm) of Oligo(DBF)s (**2**)

n	2	3	4	5	6	7	8	≥9[b]
Me–	–0.01 (t)	–0.14 (t)	–0.16 (t)	–0.20 (t)	–0.22 (t)	–0.23 (t)	–0.24 (t)	–0.25 (t)
H_A	1.88 (q)	1.69 (q)	1.61 (q)	1.55 (q)	1.53 (q)	1.51 (q)	1.50 (q)	1.49 (q)
H_B	3.05 (s)	2.87 (s)	2.68 (s)	2.56 (s)	2.51 (s)	2.48 (s)	2.47 (s)	2.46–1.86
H_C			2.67 (s)	2.45 (s)	2.34 (s)	2.28 (s)	2.25 (s)	(methylene
H_D					2.24 (s)	2.12 (s)	2.07 (s)	protons)
H_E							2.00 (s)	
H_{A1}	6.77 (d)	6.58 (d)	6.50 (d)*	6.45 (d)*	6.42 (d)†	6.40 (d)†	6.39 (d)†	5.52–6.91
H_{A2}	6.83 (dd)	6.72 (dd)	6.71 (dd)	6.68 (dd)	6.66 (dd)	6.65 (d)	6.64 (dd)	(aromatic
H_{A3}	6.98 (dd)	6.90 (dd)	6.90 (dd)	6.87 (dd)	6.86 (dd)	6.85 (d)	6.85 (dd)	protons)
H_{A4}	7.07 (d)	6.98 (d)	6.98 (d)	6.94 (d)	6.93 (d)	6.92 (d)	6.92 (d)	
H_{B1}		6.25 (d)	6.10 (d)	6.00 (d)	5.94 (d)	5.91 (d)	5.90 (d)	
H_{B2}		6.34 (dd)	6.30 (dd)	6.26 (dd)	6.24 (dd)	6.22 (dd)	6.21 (dd)	
H_{B3}		6.66 (dd)	6.65 (dd)	6.62 (dd)†	6.60 (dd)*	6.59 (dd)	6.58 (dd)	
H_{B4}		6.48 (d)	6.48 (d)*	6.45 (d)*	6.42 (d)†	6.41 (d)†	6.40 (d)†	
H_{C1}				5.90 (d)	5.81 (d)	5.75 (d)	5.72 (d)	
H_{C2}				6.22 (dd)	6.19 (dd)	6.16 (dd) ‡	6.15 (dd)‡	
H_{C3}				6.60 (dd)†	6.58 (dd)*	6.56 (dd)*	6.55 (dd)*	
H_{C4}				6.45 (d)*	6.42 (d)†	6.40 (d)†	6.39 (d)†	
H_{D1}						5.70 (d)	5.65 (d)	
H_{D2}						6.15 (dd)‡	6.13 (dd)‡	
H_{D3}						6.56 (dd)*	6.54 (dd)*	
H_{D4}						6.38 (d)†	6.36 (d)	

[a] See Scheme 1.2 for proton numbering. Spectra were recorded in $CDCl_3$ at room temperature (500 MHz). Residual $CHCl_3$ signal (7.26 ppm) was used as an internal reference. *, †, and ‡ indicate interchangeable assignments. [b] A polymer (M_n=1890 (vs oligo(DBF)), n=10.4, n≥9 mixture).

The peak assignments of the remaining main-chain methylene and aromatic protons were performed on the basis of the 1D spectral profiles and the NOESY spectra. In the 1D spectra, all oligomers indicated only one set of terminal peaks: triplet methine signals for **1** and ethyl signals consisting of a methyl triplet and methylene quartet for **2**. In addition, the number of observed peak sets for the methylene protons was only onehalf the number of existing methylene groups for the oligomers of n = 3, 5, and 7 or [(number of existing methylenes) – 1]/2 + 1 for the oligomers of n = 2, 4, 6, and 8. This profile may be explained in terms of a

conformation symmetrical with respect to the central methylene (oligomers of n = 2, 4, 6, and 8) or the central fluorene group (oligomers of n = 3, 5, and 7), such as the crystal structures of **2** (n = 6) and **5** (n = 5) shown in Figure 1.3, if the conformation is stable in solution. A fast exchange between different conformations may also lead to a simple NMR profile. However, fast conformational dynamics in solution seem unreasonable because clear NOE correlations were observed that support a stable all-trans conformation as follows.

In the NOESY spectra of all oligomers analyzed here, all in-chain methylene protons indicated correlation peaks with one or two different methylene groups in addition to aromatic protons. This finding is best interpreted assuming an all-trans conformation as illustrated in Scheme 1.2; only the neighboring groups in such a conformation will show correlation peaks in the NOESY spectra. Hence, the methylene protons were assigned as summarized in Tables 1.4 and 1.5 assuming an all-trans conformation, which is consistent with the regular numerical relations between the number of observed methylene signals and the exsiting methylene groups noted above.

The aromatic signals were assigned also using the 2D NMR information. The observed NOE signals were interpreted to correlate the protons at the 1- and 8-positions of the fluorene ring, denoted by $H_{A–D1}$ in Scheme 1.2, and the methylene groups in the vicinity. The position of each fluorene ring was assigned in this way. The peak assignments of the remaining aromatic protons were completed using the COSY information. NOE correlations between protons of neighboring fluorene units in stacked conformation were also observed, although they are not shown in Scheme 1.2 for clarity.

It is noteworthy that aromatic proton signals of all samples of **2** were within the range of 5.6–7.1 ppm. This is in stark contrast to the fact that poly(9,9-dimethyl-2-vinylfluorene)[15] which probably has a flexible conformation showed its aromatic protons signals in a much lower magnetic-field range (6–8 ppm). This supports the stable π-stacked conformation of **2** throughout the chain in solution.

The aromatic proton signals of **1** appeared in a wider chemical shift range as compared with those of **2**, suggesting that **1** may have a less regular π-stacked conformation. However, the samples of **1** (n = 4) and larger showed all aromatic signals, except for a doublet with a four-proton intensity at ca. 7.5 ppm, in the range of 5.6-7.2 ppm, similarly to all samples of **2**, indicating that most of **1** (n = 4) or larger has a regular π-stacked conformation similar to that of **2**. The exceptional four-proton intensity signals are due to the 4- and 5-positions of the

terminal fluorene rings according to the peak assignments described above. This may indicate that the terminal fluorene rings of **1** are flipped as observed in the crystal structures of **1**.

The signals of **1** (n = 2) were similar to those of fluorene in the chemical shift range, implying that this oligomer does not have a π-stacked conformation. In the sample of **1** (n = 3), both flipped and stacked conformations may exist because the spectral profile in the aromatic region is just between those of the longer oligomer and the shorter one.

To obtain information on the stability of the conformation of the oligomers, temperature effects on the NMR spectra were examined for all oligomers in the range from –50 to +60 °C. Most peaks only monotonically shifted upfield or downfield with temperature, and the shift amount was within 0.2 ppm. The peak shift was reversible with temperature. These results suggest that the π-stacked conformation in solution proposed so far is stable and does not undergo a drastic conformational mutation in this temperature range.

It should be noted here that no clear NMR information indicating the helical twist in solution was obtained even at lower temperatures. The helical structure may be in an exchange between the right- and left-handed local twists that is faster than the NMR time scale under the experimental conditions of this study.

1.5 Chemical Shift Calculation

To rationally connect the NMR spectral information to the solution conformation of the oligomers, the chemical shifts of the main-chain methylene and terminal methine or ethyl protons were computationally estimated by density functional theory (DFT)[16] calculation for some optimized conformers of **1** (n = 2), **2** (n = 2 and 4). The conformer structures optimized by the semi-empirical PM5 method[17] are shown in Figure 1.6 with their heats of formation (H_f) (PM5) and theoretical chemical shifts obtained by the LORG method[18] using B88[19] exchange and LYP[20] correlation functionals. The H_f values of the conformers having identical chemical structures were similar, indicating that all conformers shown in the figures could contribute to the experimental NMR spectra at similar probabilities.

Prior to application of the DFT method to the oligomers, the accuracy of the DFT chemical shift calculation was tested using fluorene, 9-methylfluorene, and superphane, which consist of methylene, methine, and an aromatic ring and are expected to have little conformational freedom. The experimental –CH_2– shift for fluorene was 3.95 ppm ($CDCl_3$, 500 MHz,

Me_4Si), and that for superphane was 2.98 ppm,[21] while the calculated shifts were 3.87 and 3.29 ppm for fluorene and superphane, respectively. The experimental $-CH_3$ and methine shifts for 9-methylfluorene were 1.53 and 3.95 ppm, respectively ($CDCl_3$, 500 MHz, Me_4Si), and the corresponding calculated values were 1.43 and 4.03 ppm. These results mean that the theoretical calculation in this study may contain an error of 0.1–0.3 ppm.

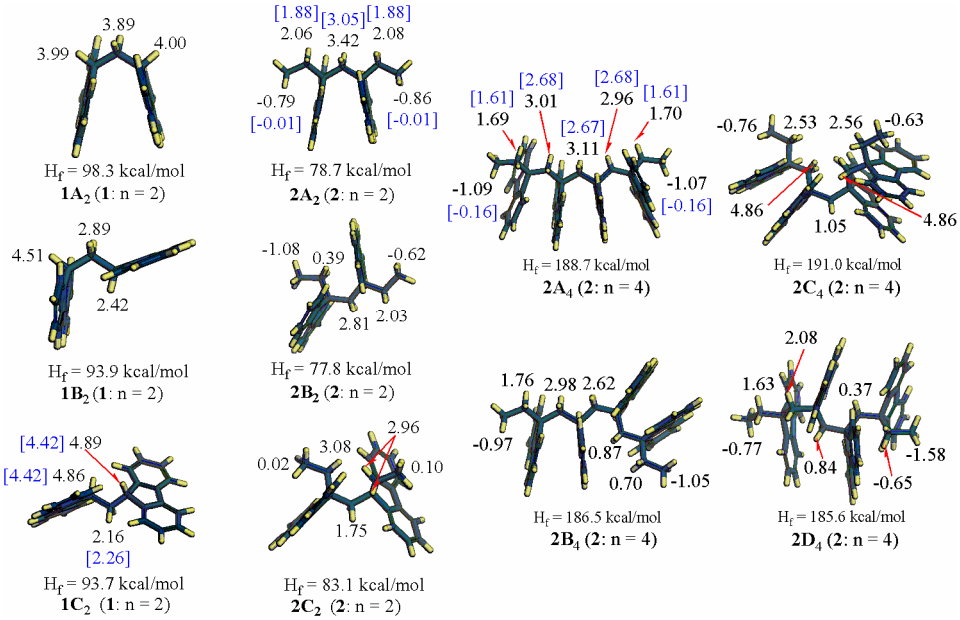

Figure 1.6 Conformers of **1** ($n = 2$) and **2** ($n = 2$ and $n = 4$) and calculated chemical shifts of methylene protons. The values in square brackets are the experimental chemical shifts.

Conformers **1A₂**–**1C₂** were evaluated for **1** ($n = 2$). The calculated methylene shift of **1A₂** deviated from the experimental value by 1.6 ppm, and one of the calculated methine shifts of **1B₂** deviated from the experimental value by 2.0 ppm, suggesting that these are not the most plausible conformers. In contrast, the deviations of the calculated methylene and methine shift of **1C₂** from the experimental values were only 0.4 and 0.1 ppm, respectively. These results suggest that **1C₂**, in which the two fluorenyl groups are flipped, is the most probable conformer although other conformers could also exist in conformational dynamics.

Conformers **2A₂**–**2C₂** for **2** ($n = 2$) were generated and subjected to shift calculations. The theoretical shifts of the central methylene protons of conformers **2A₂** and **2B₂** were rather close to the experimental shifts, while that of **2C₂** deviated from the observed value by 1.3 ppm. Therefore, **2C₂** may not be reasonable. The predicted chemical shift for one of the

terminal methylene groups of **2B$_2$** largely deviated from the experimental value, suggesting that **2A$_2$** having a π-stacked conformation is the most plausible. Although it is noticeable that the experimental terminal methyl shift of **2A$_2$** deviated from the predicted value by ca. 0.8 ppm, this may mean that the terminal ethyl groups rotate relatively fast and do not give an accurate shift in the calculation of a single conformer. Hence, flipped and stacked conformations were suggested by the NMR shift calculation for **1** (n = 2) and **2** (n = 2), respectively. As in crystal, an ethyl or a larger group may prevent the rotation of the terminal fluorene unit and force it into a stacked form.

For **2** (n = 4), four conformers, **2A$_4$**–**2D$_4$** were tested: **2A$_4$** is a model of a flawlessly stacked conformation, and **2B$_4$** and **2C$_4$** are models of stacked conformations with a "kink". Although the models with a kink were predicted to show a remarkable upfield shift of the main-chain methylene signals (δ 1–0.7 ppm) in the vicinity of the kink, no peak was observed in such a high magnetic field range in the experimental spectra. In addition, the calculated methylene shifts of **2A$_4$** were rather close to the experimental data. Therefore, **2A$_4$** is considered to be the most plausible conformation. In this case also, calculated shifts of the terminal methyl protons significantly deviated from the observed values, probably due to the relatively fast motion of the terminal ethyl group as noted above.

As described here, the chemical shift calculation appears to be an effective method of obtaining information on the oligomer conformation. Although longer oligomers and polymers were not subjected to chemical shift calculation, their experimental methylene shifts seem to converge into a value around 2 ppm, and no peaks of the methylene group were observed in a range higher than 1 ppm in the spectra. This suggests that the longer oligomers and polymers have a stable π-stacked conformation without a kink in the chain.

1.6 Conformational Calculation

Oligomer conformation was evaluated by force field and semi-empirical molecular orbital calculations. Although the relatively generic Dreiding force field[22] was used for all conformational calculations in our preliminary studies,[8] MM3*,[23] MMFF94s,[24] COMPASS[25] force fields with better energetic and structural precision and a semi-empirical PM5 method were employed in this study.

First, Monte Carlo conformational searches with MM3* and MMFF94s force fields were performed on a DBF hexamer having ethyl groups at the chain terminals (**2** (n = 6)) using a

MacroModel[26] software package. Two distinctive structures were found to be the most stable conformations using MM3* and MMFF94s force fields out of 20 000 (MM3*) and 19 550 (MMFF94s) conformers, which were generated by changing the dihedral angles around the 12 main-chain bonds at an interval of 60°, as shown in Scheme 1.3. These two most stable conformers were further minimized by the PM5 method to afford structures **2A$_6$** and **2B$_6$** shown in Figure 1.7. Structure **2A$_6$** was similar to the crystal structure (Figure 1.3), while structure **2B$_6$** had a partially trans-gauche-like structure. The two conformers indicated similar values of H_f by the PM5 method.

Scheme 1.3 Dihedral Angle Sets for the Monte Carlo Simulation of **2** of $n = 6$[a]

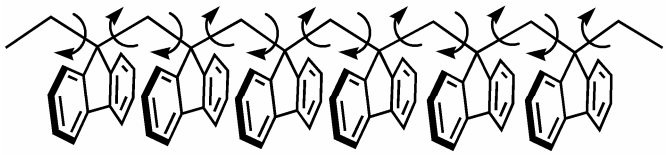

[a] Angle interval was 60°.

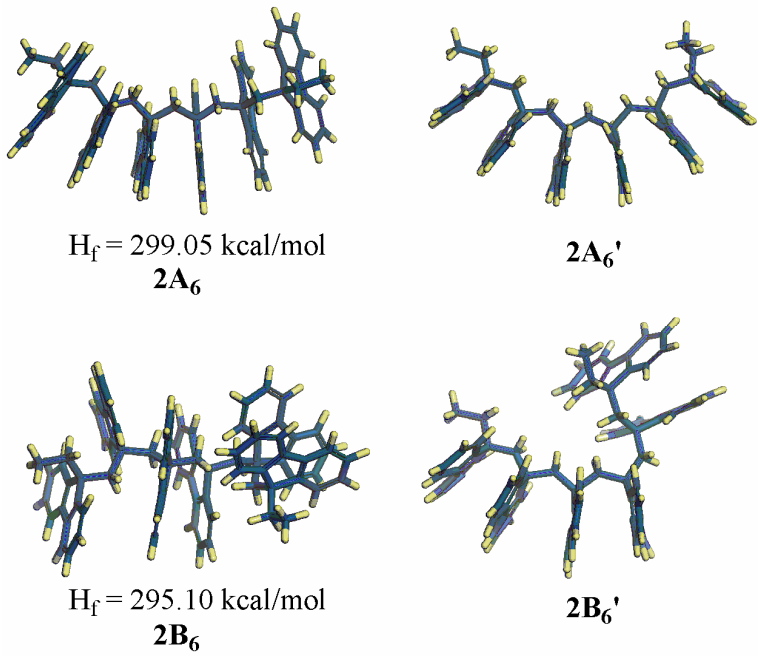

Figure 1.7 Conformers of **2** of $n = 6$ found most stable in the Monte Carlo simulation and optimized by the PM5 method, **2A6** (force field, MM3*) and **2B6** (force field, MMFF94s), and those after MD simulation, **2A6′** (300 K, 10 ns) and **2B6′** (300 K, 8.2 ns), starting from **2A6** and **2B6**, respectively.

Next, the stability of conformations **2A$_6$** and **2B$_6$** was tested by molecular dynamics (MD) simulations using the COMPASS force field under NVT conditions with Berendsen's thermostat[27] (Figure 1.7, right-hand side). While conformation **2A$_6$** did not largely change in the MD simulation at 300 K for 10 ns to give structure **2A$_6$'**, conformation **2B$_6$** quickly changed into a mostly all-trans, π-stacked conformation with a kink (gauche–gauche main-chain conformation) (**2B$_6$'**) in the middle of the chain at 300 K within 0.1 ns, and structure **2B$_6$'** did not significantly change within 8 ns. These results suggest that a π-stacked conformation is preferred under dynamic conditions while several different conformers, including the π-stacked structure, may have similar steric energies under static conditions.

The conformational stability test was extended to a model of the polymer (**2**, n = 15). An all-trans model and an alternating trans-gauche model molecular-mechanically optimized using the COMPASS force field were subjected to MD simulations (NVT) (Figure 1.8). The all-trans model remained in the π-stacked structure at 300 K in 15 ns, and the structure was only partially distorted even at 600 K. In contrast, the alternating trans-gauche model promptly changed into a preferentially alltrans, π-stacked conformation with a kink within 2 ns at 300 K.

These results suggest that the π-stacked conformation is most preferable for poly(DBF). Although some conformers with a kink in the main chain were observed in the calculations, most of the real molecules are considered to have a π-stacked structure throughout the chain, based on the discussions about the NMR spectra in the preceding section.

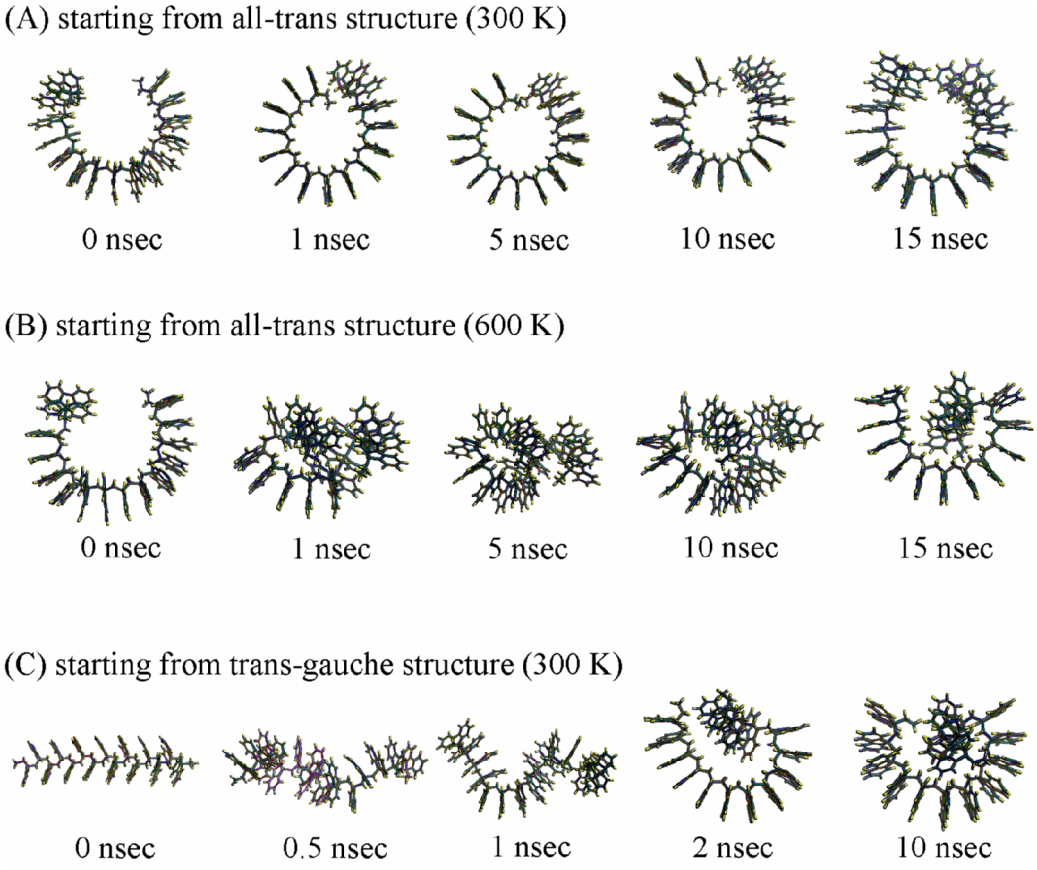

Figure 1.8 Conformations of **2** (n = 15) observed during the MD simulations: those starting from an all-trans structure at 300 K (A), those starting from an all-trans structure at 600 K (B), and those starting from an alternating trans-gauche structure at 300 K (C).

1.7 Absorption and Emission Profiles

The absorption and emission spectra of the oligomers (n = 2–8) and polymers ($n \geq 9$) of **1** and **2** indicated characteristic profiles based on their structures. The absorption spectra are shown in Figure 1.9. Oligomer **1** (n = 2) bearing two fluorene groups indicated slight hyperchromicity relative to 9-methylfluorene, the model for the monomeric unit, which is obvious in the 240–280 nm region, while oligomers **1** (n = 3–8) and the polymer (M_n = 1700, n = 9.6, mixture of $n \geq 9$) exhibited significant hypochromicity. In addition, all of the samples of **1** (n = 3) and larger showed a red shift of the absorption bands. As for oligomers **2**, all of the samples, including the one of n = 2, exhibited hypochromicity and a red shift.

Hypochromic effects have been reported for stacked base pairs in a double helical strand in DNA.[28] Therefore, the hypochromicity described above is consistent with the above discussion that the oligomers and polymers studied here have a π-stacked conformation in

solution. The degree of hypochromicity found for the oligomers and polymers in this study is larger than that for DNA. This may indicate that the π-electron systems are more densely packed in the present systems than those in DNA. The fact that **1** (n = 2) was hyperchromic[28a] while **2** (n = 2) was hypochromic supports the conclusion from the ^{1}H NMR studies that the former compound does not have a stacked conformation while the latter does.

The observed hypochromism may be interpreted in terms of the theory by Tinoco and Rhodes. According to ref 29, a parallel stacking of two aromatic molecules will result in hypochromism because the transition moment of the chromophore in question should be smaller due to interaction with induced dipoles of other chromphores in the vicinity. Because the magnitude of such interaction depends on the third power of inter chromophore distance, it should be much higher for the neighboring chromophores than those separated by longer distances. This well explains the fact that the DBF dimer showed much larger hypochromicity than the trimer and higher oligomers with respect to 9-methylfluorene (unimer model).

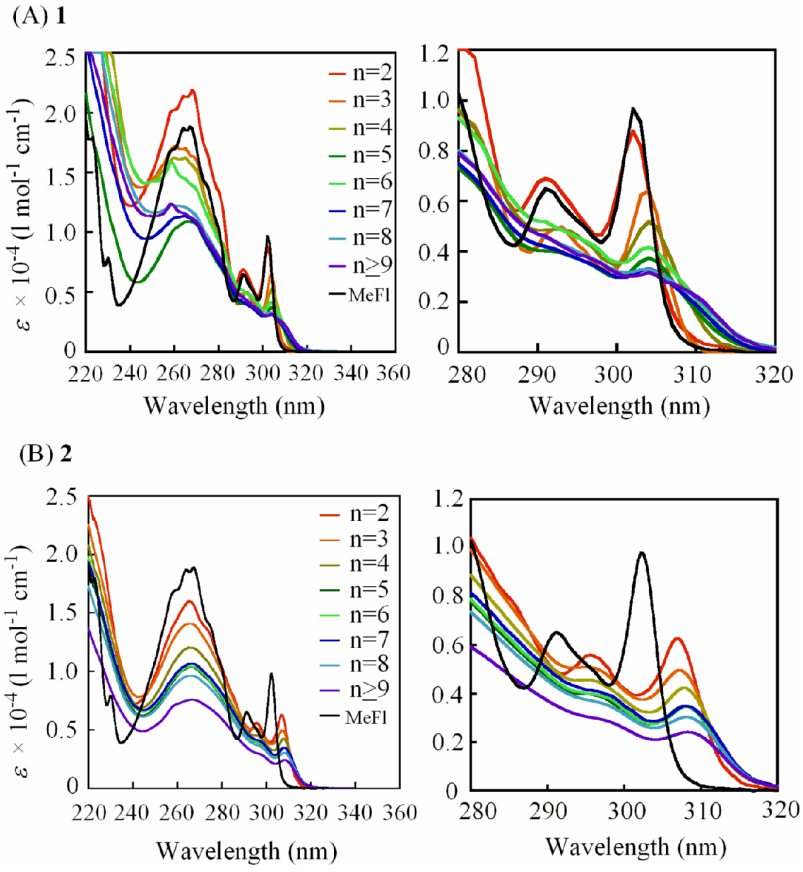

Figure 1.9 Absorption spectra of oligo(DBF)s **1** (A) , **2** (B), and 9-methylfluorene (MeFl) in THF at room temperature.

The observed red shift of the absorption bands means that electronic interaction between neighboring fluorene units in the ground state lowered the excitation energy of the oligomers or polymers. The red shift may be interpreted more accurately in terms of the exciton coupling theory by Kasha.[30] The absorption bands around 270 nm and 302 nm of fluorene moiety are ascribed to $^1L_a \leftarrow {}^1A$ and $^1L_b \leftarrow {}^1A$ transitions, respectively.[31] Both transition moments are polarized along the horizontal axis (the longer axis) of fluorene moiety. A completely co-facial arrangement of two fluorene moieties would indicate only a blue-shifted peak according to Kasha's theory due to forbidden transition corresponding to the lower-energy band among the two bands generated by energy splitting by the exciton-exciton interaction. However, the DBF oligomers experimentally exhibited red shifts. This is consistent with the fact that fluorene moieties are stacked in a slightly twisted form in a poly(DBF) chain. In main-chain conjugated polymers, a longer chain length results in a significantly reduced band gap.[32,33] Electronic interaction between closely stacked but not covalently bonded aromatic groups may also make the band gap narrower from the present results, although the effect seems to be smaller as compared with that for main-chain conjugated polymers.[33]

To more quantitatively evaluate the red shift and the hypochromicity, the wavelength and molar extinction coefficient (ε) of the lowest-energy absorption peak were plotted against the chain length (n) of oligomers **2** (Figure 1.10). The peak-top wavelength increased with the chain length and leveled off around n = 5 (Figure 1.10A). In addition, ε at the peak top decreased with n and leveled off also around n = 5 (Figure 1.10B). These results suggest that, in the ground state, the electronic interaction between the stacked fluorene groups may extend over as long as ca. five units. An exciton may be formed over ca. five successive monomeric units in a chain upon photoexcitation. However, it should be noted that the observed dependence of absorption spectra on the chain length may also be explained by considering the theories described in refs. 29 and 31 and might not have a direct connection with exciton delocalization. A more detailed investigation will be necessary to shed light on this point.

The exciton in a poly(DBF) chain may fit the Frenkel model[34] where the electron and the hole are localized in the close vicinity rather than Wannier model.[35]

Figures 1.11 and 1.12 show the wavelength-vs.-1/n and ε-vs.-1/n plots for the lowest-energy absorption peak, which suggest that the polymer has the infinite chain (1/n = 0)

would show the peak-top wavelength of 308.5 nm and ε of 1894 L mol^{-1} cm^{-1}.

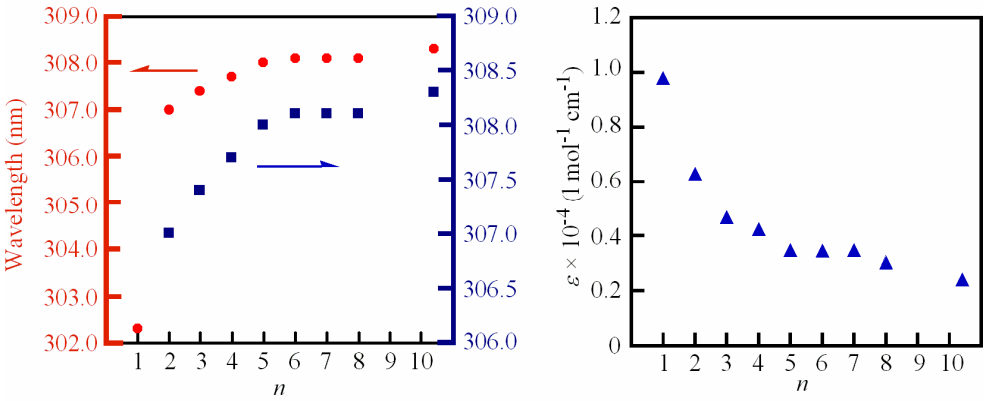

Figure 1.10 Wavelength versus n and molar extinction coefficient (ε) versus n plots for the longest wavelength absorption maxima of oligo(DBF)s **2**. Data at n = 1 are for 9-methylfluorene, and those at n = 10.4 are for a polymer (M_n = 1890 (vs oligo(DBF)), n = 10.4).

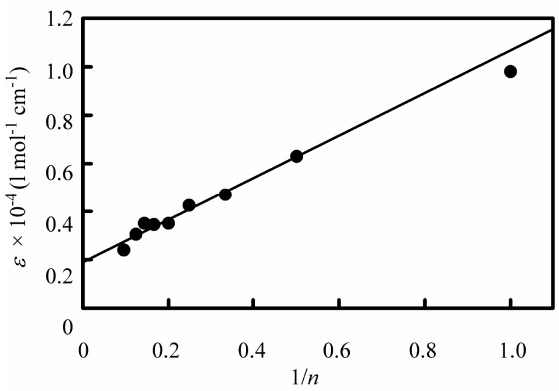

Figure 1.11 Molar extinction coefficient-vs.-1/n plots for the longest wavelength absorption maxima of oligo(DBF)s **2**. Extrapolation of the plot to 1/n = 0 gave 1890 L mol^{-1} cm^{-1} for a polymer with an infinite number of fluorene moiety. Data at 1/n = 1 are for 9-methylfluorene, and those at 1/n = 0.0962 are for a polymer (M_n = 1890 (vs. oligo(DBF)), n = 10.4).

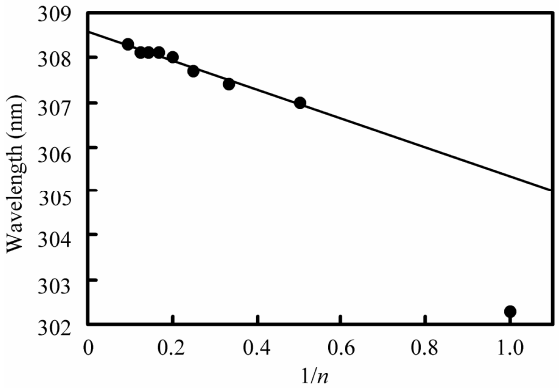

Figure 1.12 Wavelength-vs.-1/n plots for the longest wavelength absorption maxima of oligo(DBF)s **2**. Extrapolation of the plot to 1/n = 0 gave 308.6 nm for a polymer with an infinite number of fluorene moiety. Data at 1/n = 1 are for 9-methylfluorene, and those at 1/n = 0.0962 are for a polymer (M_n = 1890 (vs. oligo(DBF)), n = 10.4).

The imprecation of the "five monomeric units" may be as follows. The DBF oligomers and polymers have a π-stacked structure in solution as concluded on the basis of the NMR data and theoretical simulations. However, the π-stacked molecules should experience thermal vibration that does not largely distort the conformation. This may lead to heterogeneity of the stacked conformation; that is, the distance between the fluorene groups and main-chain torsion angle can slightly vary part by part in a chain, especially in a relatively short time range within which photoabsorption takes place. The roughly coincidental critical number of fluorene units suggests that ca. five fluorene units are always in one block of uniform stacked sequence even at a short time scale. In other words, the dynamic "persistence length" of a uniformly π-stacked sequence from the view of photoexcitation covers five monomeric units under the experimental conditions of this study.

An alternative interpretation may be that the electronic interaction of the stacked fluorene groups in the polymer side chain extends inherently up to ca. five units even for a long, completely uniform "frozen" π-stacked polymer. Absorption measurements at an extremely low temperature or in a solidstate matrix that may freeze molecular vibration might provide an answer. Computational studies on the electronic states of poly(DBF) may also be necessary. These aspects will be assessed in future studies.

Figure 1.13 shows the emission spectra of **1** and **2**. In the spectra of **1** (Figure 1.13A), those of $n \geq 4$ indicated predominant emission bands around 400 nm, while that of $n = 2$ showed a shorterwavelength emission band around 310 nm, which was similar in shape and wavelength to that of monomeric fluorene, and that of $n = 3$ indicated both bands around 310 and 400 nm. The bands around 400 nm are considered to arise from an excited dimer in which excited energy delocalizes over two neighboring, stacked fluorene units because the band wavelength is rather close to those of the fluorene excimer[36] (367 nm, in toluene) and the excited side-chain dimer of poly(2-vinylfluorene)[37] (380 nm, in THF). In contrast to **1**, all samples of **2** indicated predominant dimer emission.

Excimer formation is supported by time-resolved fluorescence spectrum measurents of a DBF pentamer (**2** ($n = 5$)). The pentamer showed a delay (ca. 0.37 nsec) in the emission at around 400 nm after excitation while it showed almost no delay in the emission at around 313 nm (monomeric fluorene emission). During the delay time, a slight change in local conformation forming the dimer emitting site (excimer site) may take place.

As discussed so far, the terminal fluorene moieties are flipped and are not stacked in

samples of **1**. The terminal-flipped conformation explains the monomeric fluorene emission from **1** (n = 2 and n = 3). However, the sample of **1** with $n \geq 4$ showed only the dimer emission. This suggests that the energy transfer from the terminal, flipped fluorene moieties to dimer forming, in-chain stacked fluorene moieties quenches monomeric fluorene in the longer oligomers of **1**. The predominant dimer emission from all **2** samples is consistent with the fact that all oligomers of **2** have a π-stacked structure throughout the chain.

The emission wavelength of the dimer emission of **1** and **2** was slightly red-shifted as compared with that of the fluorene excimer[36] and the excited side-chain dimer in poly(2-vinylfluorene),[37] which may mean that the arrangement of two fluorene molecules in the excimer is different from that of two fluorene units in the oligomers. As can be seen in the crystal structure, the side-chain fluorene moieties are so densely packed along the chain that the main chain bonds into a slightly arched shape. Such a close packing of two fluorene units probably enhances the electronic interaction between stacked π-electrons and, hence, reduces the delocalized excited energy level.

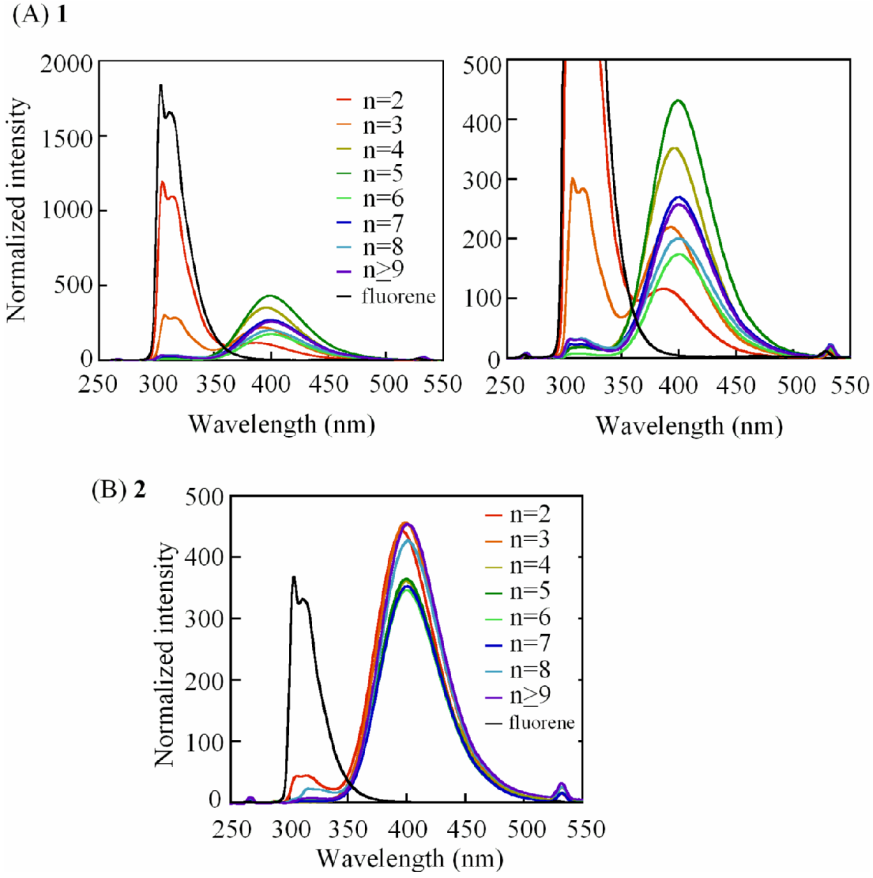

Figure 1.13 Emission spectra of oligo(DBF)s **1** (A), **2** (B), and fluorene in THF at room temperature (λ_{ex} = 267 nm). Intensity was normalized to a constant absorbance at 267 nm.

It is noteworthy that the emission profile of oligomer **1** (n = 2) is in sharp contrast to what is expected from "Hirayama's rule"[38], which predicts that a molecular array with two chromophores connected through three CH_2 groups favors excimer formation more than others with more or less CH_2 groups between the chromophores. Although in the structure of **1** (n = 2), two fluorenes are connected through three carbons, this oligomer showed only monomer emission. The conformational dynamics of this sample seem to be slower than those of the compounds tested by Hirayama that form a stacked excimer before emission.

1.8 Electrochemical Profiles

Stacked π-electron systems may facilitate charge delocalization. To obtain information on how the stacked fluorene units may affect the electronic properties, cyclic voltammetry measurements were performed for oligomers **2**. The samples showed clear oxidation peaks around 1.5–1.7 V but no clear corresponding reduction peak in the reverse scans from 2 to 0 V (Figure 1.14). In addition, the intensity of the oxidation peak gradually decreased in repeated runs, although the peak position was unchanged. These results suggest that the oxidized species may undergo some irreversible reaction on the electrode surface.

Figure 1.15 shows the dependence of oxidation potential ($E_{p/2}$) on the chain length. The oxidation potential decreased with chain length and was almost constant when an oligomer contains ca. five or more fluorene units. This may mean that a hole is stabilized by delocalization over as many as ca. five stacked fluorene units. This critical number of fluorene units coincides with those for the changes in the absorption intensity and edge wavelength depending on the chain length. As discussed in the preceding section, this may be ascribed to the proposed dynamic "persistence length" of a uniformly π-stacked sequence consisting of five fluorene units or to the nature of charge delocalization through the π-stacked structure of poly(DBF) which may inherently be limited to five fluorene units even if the chain has a longer, uniform "frozen" π-stacked structure. A lowtemperature or solid-state study minimizing thermal vibration may give an answer.

Figure 1.16 shows the plots of $E_{p/2}$ against $1/n$. Extrapolation of the plots suggests that an infinite chain ($1/n = 0$) would show a half-wave oxidation potential of 1.44 V (vs. Ag/AgCl).

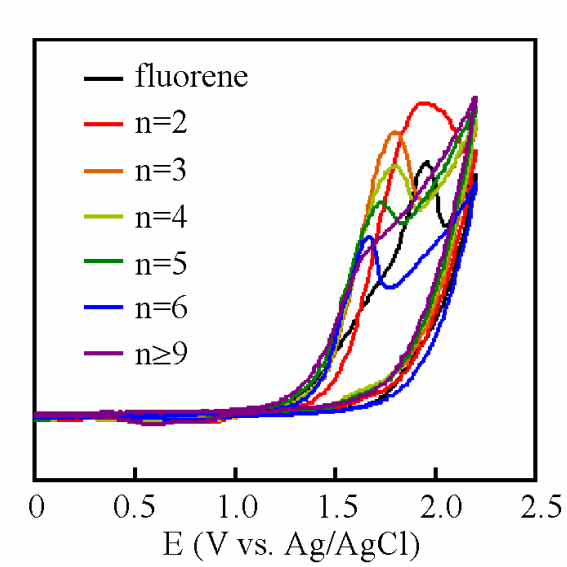

Figure 2.14 Cyclic voltammograms of oligo(DBF)s (**2**) and fluorene.

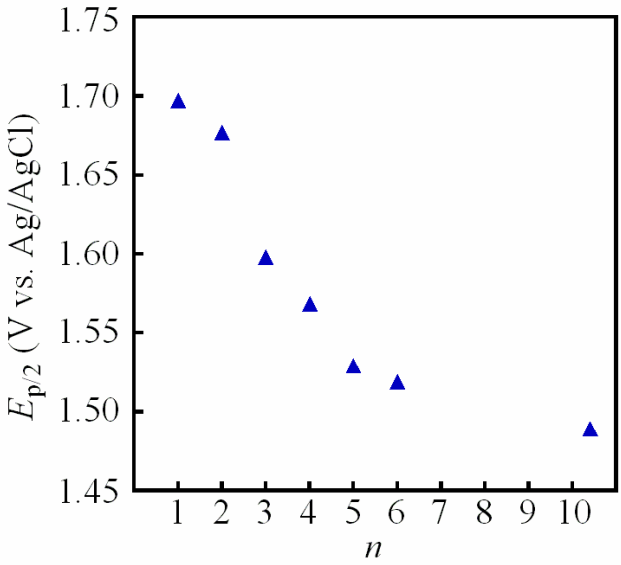

Figure 2.15 Half wave potential versus *n* plot for **2**. Data at *n* = 1 are for fluorene, and those at *n* = 10.4 are for a polymer (M_n = 1890 (vs oligo(DBF)), *n* = 10.4).

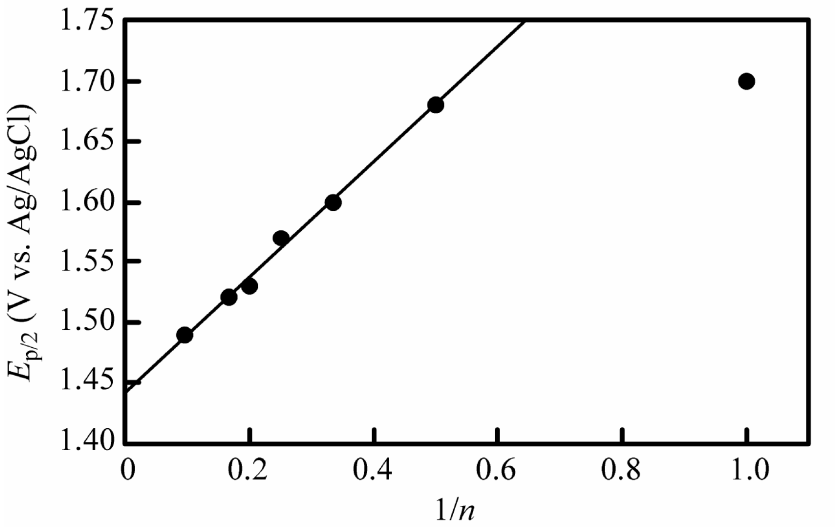

Figure 1.16 Half wave potential-vs.-1/n plots for the longest wavelength absorption maxima of oligo(DBF)s **2**. Extrapolation of the plot to 1/n = 0 gave 1.44 V vs. Ag/AgCl (1.40 V vs. SCE) for a polymer with an infinite number of fluorene moiety. Data at 1/n = 1 are for fluorene, and those at 1/n = 0.0962 are for a polymer (*Mn* = 1890 (vs. oligo(DBF)), n = 10.4).

1.9 Conclusions

DBF oligomers and polymers were proven to have π-stacked structures with the main-chain carbon–carbon bondings being almost all in the all-trans conformation not only in the solid state but also in solution. The conformation is expected to be fairly stable by the MD simulation and the NMR experiments at different temperatures. The π-stacked structure led to remarkable hypochromicity in absorption and exclusive dimer emission and facilitated charge delocalization. Among several macromolecules characterized by a π-stacked structure, a highly regular, long-range π-stacked structure of the side-chain chromophores has been achieved only for DNA so far. Poly(DBF) is the first vinyl polymer with precisely regulated π-stacked side groups. This polymer may be recognized as a new macromolecular structural motif that may be useful in photophysical and photoelectronic (e.g., molecular wire) applications.

1.10 Experimental Section

Materials

9-Fluorenylmethanol (Wako chemicals, >98%) and potassium tert-butoxide (Wako, 85%) were used as obtained. Fluorene (Wako, >95%) was recrystallized from hexane (mp 117.9 – 118.3°C). *n*-Butyllithium (*n*-BuLi) (Nacalai, 1.6 M), methyllithium (MeLi) (Kanto chemical, 1.1 M, a diethyl ether solution), and phenyllithium (PhLi) (Kanto, 1.0 M, a cyclohexane-diethyl ether solution) were used as obtained. Iodoethane (Wako, >98%) and benzyl bromide (Wako, >98%) were dried over CaH_2 and distilled immediately before use. Tetrahydrofuran (THF) (Wako) was refluxed over sodium benzophenone ketyl, distilled and stored on $LiAlH_4$ under N_2 atmosphere, and distilled under vacuum immediately before use.

Synthesis of DBF

DBF was synthesized according to the literatures[13] with modifications. 9-Fluorenylmethanol (10.7 g, 54.5 mmol) dissolved in methanol (70 mL) was mixed with a solution of potassium *tert*-butoxide (8.67 g, 77.3 mmol) in methanol (40 mL). The solution was stirred at 60°C for 20 min. The organics were extracted with a hexane-water mixture, and the hexane layer was washed with water until the wash water was neutral. Polymeric impurities were removed from the hexane layer by filtration using Celite. Removal of solvent gave colourless crystals: 8.23 g (84.9%). The monomer (purity 98.4% by ^{1}H NMR) was stored as a dry THF solution under N_2 in the dark at -20°C.

Preparation of 9-Fluorenyllithium (9-FlLi)

The reaction was carried out in a glass ampule sealed with a glass-made three-way stopcock attached to the ampule via a ground joint. The joint was completely sealed with high-vacuum grease. The ampule was flame-dried under high vacuum and flushed with N_2 immediately before use. Fluorene (838 mg, 5.00 mmol) was placed in the glass ampule, dried under high vacuum for 10 min, and purged with N_2. THF (6.0 mL) was introduced using a syringe to dissolve the fluorene. *n*-BuLi (1.6 M hexane solution, 3.1 mL, 5.0 mmol) was added to the solution at room temperature. The resulting deep-orange 9-FlLi solution (0.50 M) was used as an initiator after standing for 10 min at room temperature.

Synthesis of Oligomers

The glassware setup was the same as that for the 9-FlLi synthesis. A typical procedure is described for run 6 in Table 2.1. A THF solution of DBF (0.672 M THF solution, 14.9 mL, 10.0 mmol) and dry THF (33.1 mL) were introduced to the ampule with a syringe. The polymerization was initiated by adding the MeLi solution (1.8 mL, 2.0 mmol) to the monomer solution cooled at –78°C. After 48 h of reaction, the monomer conversion ratio was monitored by ^{1}H NMR analysis of an aliquot (ca. 0.1 mL) of the reaction mixture dissolved in $CDCl_3$ (0.6 mL). Monomer conversion was found to be 84% based on the intensity of the olefinic proton signal (s, 6.0 ppm) using the solvent signal (m, 3.7 ppm) as an internal reference. Iodoethane (2.0 ml, 25 mmol) was added to the reaction mixture. The reaction mixture was fractionated into THF-soluble and –insoluble parts with a centrifuge. Removal of the solvent from the THF-soluble parts afforded the DBF oligomers (1.42 g, yield 74.7 %) as a pale yellow solid.

Measurements

The ^{1}H NMR spectra were recorded on a JEOL JNM-ECP600NK or JEOL ECP500 spectrometer (600 and 500 MHz, respectively, for ^{1}H measurement).

Analytical scale SEC was carried out using a chromatographic system consisting of a JASCO PU-980 chromatographic pump, a JASCO UV-975 UV detector (254 nm), and a JASCO RI-930 RI detector equipped with two PL-Oligopore columns (30 × 0.72(i.d.) cm) (Polymer Laboratories) connected in series. Preparative SEC separation of oligomers was performed using a JAI LC-908 preparative recycle chromatograph equipped with JAIGEL-1H and JAIGEL-2H columns connected in series.

MALDI-mass spectra were taken on a Voyager DE-STR spectrometer equipped with a N_2

laser (337 nm, 3 ns pulse duration, frequency up to 20 Hz) under vacuum (sample chamber pressure 5.5 × 10^{-7} Torr) using the reflector mode (acceleration voltage 20 000 V). The excitation laser power was set to 3000. Samples were prepared by mixing a $CHCl_3$ solution of polymer (concentration 10 mg/mL, 1 μL), a $CHCl_3$ solution of dithranol (concentration 10 mg/mL, 20 μL), and a methanol solution of silver trifluoroacetate (concentration 0.1 mg/mL, 1 μL) and drying the mixed solution in a sample well on a gold-plated sample slide under air flow.

Single crystal X-ray data were collected at room temperature on a Rigaku R-AXIS RAPID Imaging Plate diffractometer using Mo-Kα radiation (λ = 0.71073 Å) monochromated by graphite. All calculations were performed using the teXsan software package (version 1.10b).

Absorption and emission spectra were measured at room temperature in a 1-cm quartz cell with a JASCO V-550 spectrophotometer and a JASCO FP-777W fluorescence spectrophotometer, respectively. Samples in the THF solvent were degassed by N_2 bubbling for 10 min.

Cyclic voltammetry experiments were performed with a Hokuto-Denko HSV-100 electrochemical analyzer in a THF solution containing tetrabutylammonium perchlorate as a supporting electrolyte (0.1 M) under N_2 flow. Sample solutions were degassed by N_2 bubbling for 10 min prior to the measurement. All measurements were carried out at room temperature with a conventional three-electrode configuration consisting of a platinum working electrode, an auxiliary platinum electrode, and a Ag/AgCl reference electrode at a sweep rate of 100 mV/s. The half-wave potential ($E_{p/2}$) values were determined as the potential at the current that was half of diffusion limiting current.

Computer Simulation

A Monte Carlo conformational search was carried out using MacroModel 6.0 software (Schrödinger).[26] The relative arrangements of the fluorene moieties were fixed and the main-chain torsions were changed at an interval of 60° in generating initial geometries. Each conformer generated in the Monte Carlo process was fully minimized using MM3[23] or MMFF94s[24] force field until the RMS residue went below 0.05 kcal/mol/Å or 1000 iterations were achieved. Conformers most frequently found with in 15kJ/mol energy range from the global minimum were considered to be the most stable ones.

Molecular mechanics structure optimization was effected using the COMPASS[25] force field

implemented in the Discover module of the Material Studio 2.0 (Accelrys) software package with the Fletcher-Reeves[39] conjugate gradient algorithm until the RMS residue went below 0.01 kcal/mol/Å. Molecular dynamic simulation was performed under a constant NVT condition in which the numbers of atoms, volume, and thermodynamic temperature were held constant. Berendsen's thermocouple[27] was used for coupling to a thermal bath. The step time was 1 fs and the decay constant was 0.1 ps. Conformations obtained through MD simulation were saved in trajectory files at every 5 or 10 ps and were optimized by MM simulation.

^{1}H NMR chemical shift simulations by the DFT method[16] were performed using the DGauss software in the CaChe package (Fujitsu). The models were optimized with MOPAC (Fujitsu) software by the semi-empirical PM5[17] method prior to the NMR calculations. NMR simulation was carried out using B88[19] exchange and LYP[20] correlation functionals with a DZVP basis set. LORG approximation was applied for the shift simulation to avoid the gauge problem.

H-H COSY and NOESY Spectra

Conformation of oligo(DBF)s were assessed by the spectra with peak assignments are shown in Figure 1.17-1.44.

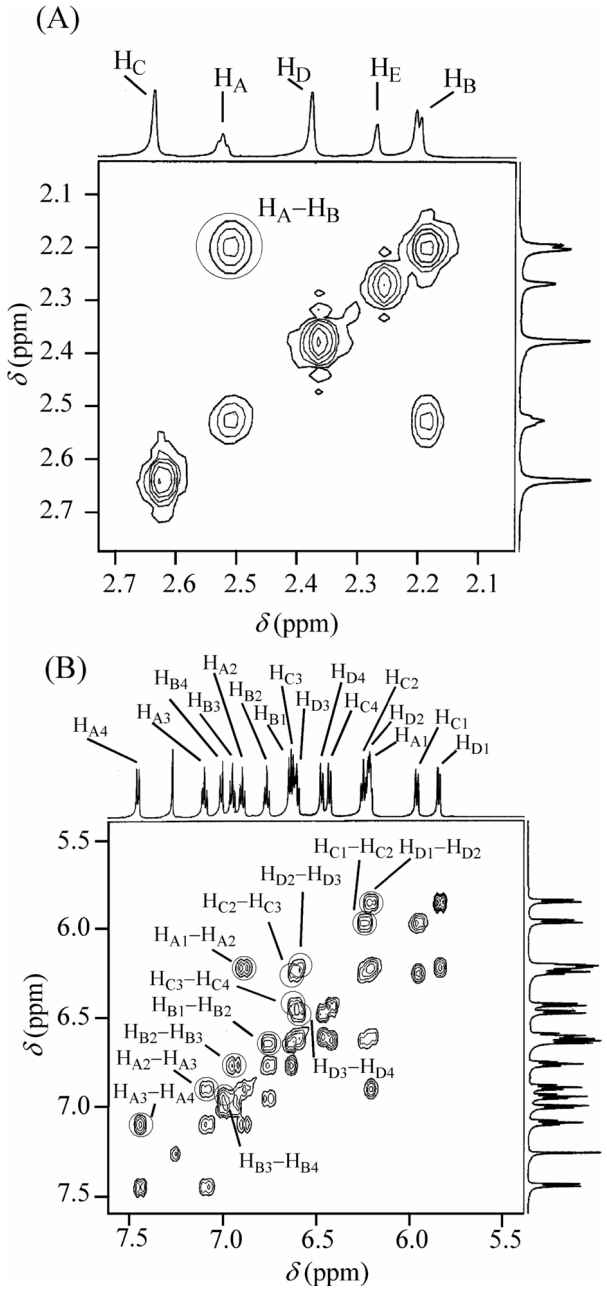

Figure 1.17 H-H COSY spectra of oligo(DBF) **1** (n = 8): alkyl region (A) and aromatic region (B) (500 MHz, $CDCl_3$, r.t.).

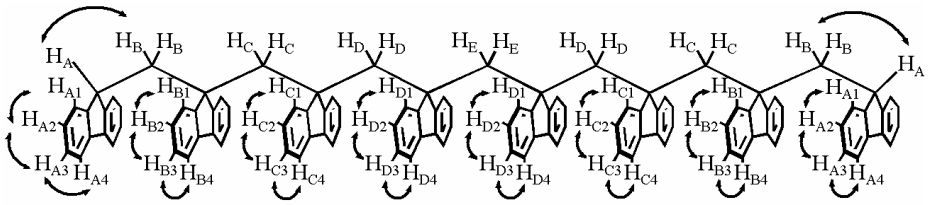

1 (n = 8)

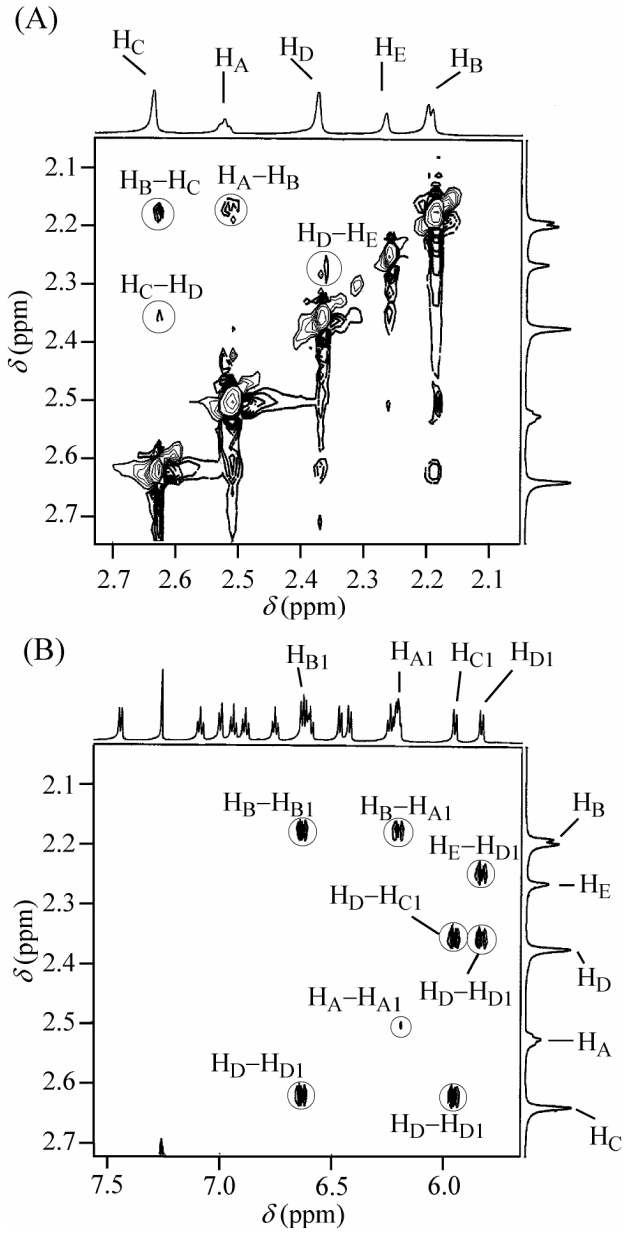

Figure 1.18 NOESY spectra of oligo(DBF) **1** (n = 8): alkyl-alkyl region (A) and alkyl-aromatic region (B) (500 MHz, $CDCl_3$, r.t.).

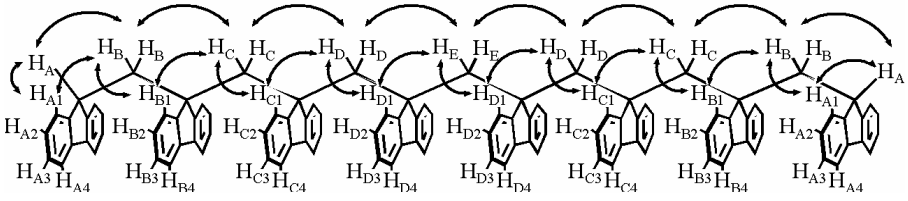

1 (n = 8)

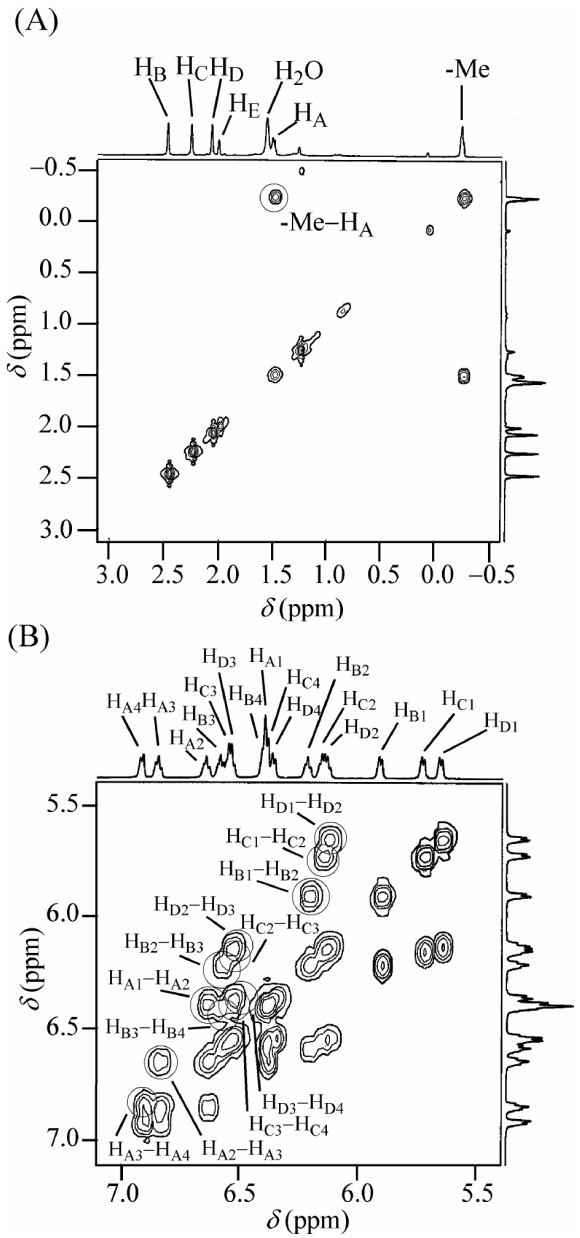

Figure 1.19 H-H COSY spectra of oligo(DBF) **2** (n = 8): alkyl region (A) and aromatic region (B) (500 MHz, $CDCl_3$, r.t.).

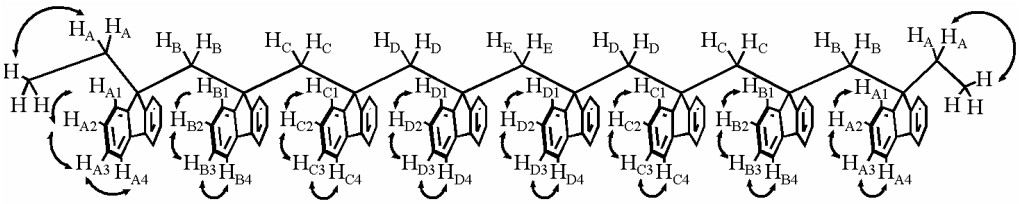

2 (n = 8)

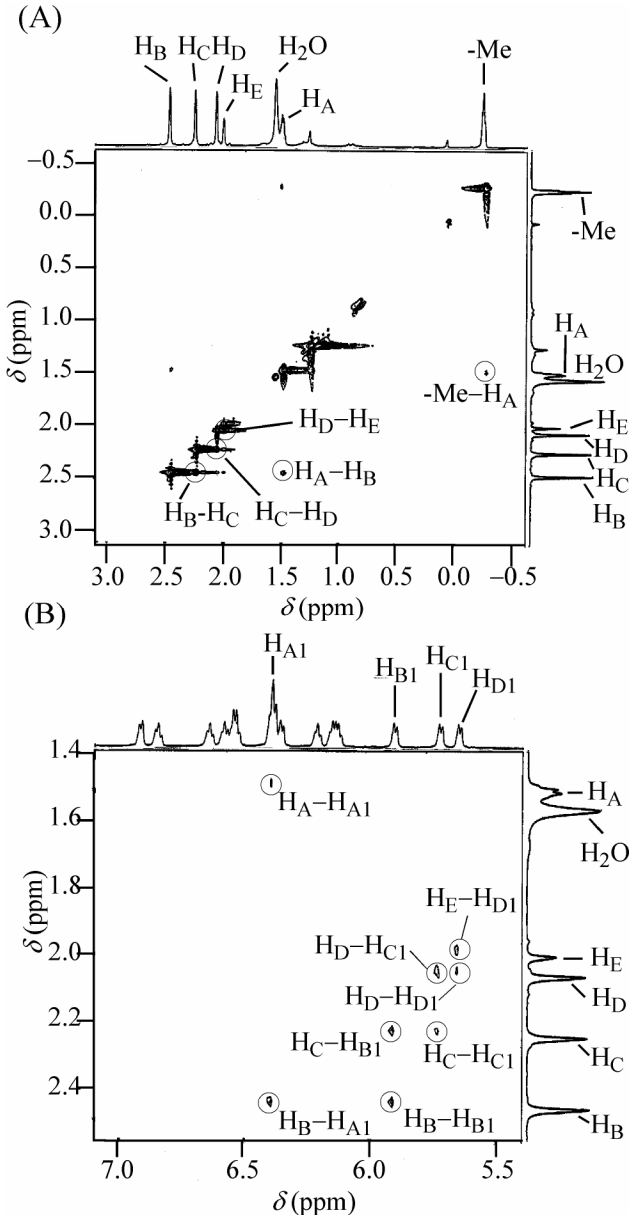

Figure 1.20 NOESY spectra of oligo(DBF) **2** (n = 8): alkyl-alkyl region (A) and alkyl-aromatic region (B) (500 MHz, $CDCl_3$, r.t.).

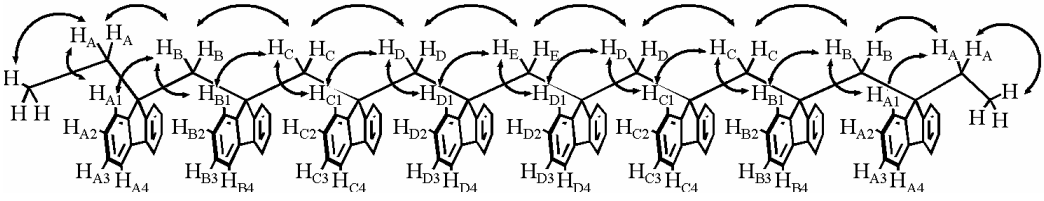

2 (n = 8)

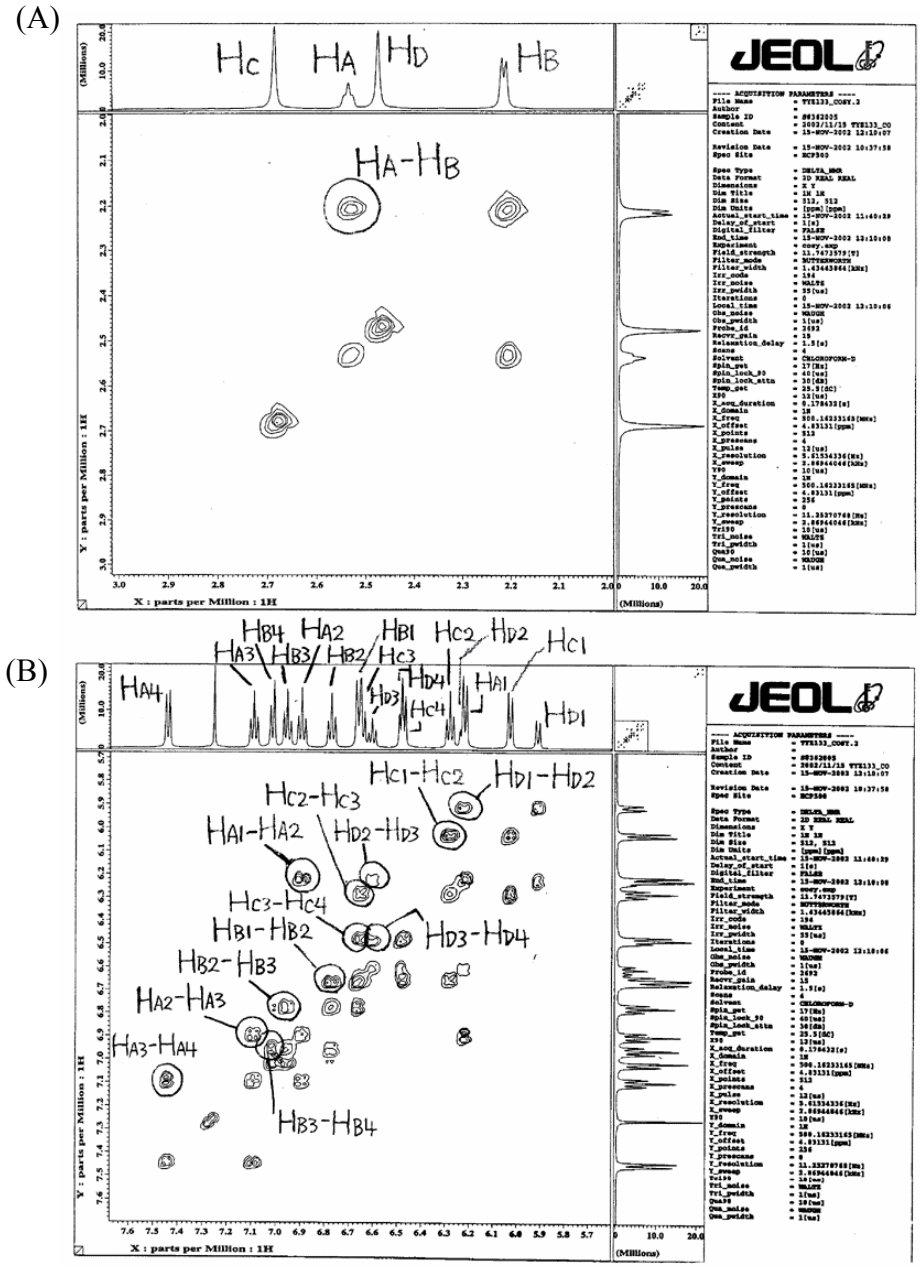

Figure 1.21 H-H COSY spectra of oligo(DBF) **1** (n = 7): alkyl region (A) and aromatic region (B) (500 MHz, $CDCl_3$, r.t.).

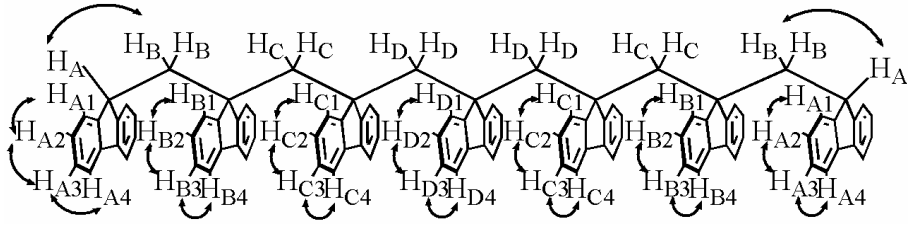

1 (n = 7)

(A)

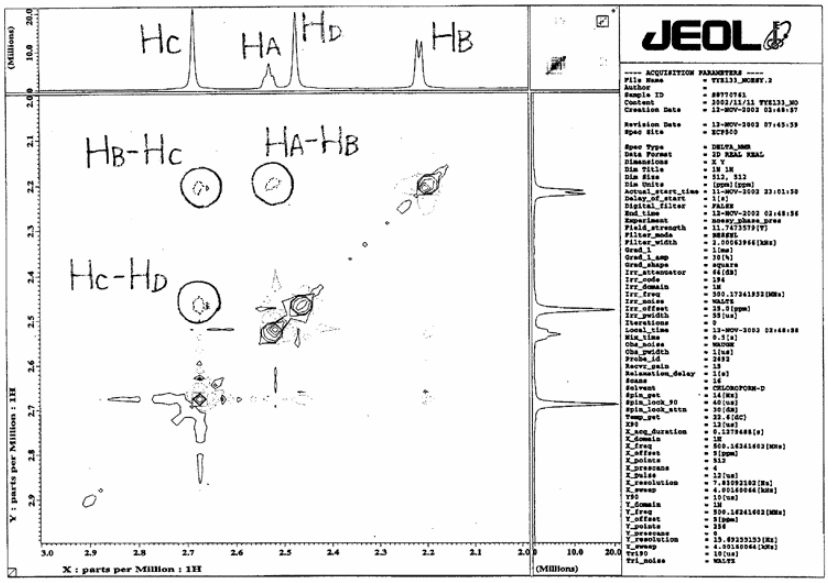

(B)

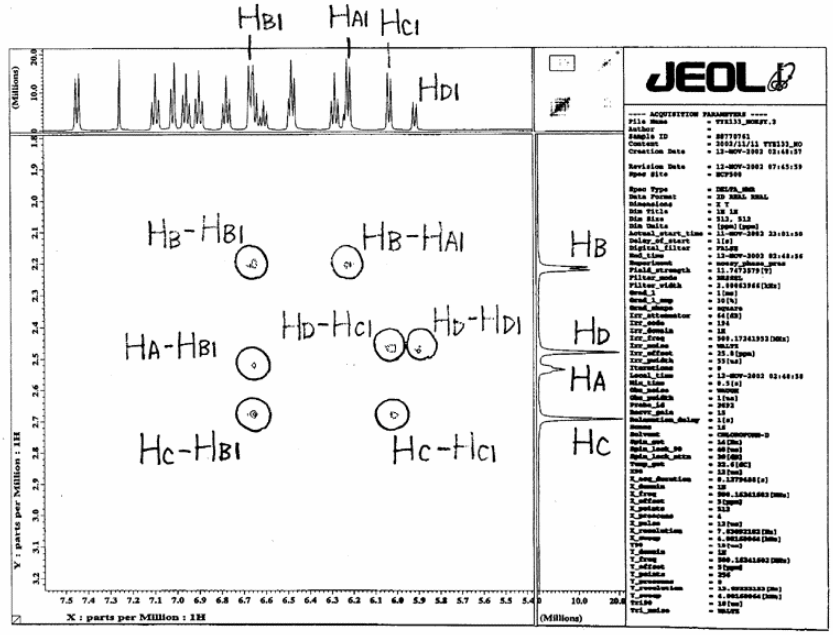

Figure 1.22 NOESY spectra of oligo(DBF) **1** (n = 7): alkyl-alkyl region (A) and alkyl-aromatic region (B) (500 MHz, $CDCl_3$, r.t.).

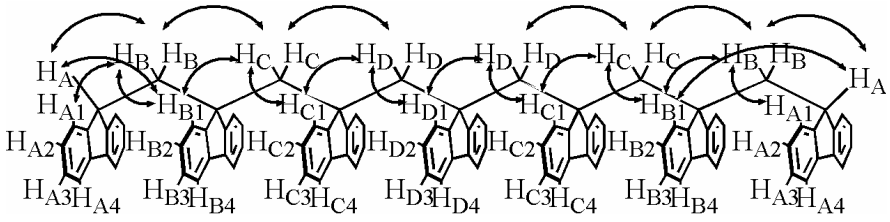

1 (n = 7)

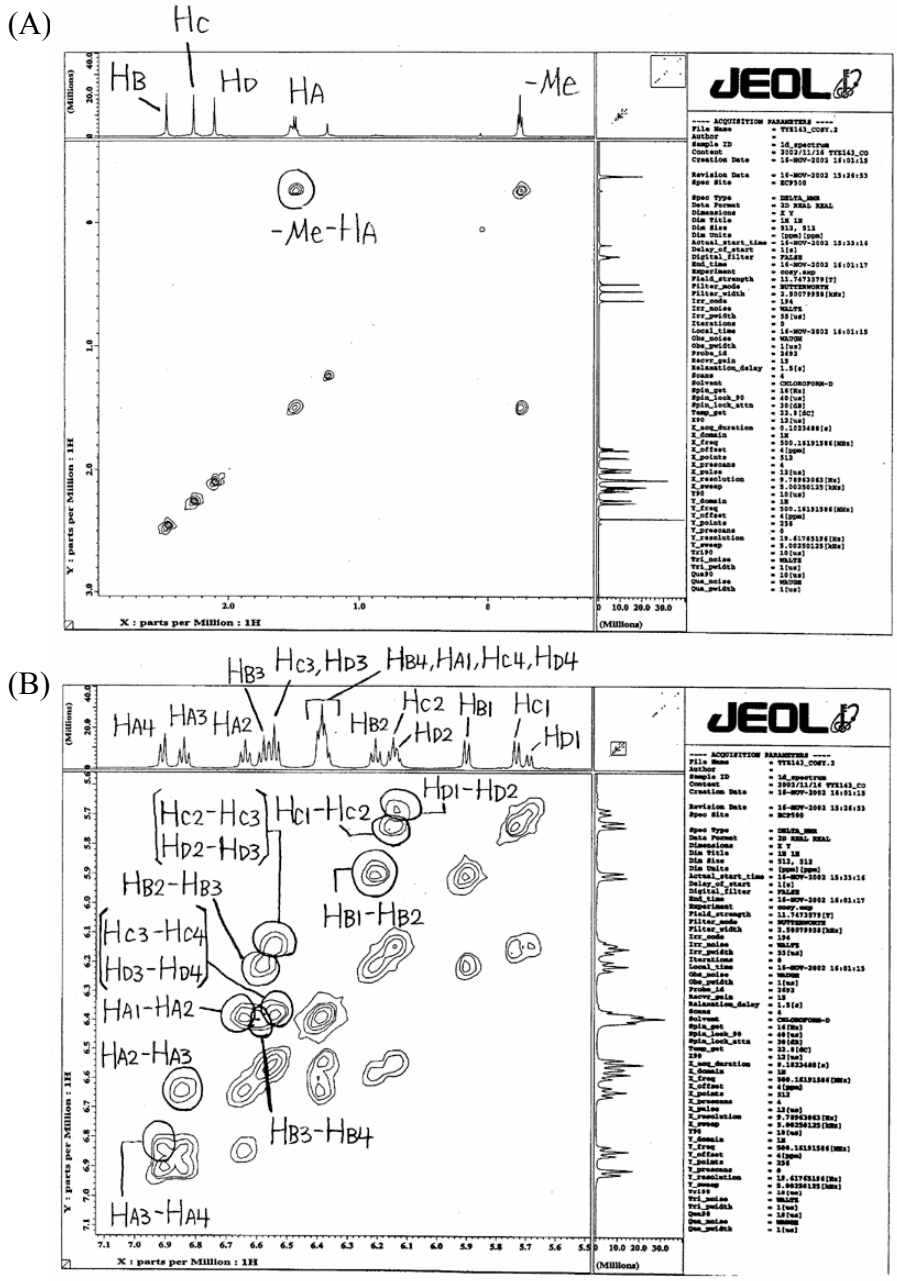

Figure 1.23 H-H COSY spectra of oligo(DBF) **2** (n = 7): alkyl region (A) and aromatic region (B) (500 MHz, $CDCl_3$, r.t.).

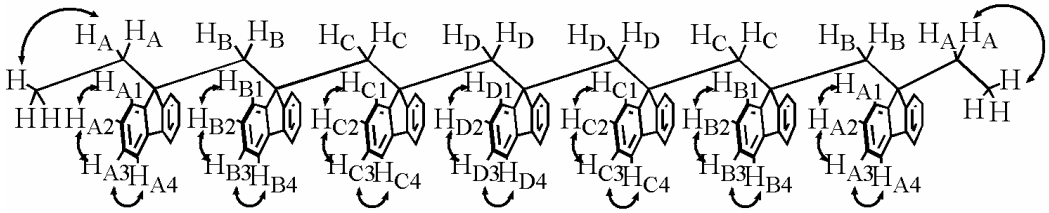

2 (n = 7)

(A)

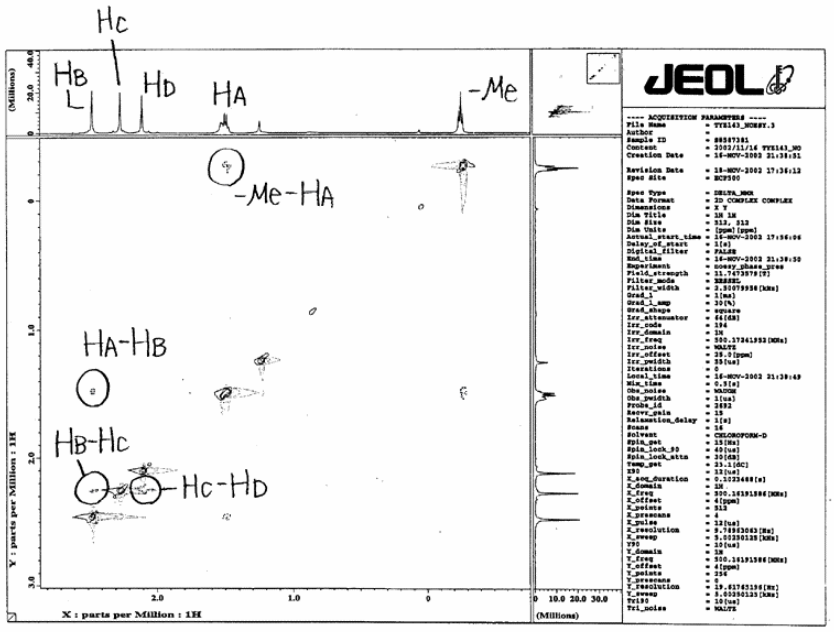

(B)

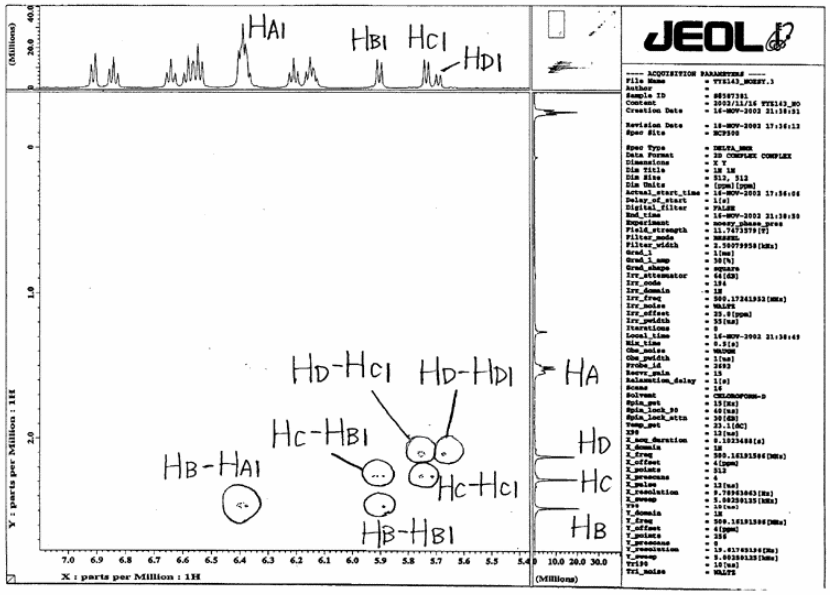

Figure 1.24 NOESY spectra of oligo(DBF) **2** (n = 7): alkyl-alkyl region (A) and alkyl-aromatic region (B) (500 MHz, $CDCl_3$, r.t.).

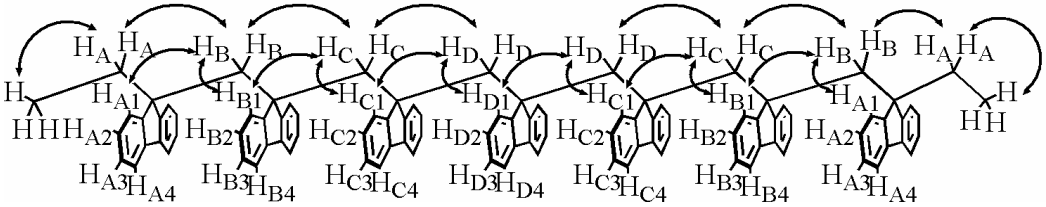

2 (n = 7)

(A)

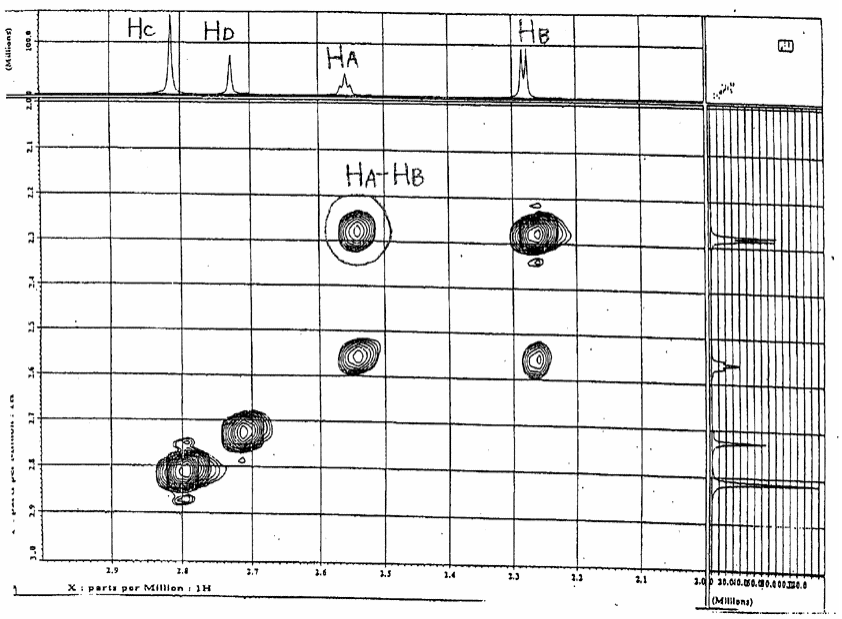

(B)

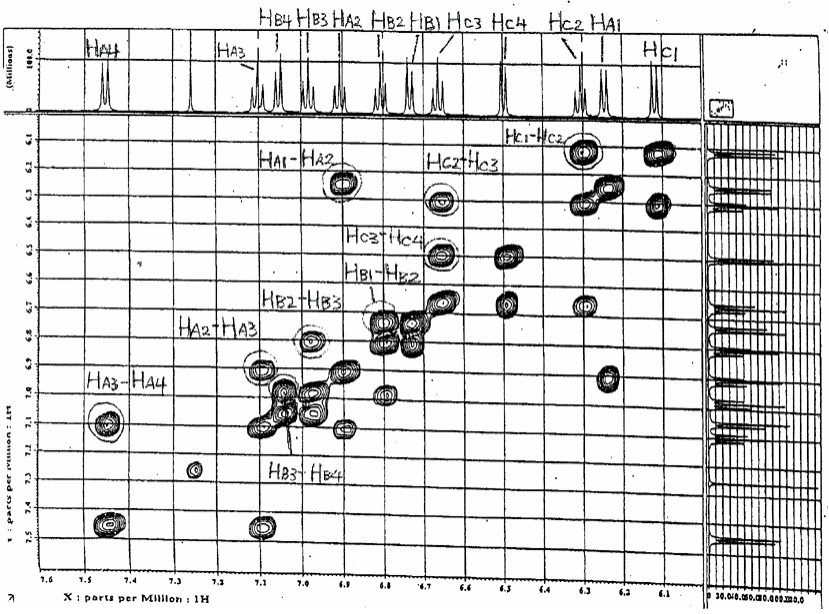

Figure 1.25 H-H COSY spectra of oligo(DBF) **1** (n = 6): alkyl region (A) and aromatic region (B) (600 MHz, $CDCl_3$, r.t.).

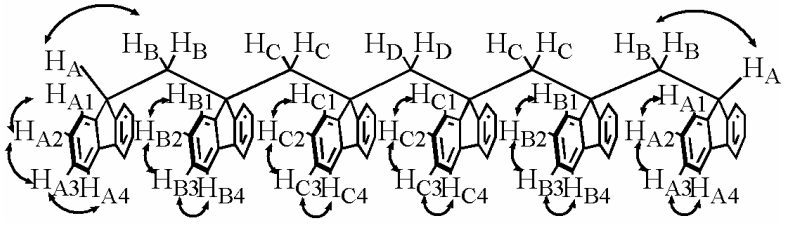

1 (n = 6)

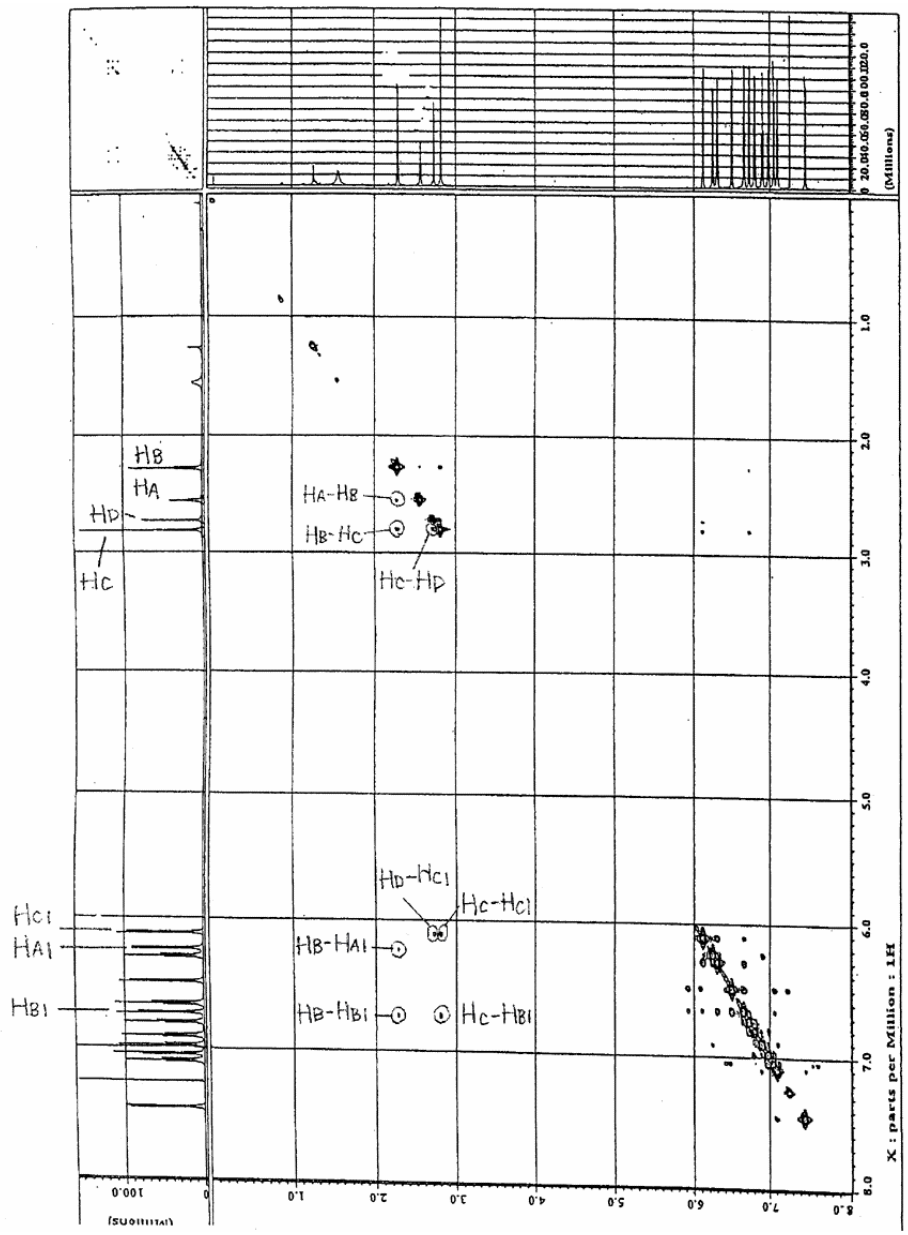

Figure 1.26 NOESY spectra of oligo(DBF) **1** (n = 6) (600 MHz, $CDCl_3$, r.t.).

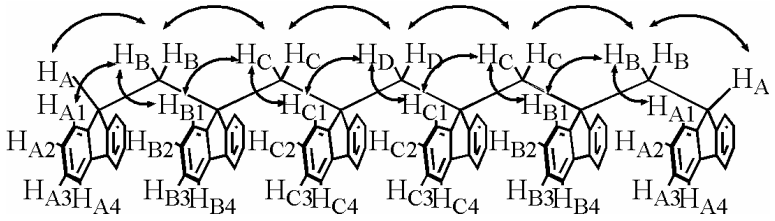

1 (n = 6)

(A)

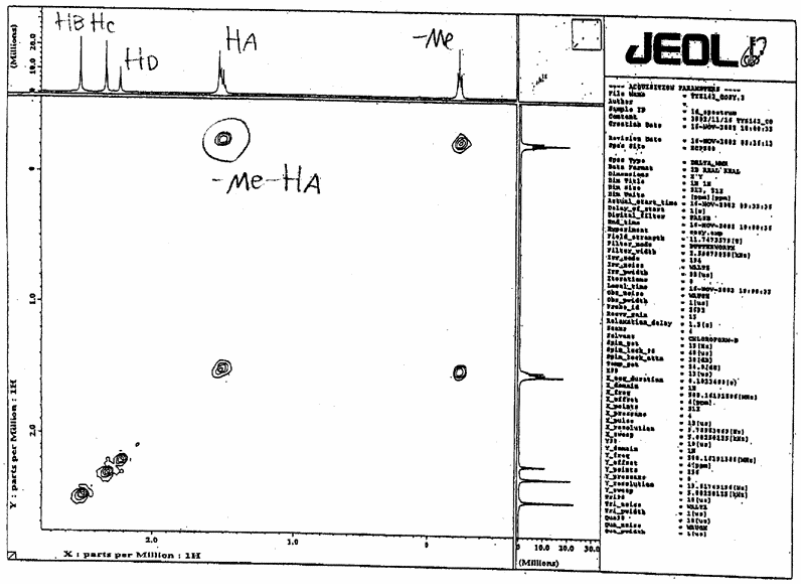

(B)

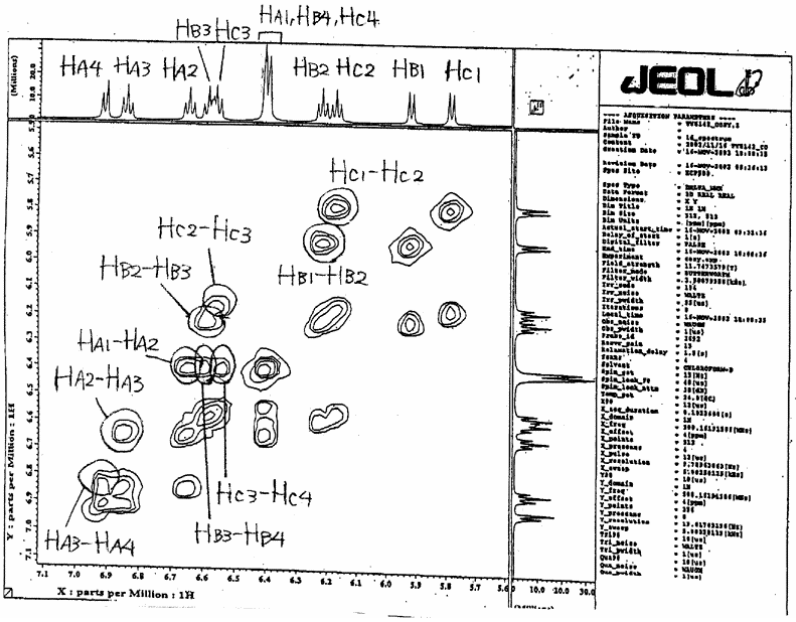

Figure 1.27 H-H COSY spectra of oligo(DBF) **2** (n = 6): alkyl region (A) and aromatic region (B) (500 MHz, $CDCl_3$, r.t.).

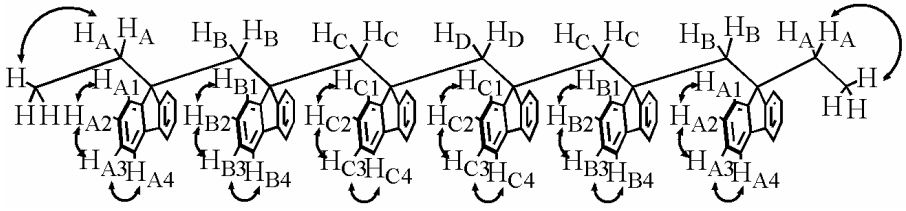

2 (n = 6)

(A)

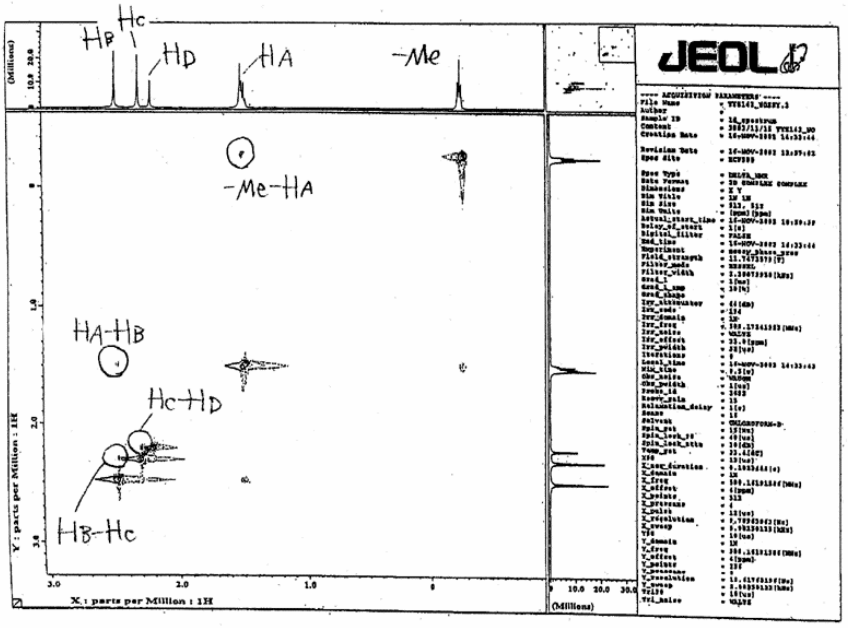

(B)

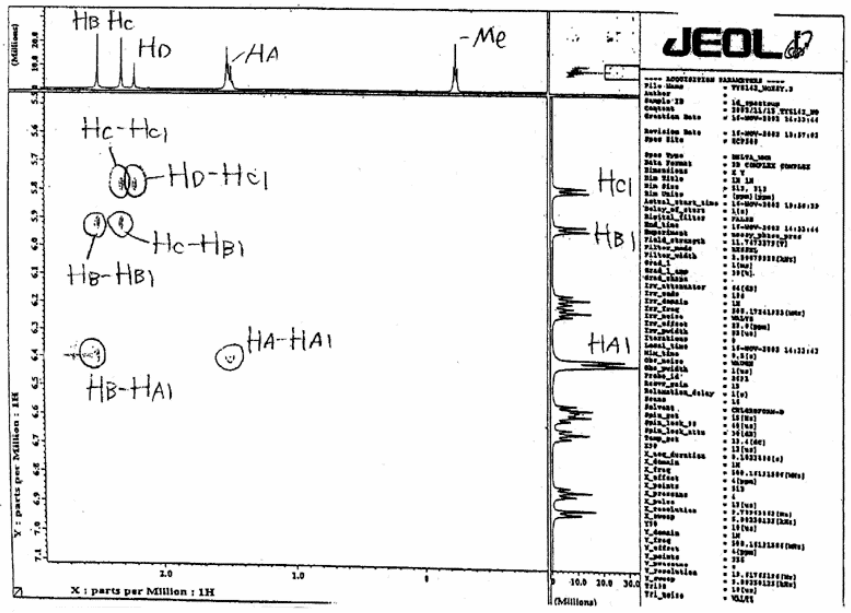

Figure 1.28 NOESY spectra of oligo(DBF) **2** (n = 6): alkyl-alkyl region (A) and alkyl-aromatic region (B) (500 MHz, $CDCl_3$, r.t.).

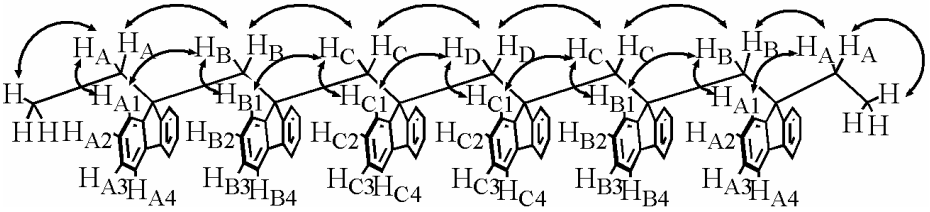

2 (n = 6)

(A)

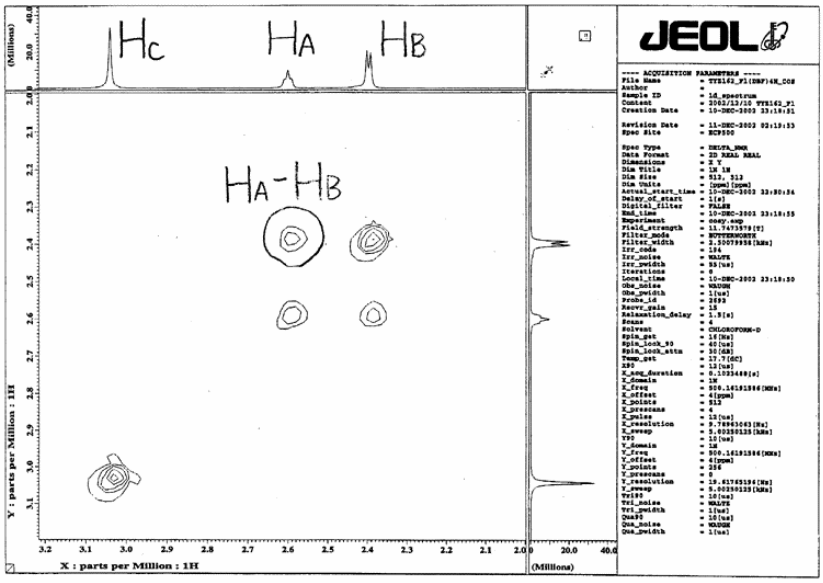

(B)

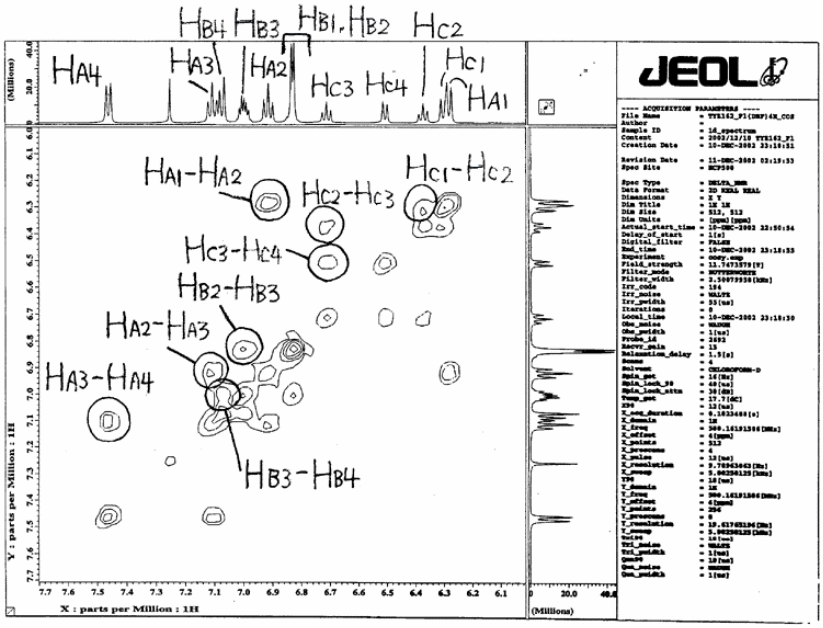

Figure 1.29 H-H COSY spectra of oligo(DBF) **1** (n = 5): alkyl region (A) and aromatic region (B) (500 MHz, $CDCl_3$, r.t.).

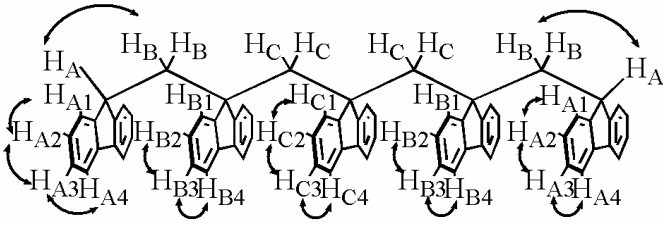

1 (n = 5)

(A)

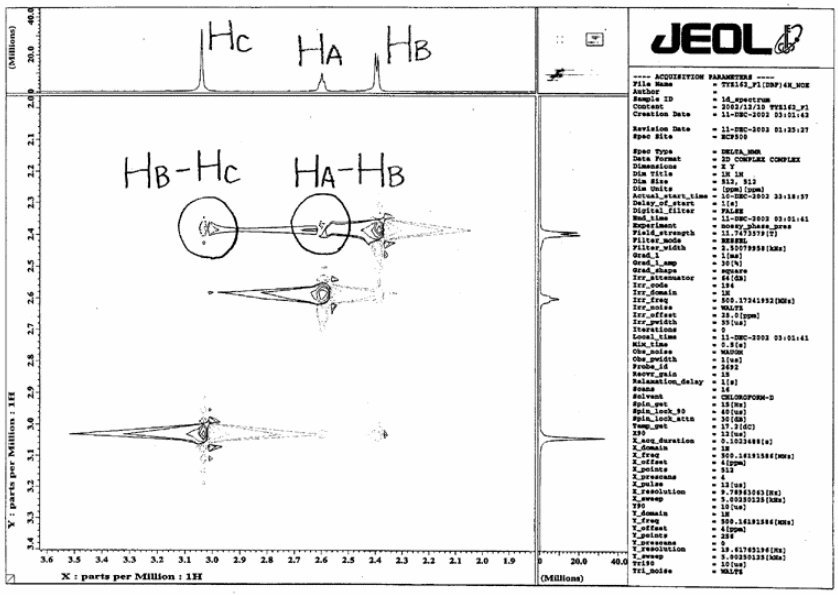

(B)

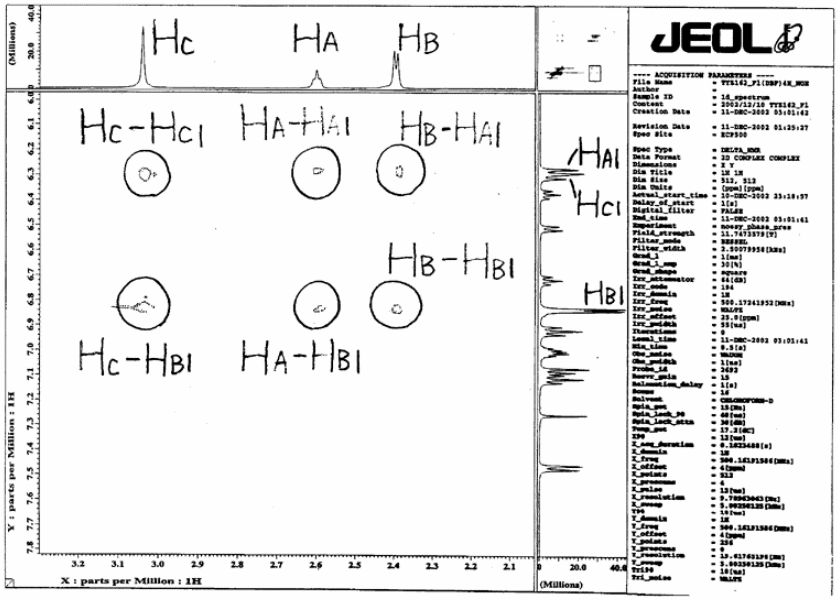

Figure 1.30 NOESY spectra of oligo(DBF) **1** (n = 5): alkyl-alkyl region (A) and alkyl-aromatic region (B) (500 MHz, $CDCl_3$, r.t.).

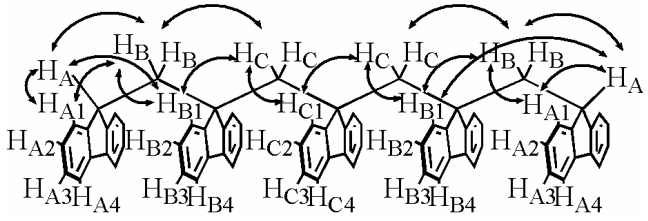

1 (n = 5)

(A)

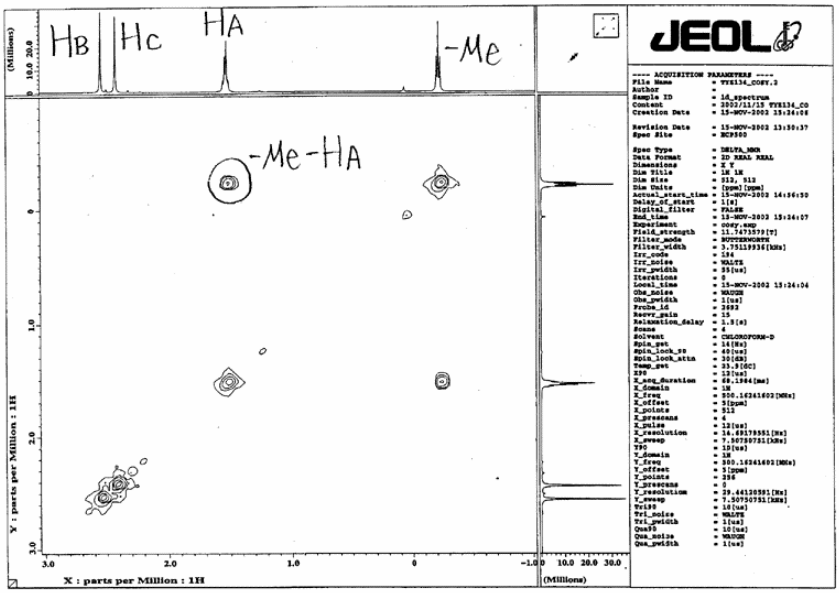

(B)

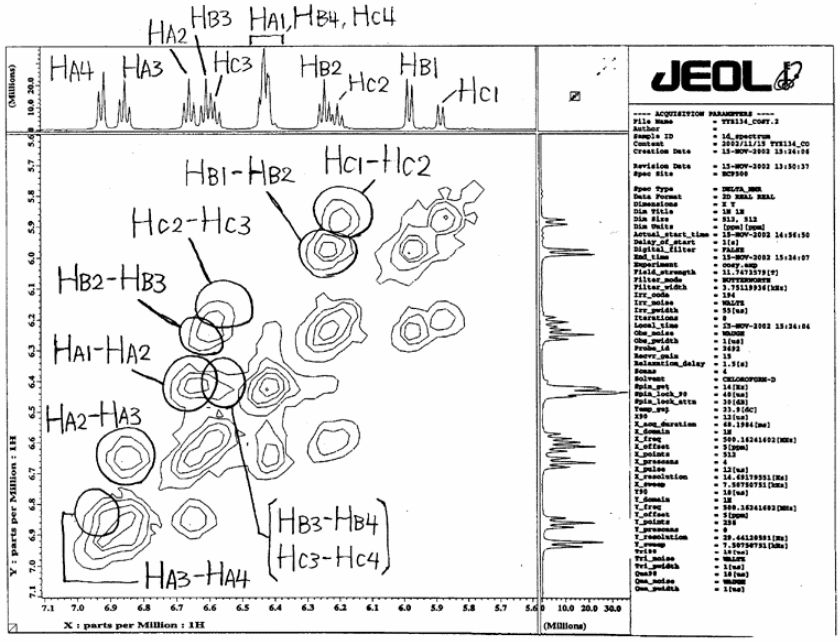

Figure 1.31 H-H COSY spectra of oligo(DBF) **2** (n = 5): alkyl region (A) and aromatic region (B) (500 MHz, $CDCl_3$, r.t.).

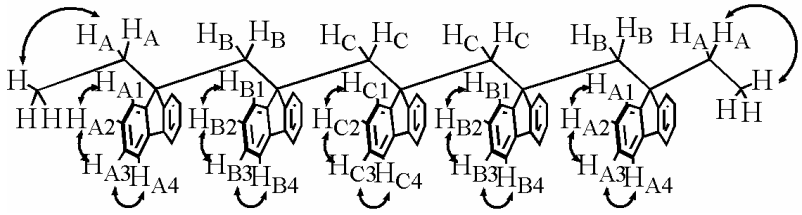

2 (n = 5)

(A)

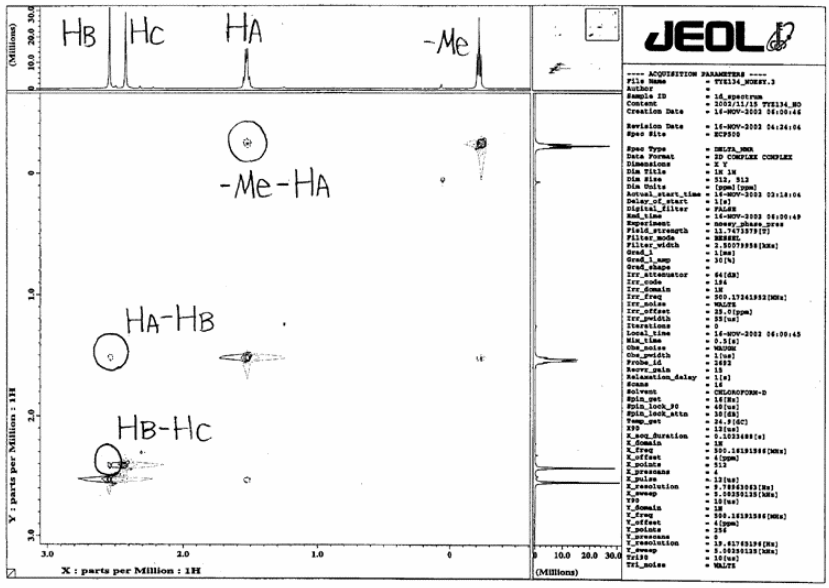

(B)

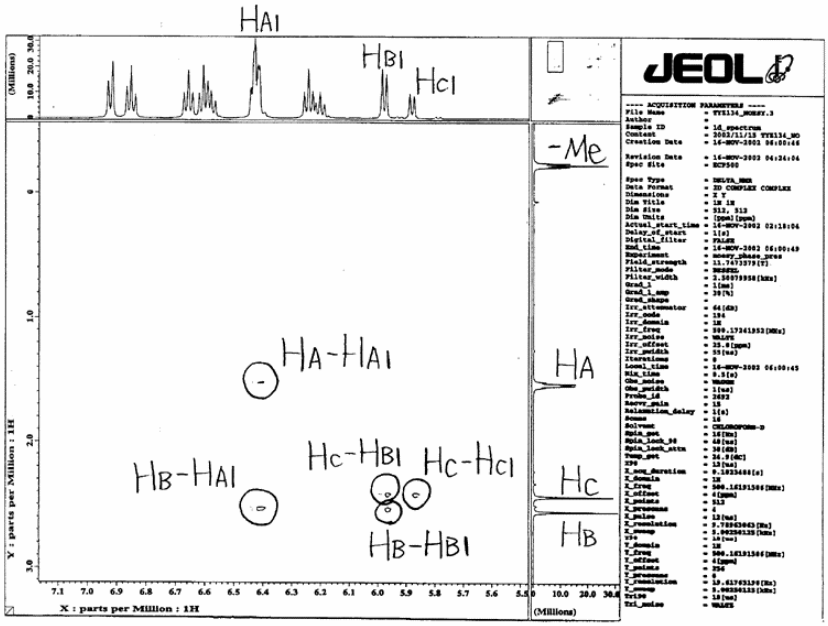

Figure 1.32 NOESY spectra of oligo(DBF) **2** (n = 5): alkyl-alkyl region (A) and alkyl-aromatic region (B) (500 MHz, $CDCl_3$, r.t.).

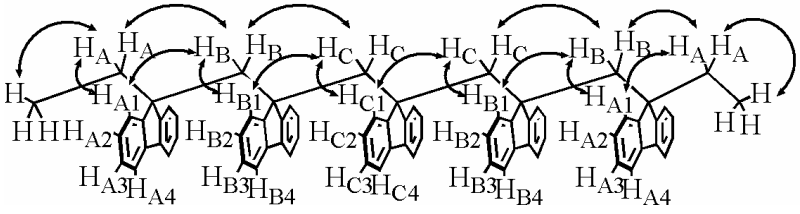

2 (n = 5)

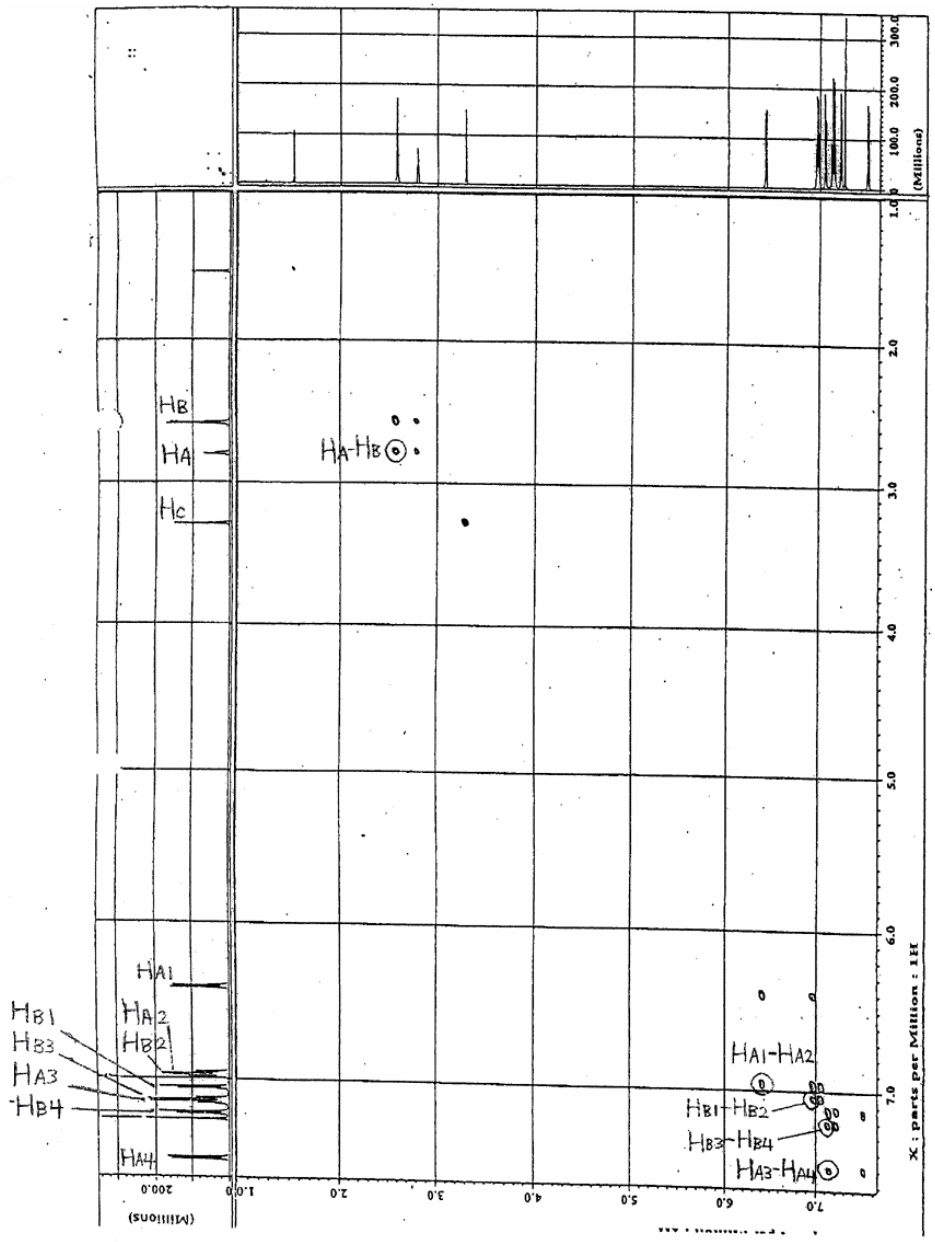

Figure 1.33 H-H COSY spectra of oligo(DBF) **1** (n = 4): alkyl region (A) and aromatic region (B) (600 MHz, $CDCl_3$, r.t.).

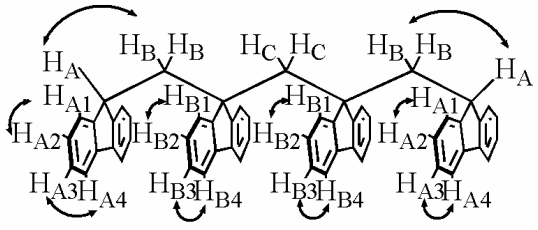

1 (n = 4)

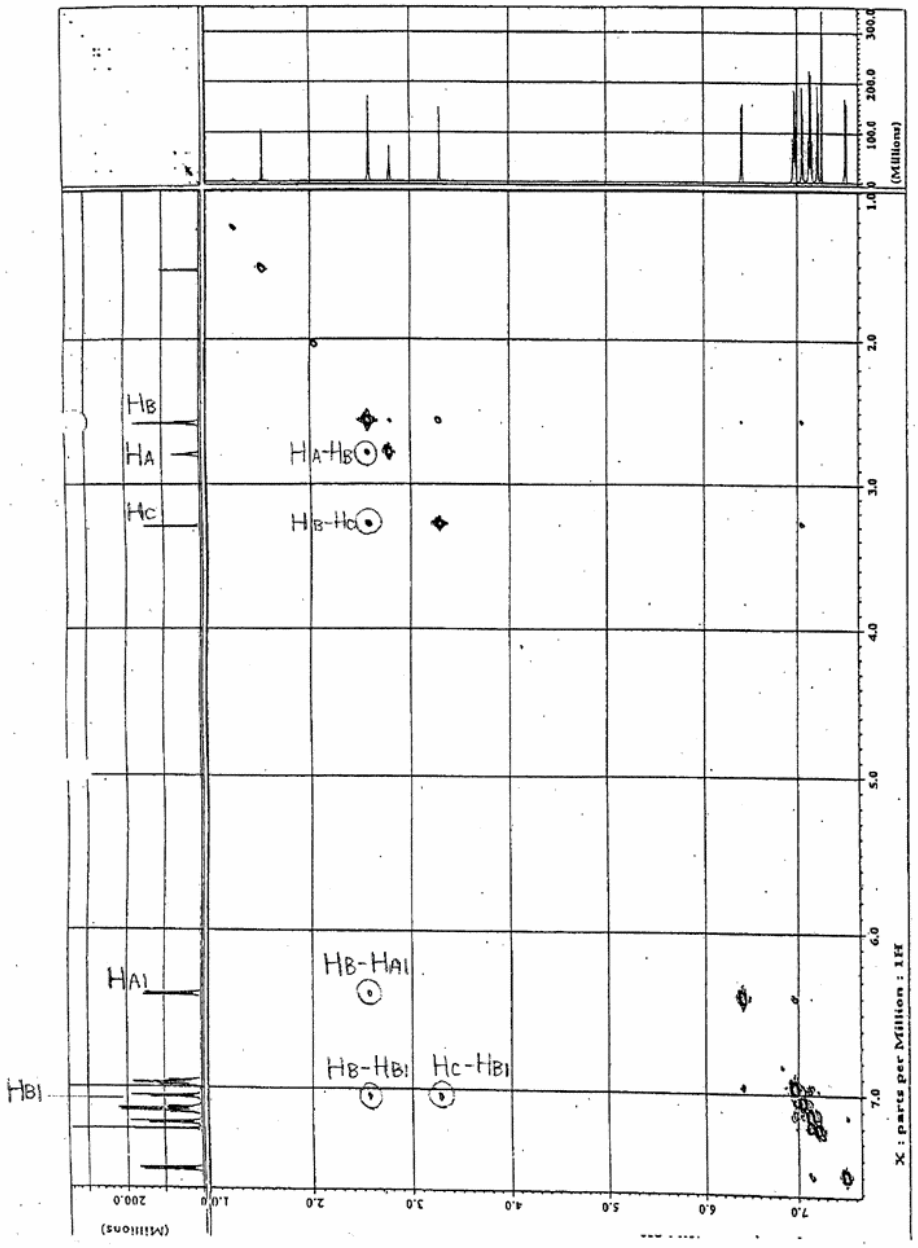

Figure 1.34 NOESY spectra of oligo(DBF) **1** (n = 4) (600 MHz, $CDCl_3$, r.t.).

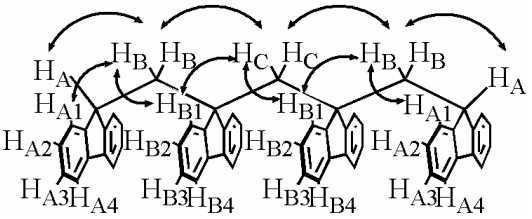

1 (n = 4)

(A)

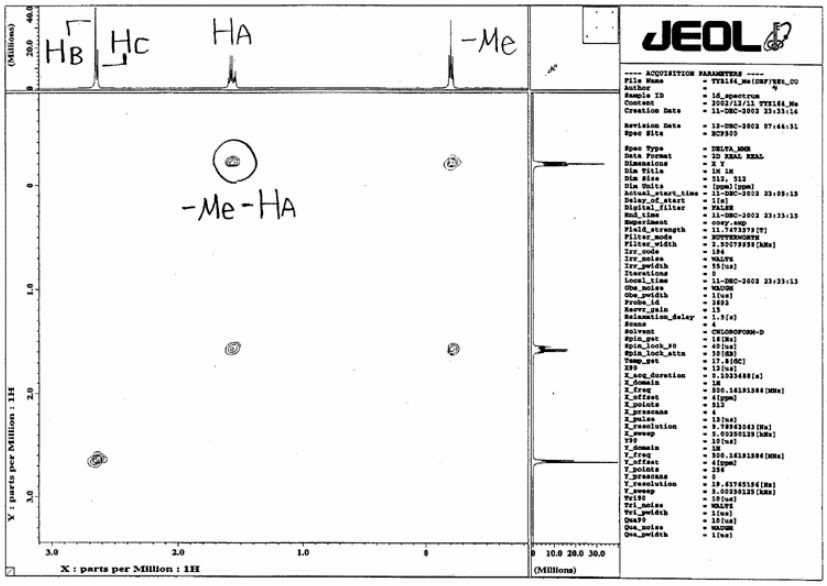

(B)

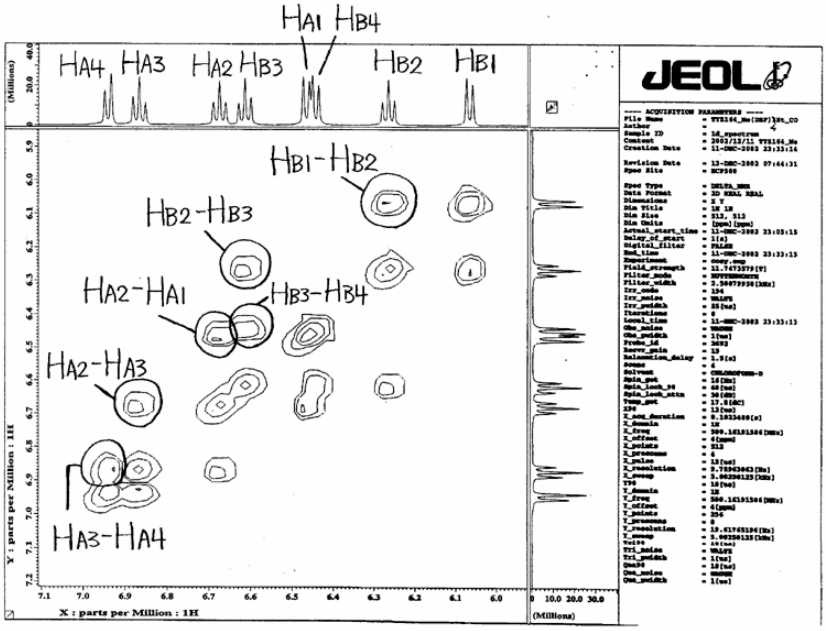

Figure 1.35 H-H COSY spectra of oligo(DBF) **2** (n = 4): alkyl region (A) and aromatic region (B) (500 MHz, $CDCl_3$, r.t.).

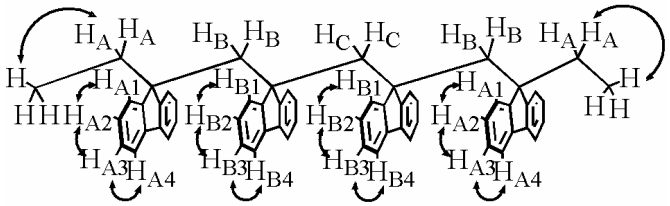

2 (n = 4)

(A)

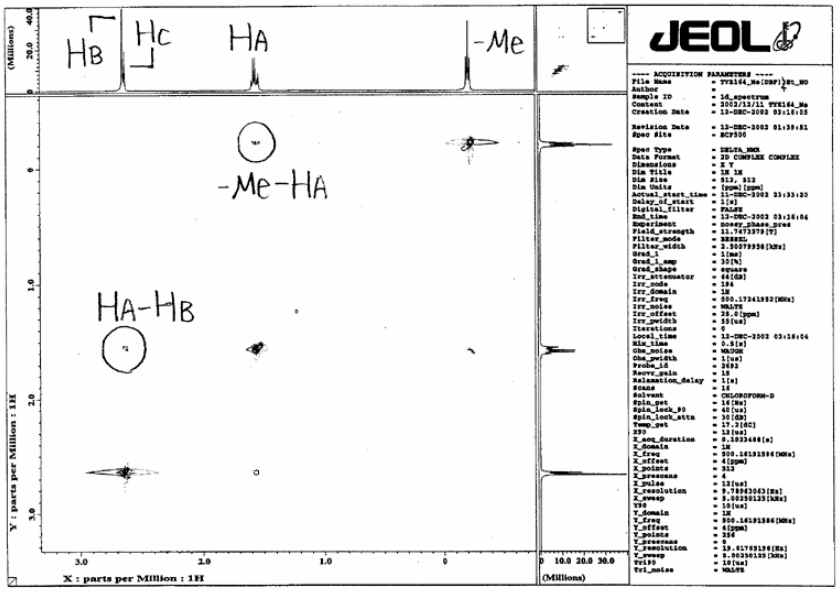

(B)

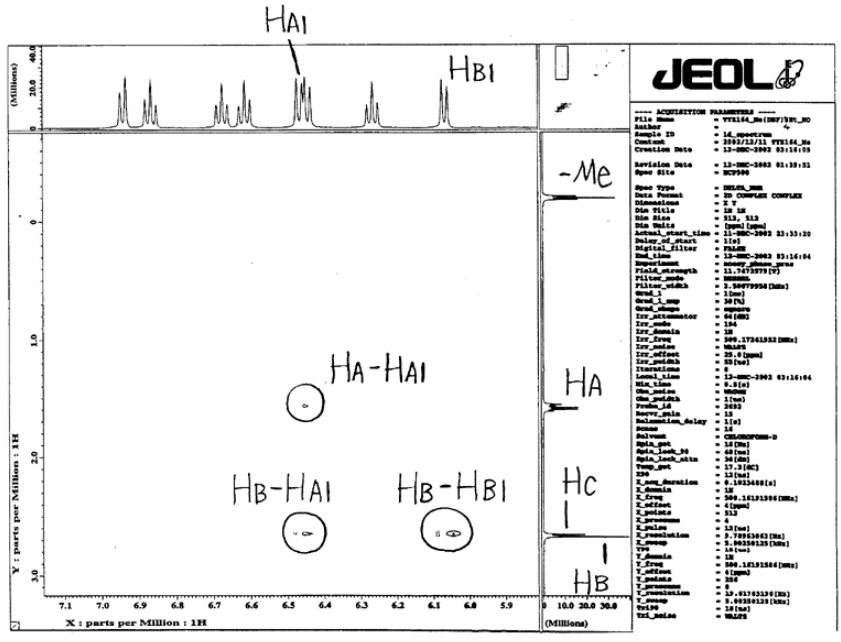

Figure 1.36 NOESY spectra of oligo(DBF) **2** (n = 4): alkyl-alkyl region (A) and alkyl-aromatic region (B) (500 MHz, $CDCl_3$, r.t.).

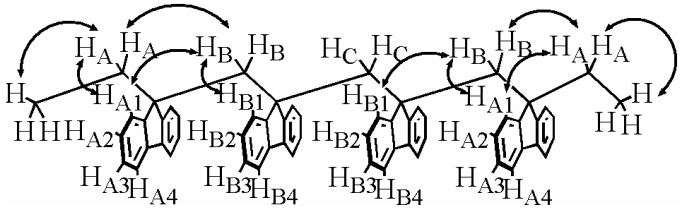

2 (n = 4)

(A)

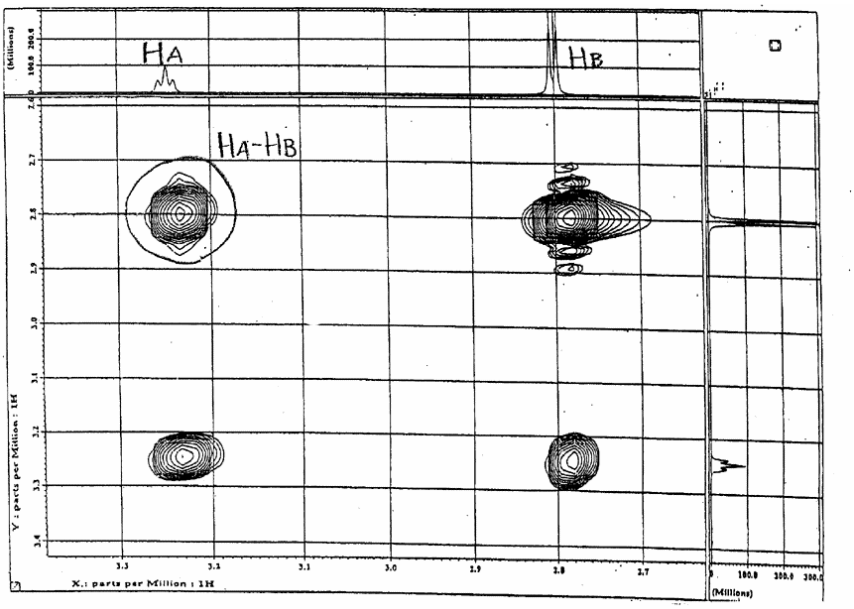

(B)

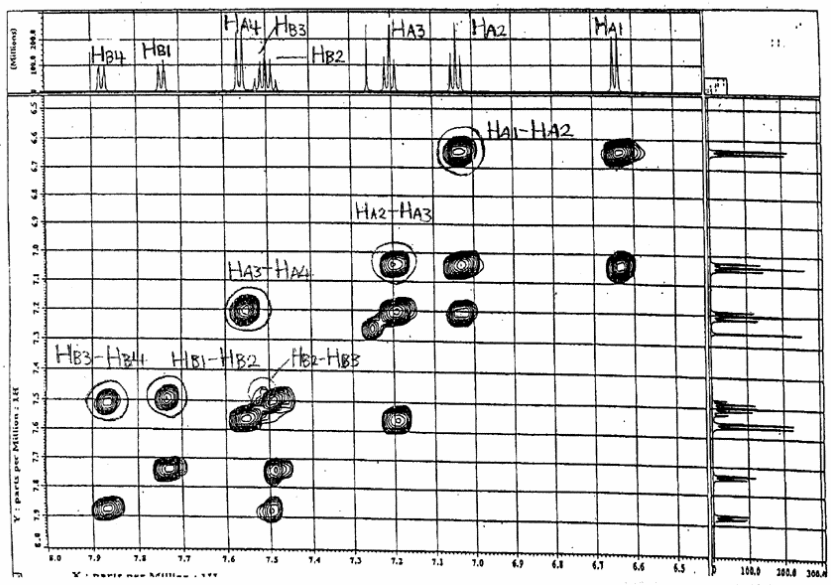

Figure 1.37 H-H COSY spectra of oligo(DBF) **1** (n = 3): alkyl region (A) and aromatic region (B) (600 MHz, $CDCl_3$, r.t.).

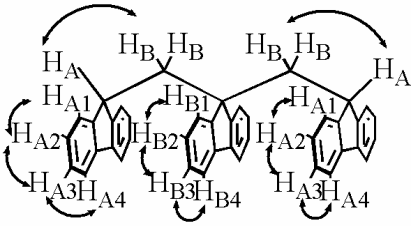

1 (n = 3)

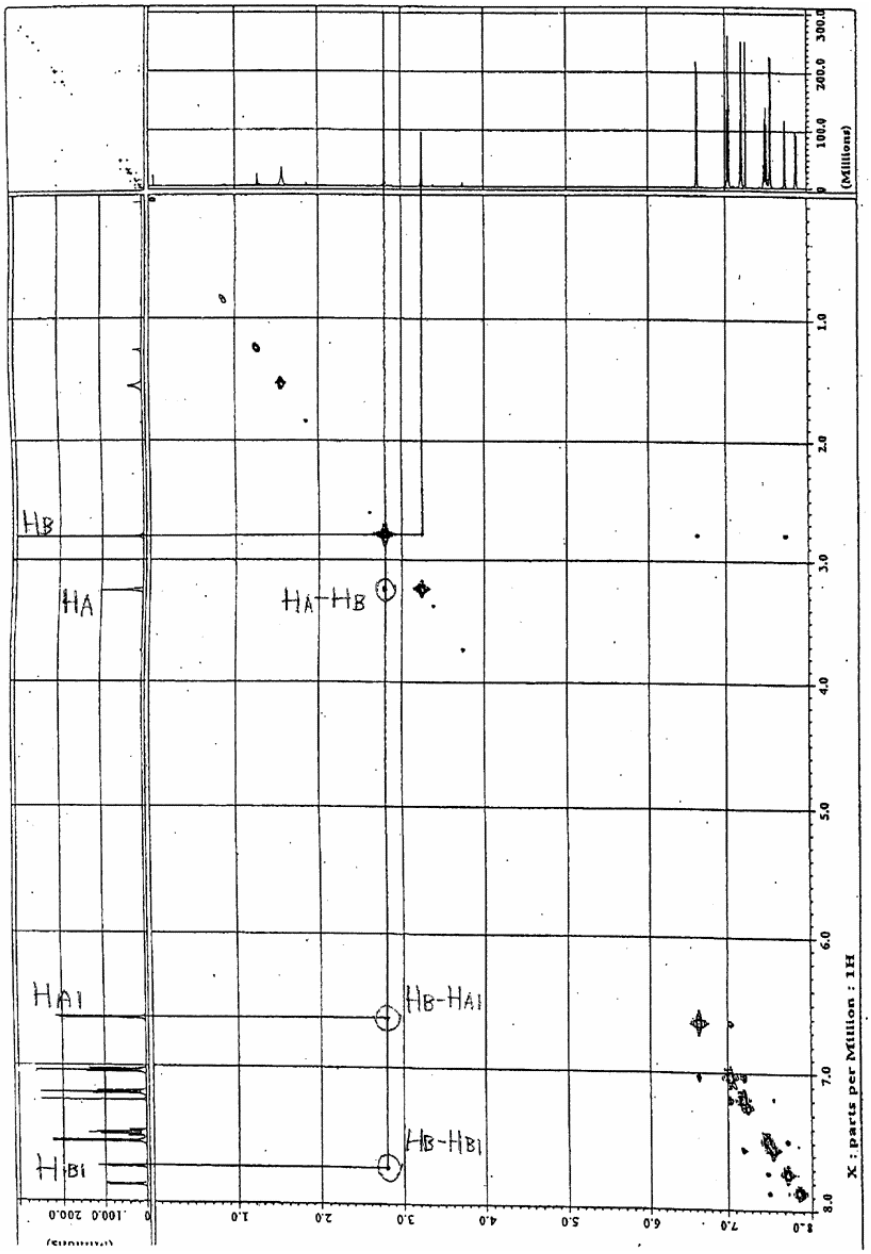

Figure 1.38 NOESY spectra of oligo(DBF) **1** (n = 3) (600 MHz, $CDCl_3$, r.t.).

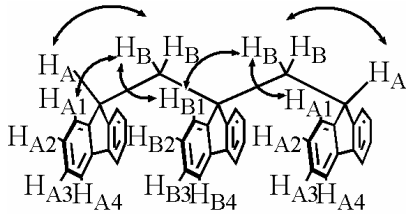

1 (n = 3)

(A)

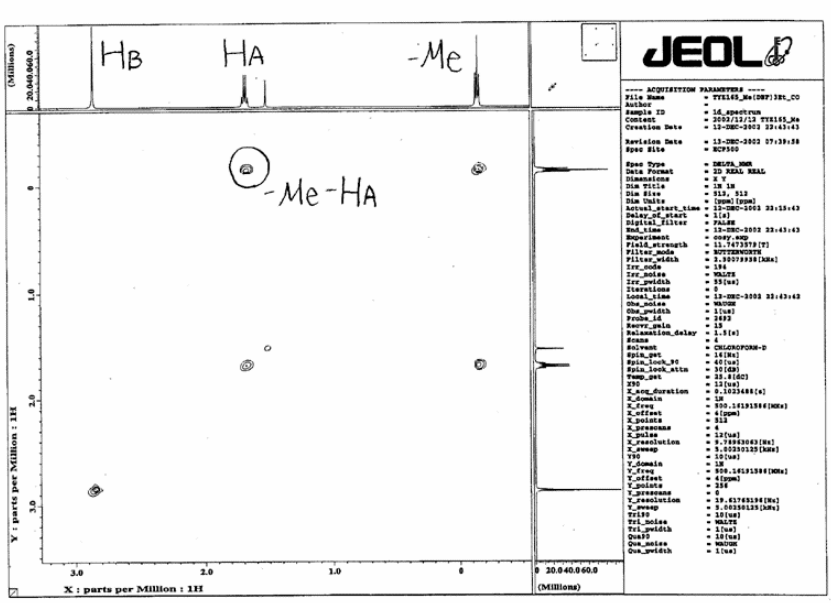

(B)

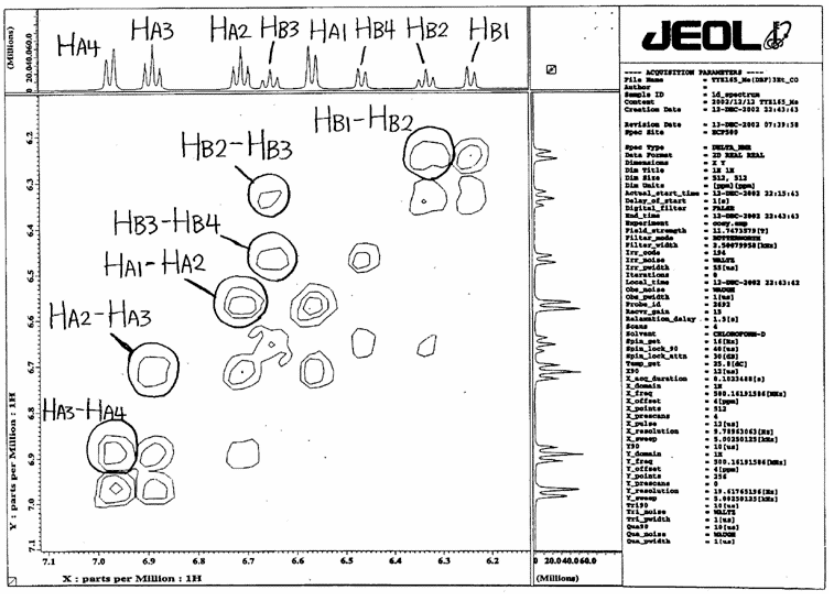

Figure 1.39 H-H COSY spectra of oligo(DBF) **2** (n = 3): alkyl region (A) and aromatic region (B) (500 MHz, $CDCl_3$, r.t.).

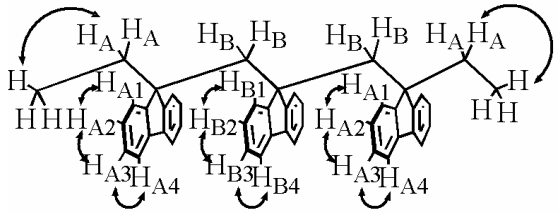

2 (n = 3)

(A)

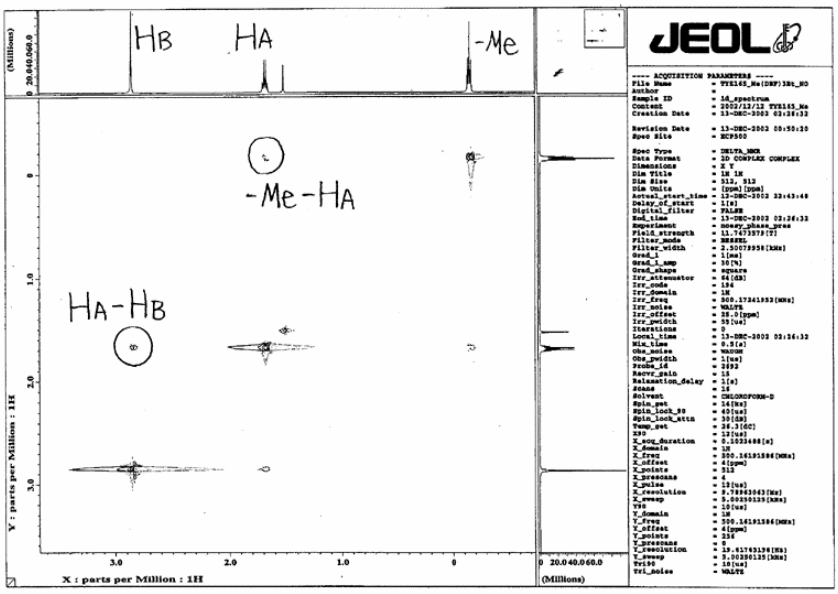

(B)

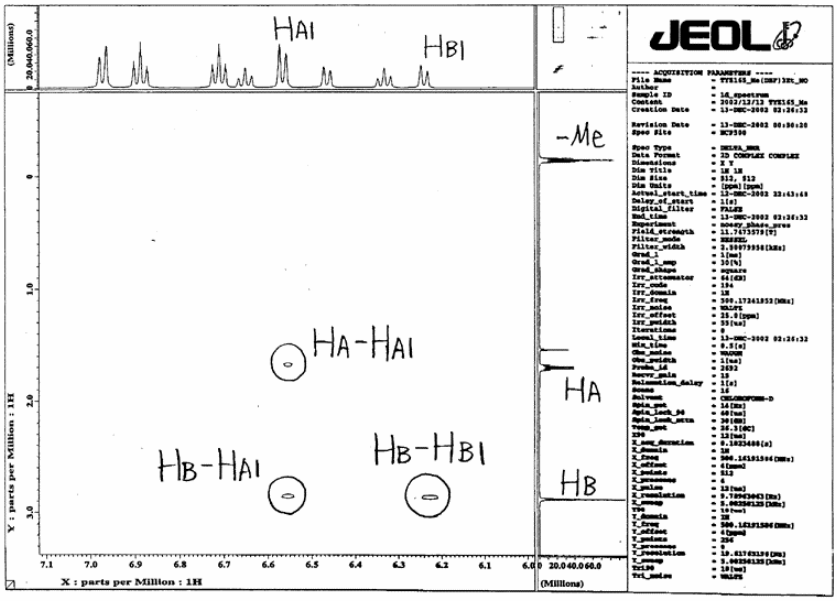

Figure 1.40 NOESY spectra of oligo(DBF) **2** (n = 3): alkyl-alkyl region (A) and alkyl-aromatic region (B) (500 MHz, $CDCl_3$, r.t.).

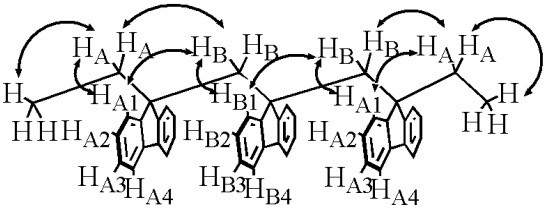

2 (n = 3)

(A)

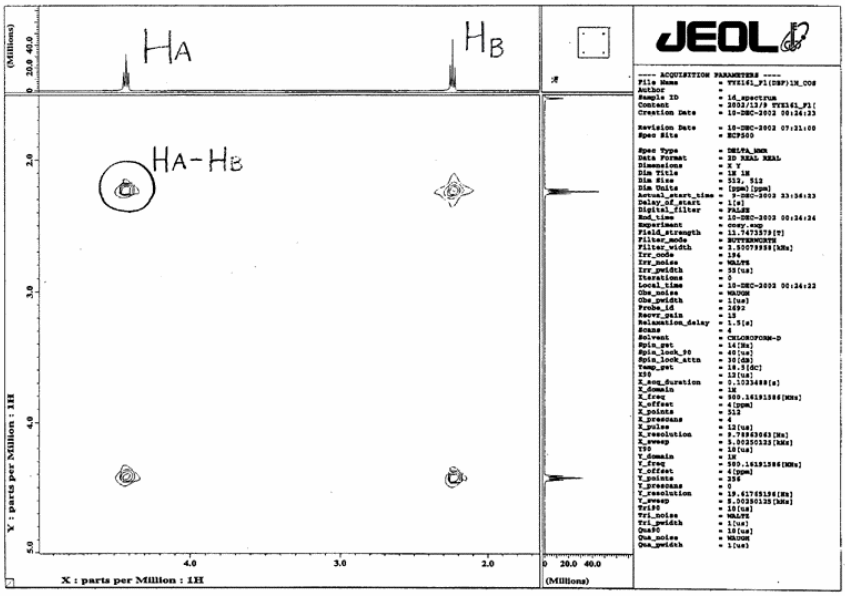

(B)

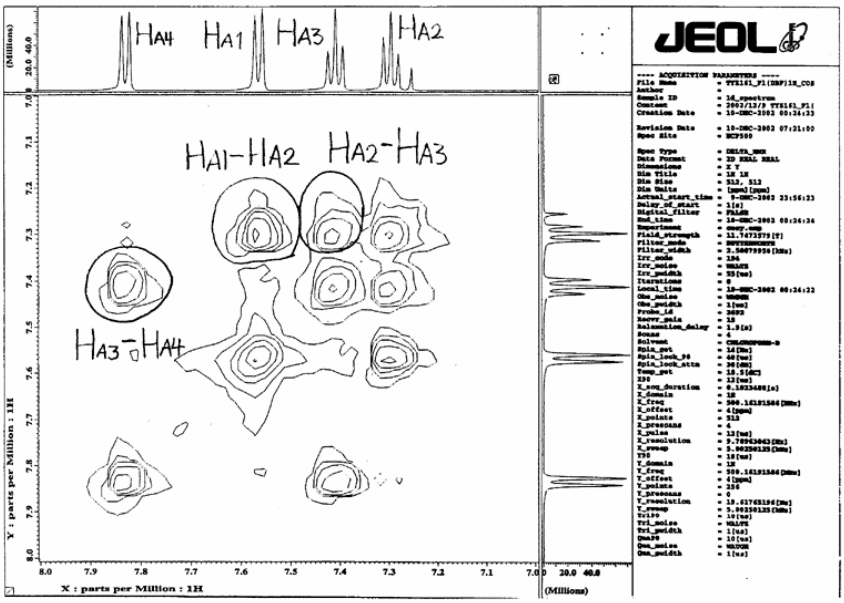

Figure 1.41 H-H COSY spectra of oligo(DBF) **1** (n = 2): alkyl region (A) and aromatic region (B) (500 MHz, $CDCl_3$, r.t.).

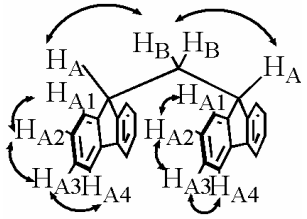

1 (n = 2)

(A)

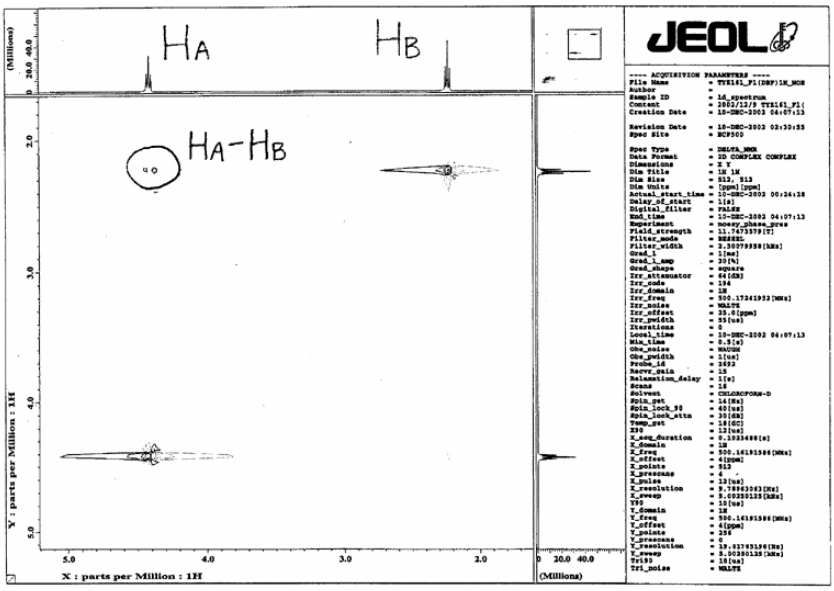

(B)

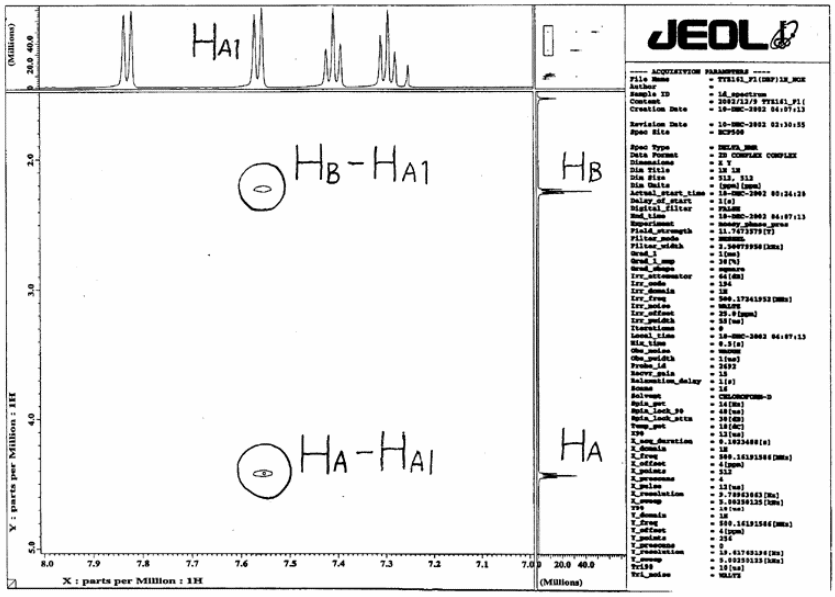

Figure 1.42 NOESY spectra of oligo(DBF) **1** (n = 2): alkyl-alkyl region (A) and alkyl-aromatic region (B) (500 MHz, $CDCl_3$, r.t.).

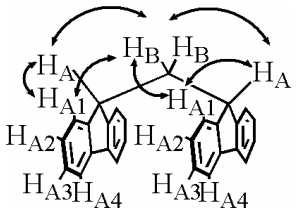

1 (n = 2)

(A)

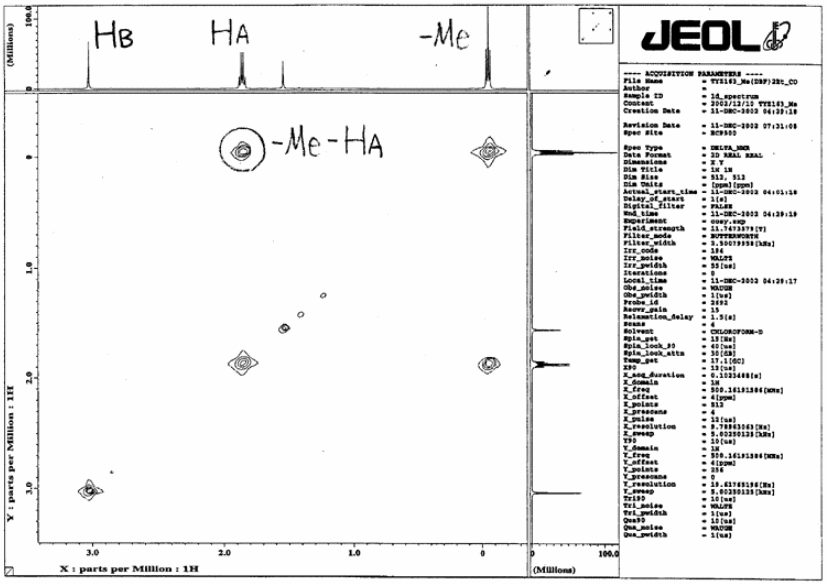

(B)

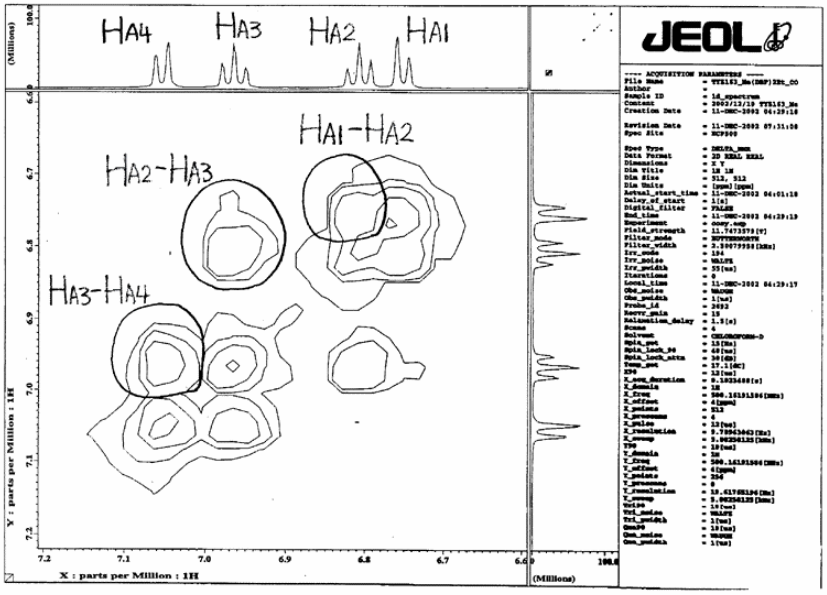

Figure 1.43 H-H COSY spectra of oligo(DBF) **2** (n = 2): alkyl region (A) and aromatic region (B) (500 MHz, $CDCl_3$, r.t.).

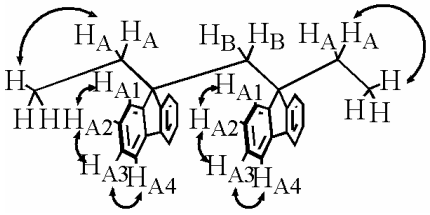

2 (n = 2)

(A)

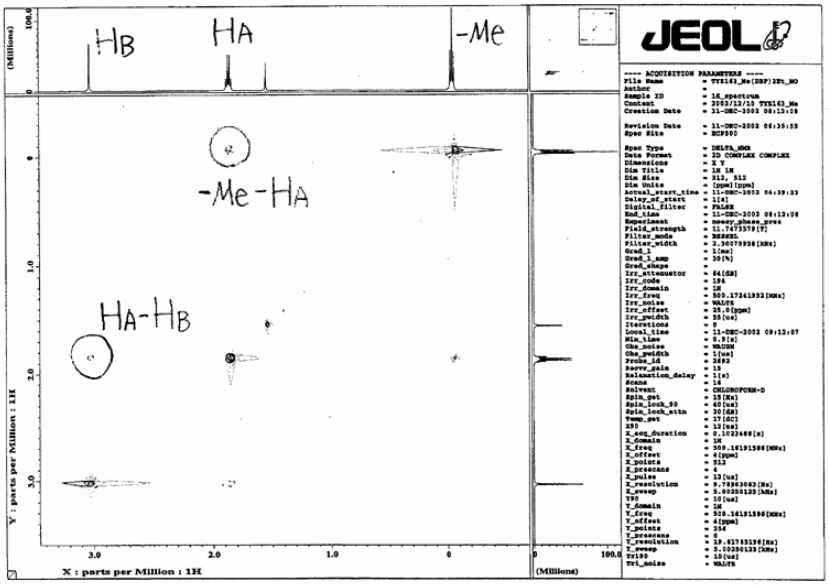

(B)

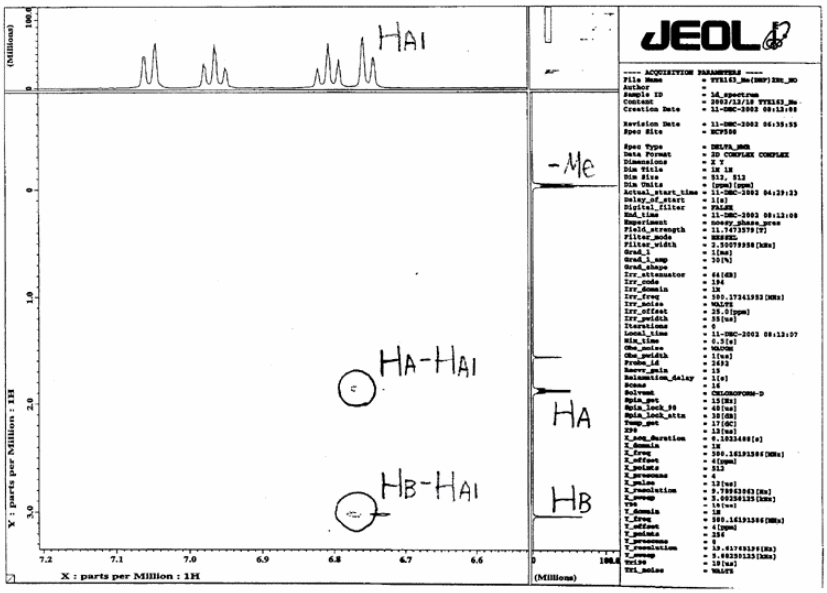

Figure 1.44 NOESY spectra of oligo(DBF) **2** (n = 2): alkyl-alkyl region (A) and alkyl-aromatic region (B) (500 MHz, $CDCl_3$, r.t.).

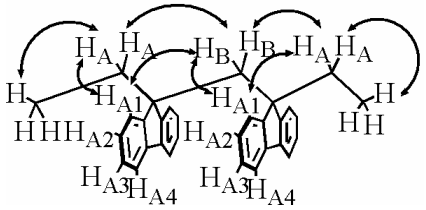

2 (n = 2)

References

(1) (a) Okamoto, Y.; Nakano, T. *Chem. Rev.* **1994**, *94*, 349. (b) Green, M. M.; Peterson, N. C.; Sato, T.; Teramoto, A.; Cook, R.; Lifson, S. *Science* **1995**, *268*, 1860. (c) Gellman, S. H. *Acc. Chem. Res.* **1998**, *31*, 173. (d) Green, M. M.; Park, J.-W.; Sato, T.; Teramoto, A.; Lifson, S.; Selinger, R. L. B.; Selinger, J. V. *Angew. Chem., Int. Ed.* **1999**, *38*, 3138. (e) Srinivasarao, M. *Curr. Opin. Colloid Interface Sci.* **1999**, *4*, 370. (f) Fujiki, M. *Macromol. Rapid Commun.* **2001**, *22*, 539. (g) Hill, D. J.; Mio, M. J.; Prince, R. B.; Hughes, T. S.; Moore, J. S. *Chem. Rev.* **2001**, *101*, 3893. (h) Nakano, T.; Okamoto, Y. *Chem. Rev.* **2001**, *101*, 4013. (i) Conrnelissen, J. J. L. M.; Rowan, A. E.; Nolte, R. J. M.; Sommerdijk, N. A. J. M. *Chem. Rev.* **2001**, *101*, 4039. (j) Brunsveld, L.; Folmer, B. J. B.; Meijer, E. W.; Sijbesma, R. P. *Chem. Rev.* **2001**, *101*, 4071.

(2) Watson, J. D.; Crick, F. H. C. *Nature* **1953**, *171*, 737.

(3) Nelson, J. C.; Saven, J. G.; Moore, J. S.; Wolynes, P. G. *Science* **1997**, *277*, 1793.

(4) (a) Lokey, R. S.; Iverson, B. L. *Nature* **1995**, *375*, 303. (b) Nguyen, J. Q.; Iverson, B. L. *J. Am. Chem. Soc.* **1999**, *121*, 2639.

(5) Wang, W.; Li, L.-S.; Helms, G.; Zhou, H.-H.; Li, A. D. Q. *J. Am. Chem. Soc.* **2003**, *125*, 1120. (b) Li, A. D. Q.; Wang, W.; Wang, L.-Q. *Chem.-Eur. J.* **2003**, *9*, 4594. (c) Wang, W.; Han, J. J.; Wang, L.- Q.; Li, L.-S.; Shaw, W. J.; Li, A. D. Q. *Nano Lett.* **2003**, *3*, 455.

(6) Kuran, W. *Principles of Coordination Polymerization*; Wiley: Chichester, Sussex, 2001; pp 245-274.

(7) (a) Okamoto, K.-I.; Itaya, A.; Kusabayashi, S. *Chem. Lett.* **1974**, 1167. (b) Pearson, J. M.; Stolka, M. *Poly(N-Vinylcarbazole)*; Gordon and Breach: New York, NY, 1981.

(8) Nakano, T.; Takewaki, K.; Yade, T.; Okamoto, Y. *J. Am. Chem. Soc.* **2001**, *123*, 9182.

(9) (a) Evans, A.; George, D. *J. Chem. Soc.* **1961**, 4653. (b) Evans, A.G.; George, D. B. *J. Chem. Soc.* **1962**, 141. (c) Yuki, H.; Hotta, J.; Okamoto, Y.; Murahashi, S. *Bull. Chem. Soc. Jpn.* **1967**, *40*, 2659. (d) Richards, D. H.; Scilly, N. F. *J. Polym. Sci., Polym. Lett.* **1969**, *7*, 99-101.

(10) Rathore, R.; Abdelwahed, S.; Guzei, I. A. *J. Am. Chem. Soc.* **2003**, *125*, 8712.

(11) (a) Ferraris, J. P.; Cowan, D. O.; Walatka, V., Jr.; Perlstein, J. H. *J. Am. Chem. Soc.* **1973**, *95*, 948. (b) Je´rome, D.; Mazaud, M.; Ribault, M.; Bechgaard, K. *J. Phys., Lett.* **1980**, *41*, L95-L98.

(12) (a) Murphy, C. J.; Arkin, M. R.; Jenkins, Y.; Ghatlia, N, D.; Bossman, S. H.; Turro, N.

J.; Barton, J. K. *Science* **1993**, *262*, 1025. (b) Okahata, Y.; Kobayashi, T.; Tanaka, K.; Shimomura, M. *J. Am. Chem. Soc.* **1998**, *120*, 6165. (c) Fink, H.-W.; Schönenberger, C. *Nature* **1999**, *398*, 407. (d) Porath, D.; Bezryadin, A.; de Vries, S.; Dekker, C. *Nature* **2000**, *403*, 635. (e) Priyadarshy, S.; Risser, S. M.; Beratan, D. N. *J. Phys. Chem.* **1996**, *100*, 17678. (f) Braun, E.; Eichen, Y.; Sivan, U.; Ben-Yoseph, C. *Nature* **1998**, *391*, 775. (g) Debije, M. G.; Milano, M. T.; Benhard, W. A. *Angew. Chem., Int. Ed.* **1999**, *38*, 2752. (h) Maiya, B. G.; Ramasarma, T. *Curr. Sci.* **2001**, *80*, 1523.

(13) (a) Greenhow, E. J.; McNeil, D.; White, E. N. *J. Chem. Soc.* **1952**, 986. (b) More O'Ferrall, R. A.; Slae, S. *J. Chem. Soc., Chem. Commun.* **1969**, 486.

(14) Sanders, J. K. M.; Hunter, B. *Modern NMR Spectroscopy*, 2nd ed.; Oxford University Press: New York, NY, 1993.

(15) Zhang, X.; Hogen-Esch, T. E. *Macromolecules* **2000**, *33*, 9176.

(16) Koch, W.; Holthausen, M. C. *A Chemist's Guide to Density Functional Theory*; Wiley-VCH: New York, 2000; pp 197-216.

(17) Stewart, J. J. P. MOPAC2002 software; Fujitsu Limited: Tokyo, Japan, 2001.

(18) Bouman, T. D.; Hansen, A. E. *Chem. Phys. Lett.* **1988**, 149, 510.

(19) Becke, A. D. *Phys. Rev. A* **1988**, *38*, 3098.

(20) Lee, C.; Yang, W.; Parr, R. G. *Phys. Rev. B* **1988**, *37*, 785.

(21) Sekine, Y.; Brown, M.; Boekelheide, V. *J. Am. Chem. Soc.* **1979**, *101*, 3126.

(22) Mayo, S. L.; Olafson, B. D.; Goddard, W. A. *J. Phys. Chem.* **1990,** *94*, 8897.

(23) Allinger, N. L.; Yuh, Y. H.; Lii, J.-H. *J. Am. Chem. Soc.* **1989**, *111*, 8551.

(24) Halgren, T. A. *J. Comput. Chem.* **1999**, *20*, 730.

(25) Sun, H. *J. Phys. Chem.* **1998**, *102*, 7338.

(26) Mohamadi, F.; Richards, N. G. J.; Guida, W. C.; Liskamp, R.; Lipton, M.; Caufield, C.; Chang, G.; Hendrickson, T.; Still, W. C. *J. Comput. Chem.* **1990**, *11*, 440.

(27) Berendsen, H. J. C.; Postma, J. P. M.; van Gunsteren, W. F.; DiNola, A.; Haak, J. R. *J. Chem. Phys.* **1984**, *81*, 3684.

(28) (a) Tinoco, I. *J. Am. Chem. Soc.* **1960**, *82*, 4785. (b) Rohdes, W. *J. Am. Chem. Soc.* **1961**, *83*, 3609.

(29) Cantor, C. R.; Schimmel, P. R. *Biophysical Chemistry*; W. H. Freeman and Company: New York, 1980; Vol. 2, Chapter 7.

(30) Kasha, M.; Rawls, H. R.; El-Bayoumi, M. A. *Pure Appl. Chem.* **1965**, *11*, 371.

(31) Sagiv, J.; Yogev, A.; Mazur, Y. *J. Am. Chem. Soc.* **1977**, *99*, 6861.

(32) Ellis, J. R. In *Handbook of Conducting Polymers*; Skotheim, T. A., Ed.; Marcel Dekker: New York, 1986; Vol. 1, Chapter 13.

(33) Houk, K. N.; Lee, P. S.; Nendel, M. *J. Org. Chem.* **2001**, *66*, 5517.

(34) Frenkel, *J. Phys. Rev.* **1931**, *37*, 17.

(35) (a) Wannier, G. H. *Phys. Rev.* **1937**, *52*, 191. (b) Davydov, A. S. *Theory of Molecular Excitons*; Plenum: New York,1971.

(36) Horrocks, D. L.; Brown, W. G. *Chem. Phys. Lett.* **1970**, *5*, 117.

(37) Matsuda, M.; Watanabe, A. In *Recent Advances in Anionic Polymerization*; Hogen-Esch, T. E., Smid, J., Eds.; Elsevier: New York, 1987; p 73.

(38) Hirayama, F. *J. Chem. Phys.* **1965**, *42*, 3163.

(39) Fletcher, R.; Reeves, C. M. *Comput. J.* **1964**, *7*, 149.

Chapter 2
Radical Polymerization of Dibenzofulvene

2.1 Introduction

Stereoregulation in polymerization is an important goal in macromolecular science because the stereostructure of a polymer molecule often significantly affects properties and functions of materials derived therefrom. Aiming at novel functional polymeric materials, various polymers with regulated configuration and conformation have been synthesized. Regarding the polymers with a regulated conformation, our group recently reported the anionic synthesis of poly(dibenzofulvene) (poly(DBF)) and its derivatives having a π-stacked conformation in which the main-chain C-C bonds are nearly all trans and the side-chain fluorene moieties are stacked on top of each other,[1-4] while most of the publications about polymers having a specific conformation deal with helical structures.[5] Precise stereoregulation has been achieved for various monomers mainly by anionic or coordination polymerization so far. Although radical polymerization is more versatile and convenient than anionic or coordination polymerization, it is generally less effective in stereoregulation except for limited examples.[6] As an exceptional example, it has been reported that radical polymerizations of bulky acrylic monomers such as 1-phenyldibenzosubery methacrylate and triphenylmethyl methacrylate proceeds in a highly configuration- and conformation-specific manner, giving a highly isotactic, helical polymer.[7-9] As shown by these examples, it is of significant benefit if a polymer with a regulated conformation can be obtained by facile radical polymerization rather than the anionic polymerization which requires a strict control of reaction conditions.

As discussed in the previous chapter, the anionic polymerization of DBF leads to a perfectly π-stacked conformation.[2] However, no details of the radical polymerization including the stereochemical aspect have been known. This chaptor describes the polymerization of DBF using radical initiators under various conditions and the structure and photophysical and solubility properties of the obtained polymers.

2.2 Chemical Structure of Radical Polymerization Products

Radical polymerization was carried out with and without initiator in several solvents (Table 2.1). Despite the bulky structure resembling 1,1-diphenylethylene (DPE), which dose not

homopolymerize,[10] DBF afforded polymers by polymerization using the radical initiators. The relatively low monomer conversions may suggest a relatively low ceiling temperature due to the bulkiness of the monomer. In all cases, the products consisted of $CHCl_3$-insoluble and –soluble parts. The $CHCl_3$-soluble and -insoluble parts of the polymer from run 1 in Table 2.1 indicated virtually the same IR spectral pattern, suggesting that they have the same chemical structure. The insoluble part is assumed to be produced by molecular aggregation of rigid polymer molecules and not by cross-linking. It is known that higher-molecular-weight fractions tend to form insoluble aggregates for helical polymethacrylates having a rigid, regulated chain structure.[11]

Table 2.1 Radical Polymerization of DBF[a]

							$CHCl_3$-	$CHCl_3$-soluble part		
			temp	$[monomer]_0$	$[initiator]_0$	conv[b]	insoluble part	yield	M_n[d]	M_n[e]
run	initiator	solvent	(°C)	(M)	(M)	(%)	yield (%)	(%)	(vs St)	(vs DBF)
1	AIBN	benzene	60	0.40	0.020	54	40	14	1000[f]	1730[f]
2	$(i$PrOCOO$)_2$	toluene	40	0.40	0.020	73	40	33	1070[f]	1560[f]
3	none	benzene	60	0.40	0	45	42	17	2190[g]	n.d.
4	AIBN	toluene	60	0.40	0.020	39	26	13	950	1370
5	AIBN	THF	60	0.40	0.020	24	8	16	770	1080
6	AIBN	$CHCl_3$	60	0.42	0.020	27	8	19	780	1090
7	AIBN	MeOH	60	0.20	0.020	40	28	12	1100	1620
8	AIBN	Hexane	60	0.40	0.020	45	22	23	1550	2340
9	AIBN	benzene	60	0.16	0.008	23	9	18	670	820
10	AIBN	benzene	60	0.08	0.004	22	4	18	510	690
11	AIBN	toluene	80	0.40	0.020	36	8	28	250	320
12	BPO-DMA[h]	toluene	0	0.40	0.020	n.d.	34	n.d.	870	n.d.

[a] Time = 24 h (runs 1-11), 48 h (run 12). [b] Determined by ^{1}H NMR analysis of the reaction mixture. [c] $CHCl_3$-soluble part was a mixture of oligomers and unreacted monomer. The yield of this part was calculated excluding the weight of the unreacted monomer. [d] Determined by SEC using two OligoPore columns connected in series with oligostyrenes as the standard samples (eluent: THF). [e] Determined by SEC using two OligoPore columns connected in series with oligo(DBF)s as the standard samples (eluent: THF). [f] Two TSKgel G1000HHR columns connected in series were used for SEC analysis. [g] Determined by SEC using TSKgel G6000HHR and G3000HHR columns connected in series with polystyrene as the standard sample (eluent: THF). [h] DMA = *N*,*N*-dimethylaniline, $[BPO]_0/[DMA]_0 = 1$.

Interestingly, the reaction without an initiator also led to a polymer (run 3 in Table 2.1). A trace amount of oxygen in the reaction system might be responsible for the formation of an initiating radical[4] although generation of a Diels-Alder dimer similar to that reported for the thermal polymerization of styrene[12] cannot be ruled out. No more details have been investigated about this aspect.

To establish that the polymerization took place in vinyl fashion, the structure of the

$CHCl_3$-soluble polymer obtained in run 1 was investigated by NMR and IR spectra. Figure 2.1 compares the ^{1}H NMR spectrum of the polymer from run 1 with that of the poly(DBF) obtained by anionic polymerization with MeLi as initiator and EtI as terminator[2] (M_n 1890). The two spectra had a very similar shape with the only clear difference in the signals of the terminal groups. These results suggest that the radical polymerization took place in vinyl fashion.

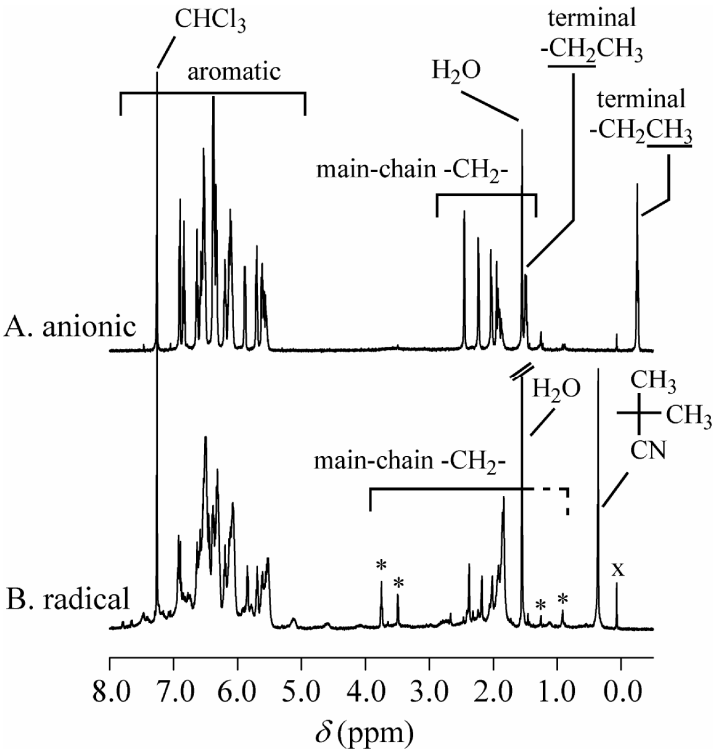

Figure 2.1 ^{1}H NMR spectra of poly(DBF)s prepared by anionic polymerization using MeLi as initiator and EtI as terminator (M_n = 1890 (vs oligo(DBF)s))[2] (A) and by radical polymerization using AIBN (run 1 in Table 2.1) (B). The signals marked by an asterisk in (B) may be based on conformational defects [500 MHz, $CDCl_3$, rt].

The ^{13}C NMR and IR spectra of the poly(DBF) obtained by radical polymerization (run 1 in Table 2.1) were compared with those of the anionically synthesized poly(DBF)s,[2] in Figures 2.2 and 2.3, respectively. The aromatic ^{13}C NMR spectrum in Figure 2.2 and the overtone/combination IR bands in Figure 2.3 are sensitive to the aromatic ring substitution pattern. The fact that the radical and the anionic polymerization products showed very similar patterns both in the ^{13}C NMR and the IR spectra indicates that isomerization of the growing radical[13] or aromatic substitution did not significantly contribute to the

polymerization although such reactions are not completely ruled out because there still are minor differences between the two ^{13}C spectra which cannot be immediately explained.

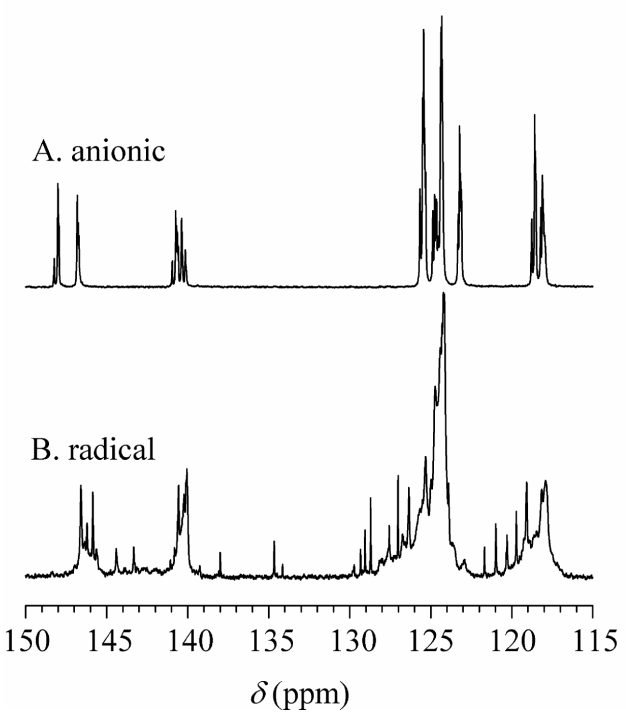

Figure 2.2 ^{13}C NMR spectra of poly(DBF)s prepared by anionic polymerization using MeLi as initiator and EtI as terminator (M_n = 770, DP = 2–8 mixture) (A) and by radical polymerization using AIBN (run 1 in Table 2.1) (B) [150 MHz, $CDCl_3$, rt].

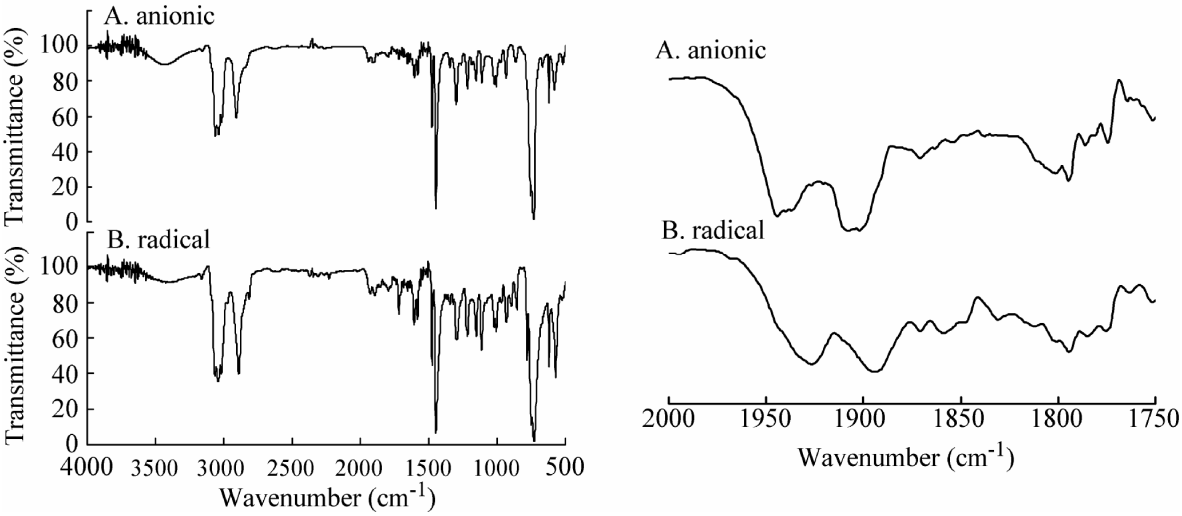

Figure 2.3 IR spectra of polymers prepared by anionic polymerization using MeLi as initiator and EtI as terminator (M_n = 1890 (vs. oligo(DBF)s)) (A) and by radical polymerization using AIBN (run 1 in Table 2.1) (B): full (left) and overtone/combination band region (right) spectra.

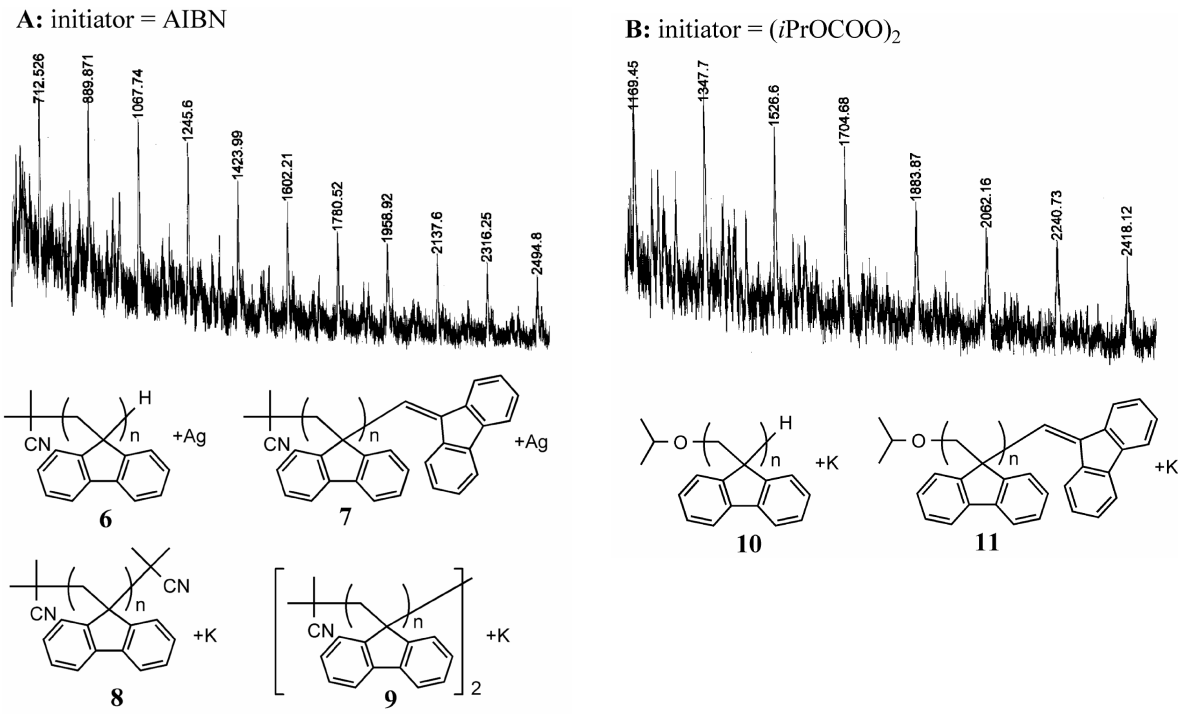

Figure 2.4 MALDI-TOF mass spectra of poly(DBF)s prepared by radical polymerization using AIBN (run 1 in Table 2.1) (A) and (*i*PrOCOO)$_2$ (run 2 in Table 2.1) (B) (matrix: dithranol and TFA-Ag).

Figure 2.4 shows the MALDI-TOF mass spectra of the $CHCl_3$-soluble polymer obtained using AIBN and (*i*PrOCOO)$_2$ (runs 1 and 2 in Table 2.1). The spectra indicated the periodic mass peaks separated from each other by a mass number of ca. 178 corresponding to the molecular mass of DBF monomeric unit. In the spectrum of the polymer synthesized using AIBN (run 1 in Table 2.1), the mass numbers of the major peaks were close to those of molecular ions associated with Ag corresponding to structures **6** and **7** which may be produced by disproportionation or hydrogen abstraction from solvent. The mass numbers were also close to those of molecular ions associated with K corresponding to structures **8** and **9** having two $(CH_3)_2C(CN)$- groups at the chain terminals which may be obtained through primary radical termination and recombination termination, respectively; however, these structures are less plausible because the DP of the products from run 1 in Table 2.1 calculated from the ^{1}H NMR spectra in Figure 2.1B assuming structures **6** and **7** (DP = 15) was much closer than that calculated assuming structures **8** and **9** (DP = 30) to the DP of ca. 10 derived from the M_n estimated by SEC (M_n 1730 by SEC with oligo(DBF)s as reference samples).

On the other hand, the spectrum of the polymer obtained using (iPrOCOO)$_2$ (run 2) showed the mass numbers close to those of the molecular ions associated with K corresponding to structures **10** and **11** and no signals matching to the mass numbers of primary radical termination or recombination termination products. Hence, in the radical polymerization of DBF with AIBN or (iPrOCOO)$_2$ examined here, the termination reaction may occur mainly through disproportionation or hydrogen abstraction from solvent.

2.3 Stereochemistry of Radical Polymerization

Because poly(DBF) with a vinyl polymer structure has no asymmetric centers, conformation is the only aspect of the stereochemistry to be discussed. The ^{1}H NMR spectra shown in Figure 2.1 provide important information on the stereostructure (conformation) of the polymer obtained by the radical polymerization. The detailed studies on the completely π-stacked poly- and oligo(DBF)s have indicated that the aromatic proton signals are in the range of 5.5–6.9 ppm due to the shielding effect and the main-chain –CH_2– signals are in the range of 1.8–2.6 ppm.[2] It has also been predicted by density functional theory (DFT) calculations that the main-chain –CH_2– chemical shifts are sensitive to polymer conformation, and defective conformations (not-π-stacked parts) will shift the main-chain –CH_2– signals to a higher or a lower magnetic field from the 1.8–2.6 ppm range.[2]

The spectrum of the polymer obtained by the radical polymerization in benzene using AIBN (Figure 2.1B) indicated the most main-chain –CH_2– peaks in the range of 1.8–2.8 ppm and the aromatic peaks in the range of 5.5–7 ppm. This indicates that the polymer prepared by radical polymerization has a π-stacked conformation similar to that of the polymer by anionic polymerization. Hence, the radical polymerization of DBF was shown to be almost as conformation-specific as well as the anionic polymerization. However, the radically synthesized polymer may contain a small amount of some defective conformation, because the peaks marked by an asterisk in Figure 2.1B of low intensities probably due to –CH_2– protons are observed in the 0.8–1.5 ppm and the 3–4 ppm regions where the peaks due to π-stacked conformation should not show. It is important to note that these peaks are considered not to arise from some low-molecular-weight impurities because the shapes and intensities of the peaks were unchanged through purification by reprecipitating in hexane seven times to remove silicon grease residue and also because no signals of such impurities were found by SEC analyses.

2.4 Effects of Solvent, Temperature, and Monomer Concentration on the Reaction Stereochemistry

Although solvent, monomer concentration, and temperature generally do not have a significant effect on radical polymerization stereochemistry, such factors have been reported to significantly affect the stereochemistry of triphenylmethyl methacrylate (TrMA) polymerization which leads to a polymer with a rigid, helical conformation.[14] These effects have been interpreted in terms of the proposed two growing species whose conformations differ in the vicinity of the active radical end, and the followings have been proposed for the species: (1) one of the two adds monomer in a highly isotactic-specific manner while the other leads to lower stereospecificity in monomer addition, (2) the latter is formed on monomer addition and mutates to the former at a rate comparable to that of monomer addition, and (3) the mutation takes more obvious effects on the polymerization stereochemistry in a proper solvent, at a lower monomer concentration, and at a higher temperature. A similar situation might be possible for the radical polymerization of DBF because both poly(DBF) and poly(TrMA) have a rigid structure with a specific conformation.

To test this possibility, the polymerization of DBF was carried out in different solvents, at different monomer concentrations, and at different temperatures. First**,** solvent effects were examined by polymerization at 60°C using benzene, toluene, tetrahydrofuran (THF), $CHCl_3$, methanol, and hexane as solvents (runs 1 and 4-8 in Table 2.1). Polymers were obtained in all solvents. Although polymer yields and molecular weights varied depending on solvents, all $CHCl_3$-soluble polymers obtained here showed very similar ^{1}H NMR spectral patterns which resemble to the spectrum of a π-stacked polymer obtained by anionic polymerization (Figure 2.1A). This means that the stereochemistry was little affected by solvents in the DBF polymerization unlike in the TrMA polymerization.

Monomer concentration effects were next examined by polymerizations in benzene using AIBN at 60°C (runs 1, 9, and 10 in Table 2.1). Polymerization reaction took place at all concentrations. The ^{1}H NMR spectra of the products obtained at $[M]_o$ = 0.08 M and 0.16 M are shown in Figure 2.5A and B. The spectra were clearly different in pattern from that of the polymer obtained at $[M]_o$ = 0.40 M (Figure 2.1B): the aromatic signals are significantly less upfield shifted, and signals probably due to $-CH_2-$ were observed in a much wider chemical shift range.

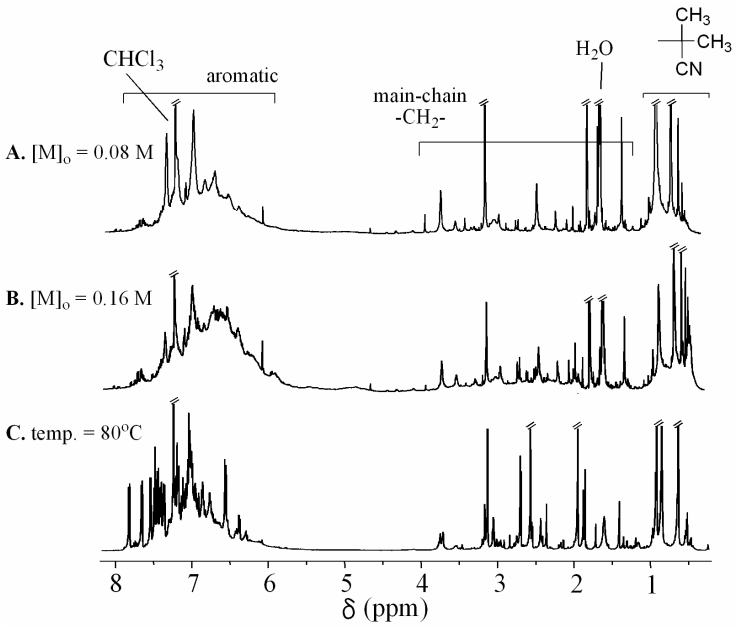

Figure 2.5 ^{1}H NMR spectrum of the radical polymerization products obtained in benzene at 60°C at 0.08 M (run 10 in Table 2.1) (A) and $[M]_0$ = 0.16 M (run 9 in Table 2.1) (B) and in toluene at 80°C at $[M]_0$ = 0.40 M (run 11 in Table 2.1) (C) [500 MHz, $CDCl_3$].

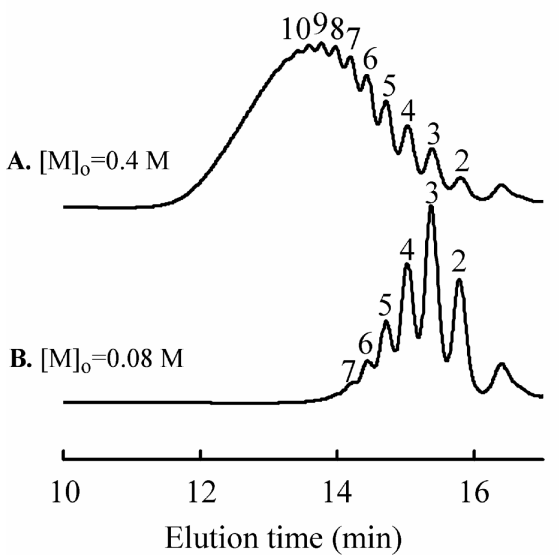

Figure 2.6 SEC curves of the radical polymerization products obtained at different initial monomer concentrations: $[M]_0$ = 0.40 M (run 1 in Table 2.1) (A) and 0.08 M (run 10 in Table 2.1) (B) [UV detection at 254 nm].

Although the products obtained at $[M]_o$ = 0.08 M had a much lower average molecular weight than that obtained at $[M]_o$ = 0.4 M and were oligomers with dimer, trimer, and tetramer as the major components (Figure 2.6A and B), the NMR profiles noted above are not

due to the low DPs of the products because π-stacked oligomers (DP = 2–8) obtained by anionic polymerization did not show –CH_2– signals in such a wide range. Some of the –CH_2– signals in Figure 2.5 A and B may be due to some defective, not-π-stacked conformation.

Next, to investigate temperature effects on the polymerization stereochemistry, polymerization was carried out in toluene using AIBN at 80°C, 60°C, and 40°C and using benzoyl peroxide–*N*,*N*-dimethylaniline (BPO–DMA) at 0°C (runs 2, 4, 11, and 12 in Table 2.1). While the products at 0–60°C showed similar ^{1}H NMR spectra resembling to that of the anionic polymerization products, the reaction products obtained at 80°C indicated a spectral pattern similar to those of the products obtained at $[M]_o$ = 0.08 M and 0.16 M at 60°C (Figure 2.5C). Again, this is considered not to arise from the low molecular weight of the products as discussed above.

Thus, a lower monomer concentration and a higher reaction temperature seem to lead to a defective conformation. To obtain information on the conformation produced under such conditions, the trimer fraction (the peak marked by "3" in Figure 2.6B) was isolated using a preparative SEC system and subjected to structural analyses. The MALDI-mass spectra of this isolated fraction indicated major molecular ion peaks at *m*/*z* = 692.883 and 708.905 which correspond to the mass numbers of a DBF trimer having two $(CH_3)_2C(CN)$- groups (structure **3** in Figure 2.4A with n = 3) associated with Na and K, respectively. This structure is produced through primary radical termination of a trimer radical. In the low-molecular-weight range, primary radical termination appears to contribute to the polymerization, which is in contrast to the production of structures **1** and **2** in Figure 2.4A in the higher molecular-weight range as discussed earlier.

Figure 2.7A shows the ^{1}H NMR spectrum of the isolated trimer. The two peaks in the 0.5–0.8 ppm range are assigned to the two $(CH_3)_2C(CN)$– groups on the basis of their intensities relative to that of aromatic signals. Several peaks probably due to –CH_2– groups were in the 0.8–4 ppm range whereas –CH_2– protons of a completely π-stacked trimer appear only at 2.8 ppm. To explain these chemical shift characteristics, a trimer structure with a gauche–gauche part in the main chain is proposed, as shown in Scheme 2.1A. From the published DFT calculation on the DBF oligomers,[2] the –CH_2– protons marked by red and blue circles are expected to be down-field- and up-field-shifted, respectively, compared with those in a completely π-stacked conformation with all-trans main chain on the basis of the

published DFT calculations. Therefore, the proposed oligomer structure explains that the –CH_2– signals were observed in a wide range though precise peak assignments have not been achieved. Because the total number of signals in the –CH_2– region was greater than the number of –CH_2– groups of a trimer, three, the fractionated sample may contain several conformational variations.

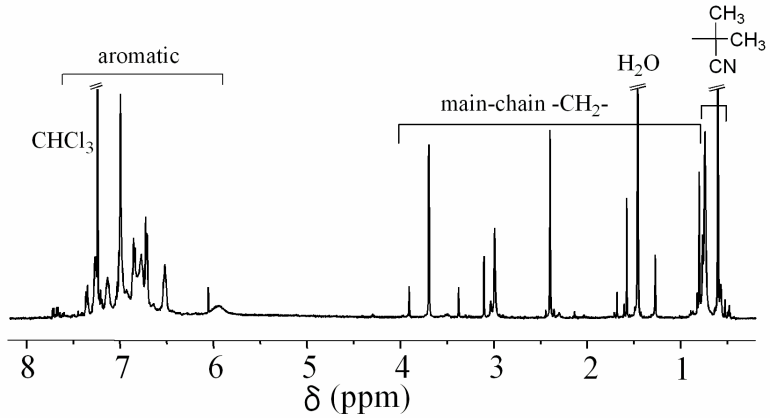

Figure 2.7 ^{1}H NMR spectrum of the trimer fraction isolated by SEC. See Figure 2.6B for the analytical SEC curve.

Scheme 2.1 A Defective, Not-π-Stacked, Conformation of a DBF Trimer Having $(CH_3)_2C(CN)$- Groups at Chain Terminals: Side (Left) and Top (Right) Views[a]

A. Trimer structure with a defective conformation

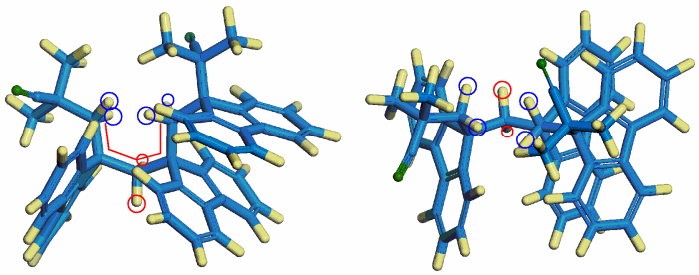

B. A π-stacked chain with a gauche-gauche part (defective conformation).

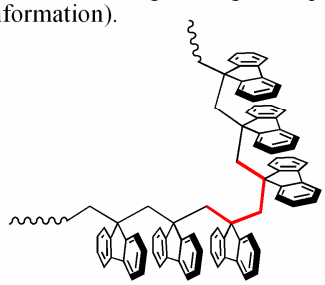

[a] The red bars indicate the gauche–gauche part of the main chain (conformational defect), and the red and blue circles indicate protons expected to be upfield and downfield shifted, respectively, compared with the –CH_2– protons in a completely π-stacked chain, by DFT calculations.[2]

The proposed conformer was found to be stable in molecular dynamics (MD) simulations at 298 K in the duration periods of 9.99 ns. Although three other possible, defective conformers were examined under the same simulation conditions, they turned to a completely π-stacked structure within the duration time of ca. 500 ps. This supports the plausibility of the proposed conformation in Scheme 2.1A.

On the basis of the discussions here, poly(DBF) obtained by radical polymerization may possibly have gauche–gauche parts as a conformational defect in the mostly π-stacked, all trans chain as shown in Scheme 2.1B. Such a part may result in the $-CH_2-$ signals out of the 1.8–2.8 ppm range in ^{1}H NMR spectra (the signals marked by an asterisk in Figure 2.1B). Due to steric repulsion, energy barriers for trans to gauche and reversed conformational transitions are expected to be very large. Hence, a local conformation determined kinetically during the course of polymerization can be maintained in a polymer chain even if it is a thermodynamically disfavored structure.

2.5 Proposed Stereochemical Mechanism of Polymerization

To explain the fact that the defective structures are produced at a lower monomer concentration and at a higher reaction temperature, the author propose a reaction mechanism involving different conformations of the growing radical which lead to different conformations of the terminal diad on the reaction with a monomer (radicals **a** and **b** in Scheme 2.2). Radical **a** has a loosely π-stacked conformation at the growing terminal and gives a π-stacked diad on monomer addition while radical **b** has a flipped fluorene moiety at the growing terminal and gives a flipped diad with a gauche main-chain conformation on monomer addition. Radical **a** is less stable than radical **b** and can mutate to radical **b**. This mechanism explains the generation of defective structures at a lower monomer concentration where radical **a** has a larger chance to mutate to **b** before it attacks to a monomer and at a higher temperature where the mutation is faster. While the more stable growing species was the more stereospecific species in the proposed mechanism of TrMA polymerization,[14] the species giving a defective conformation is more stable in this case.

Validity of the proposed radicals **a** and **b** was checked by the semi-empirical PM5[15] calculations of two model trimer radicals bearing an ethyl group at the initiation terminal (Scheme 2.3). The optimized trimer radical structures, **A** and **B** in Scheme 2.3, have similar shapes to those of the growing end of the proposed radicals, **a** and **b** in Scheme 2.2,

respectively, and are likely to give a stacked and a flipped diads, respectively, on monomer addition. The heat of formation (H_f) for **A** was 168.75 kcal/mol and that for **B** was 165.77 kcal/mol, indicating that the latter is slightly more stable. Steric repulsion between the terminal and penultimate fluorene moieties may destabilize **A**. In addition, the rotation barrier between **A** and **B** was estimated to be ca. 10 kcal/mol by calculating the energies of 20 conformers generated by changing the dihedral angle marked by the curved arrows shown in Scheme 2.3 at the angle interval of 10°. Thus, the proposed mechanism that radical **a** mutates to radical **b** (Scheme 2.2), the more stable conformer, may be reasonable. Because the main-chain C-C bonds are the only rotatable bonds in poly(DBF), the molecular simulations presented here are expected to be reasonably accurate.

Scheme 2.2 Proposed Reaction Mechanism Involving Two Conformers of the Growing Radical

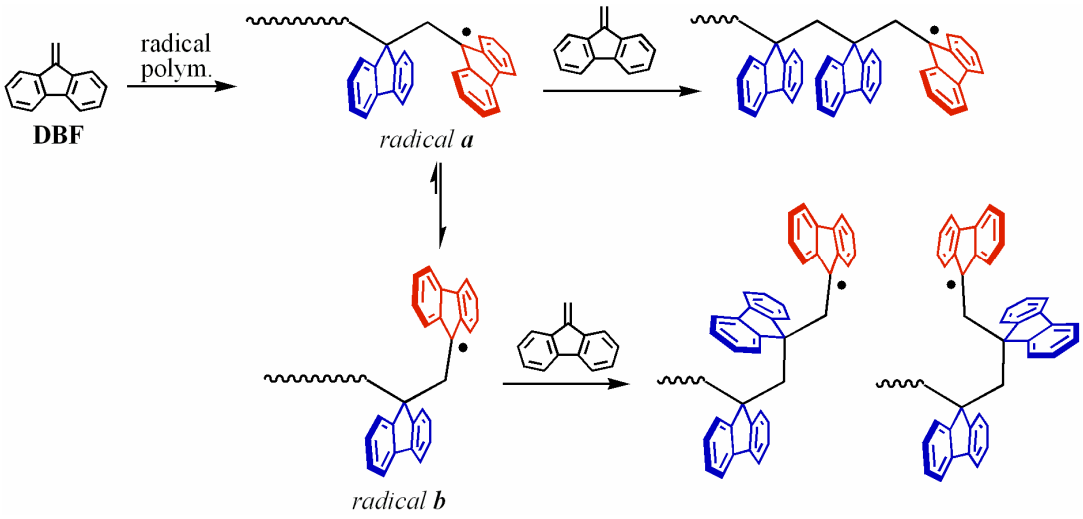

Scheme 2.3 Structures and Heat of Formation (H_f) Values of Loosely π-Stacked (A) and Flipped (B) Trimer Growing Radical Models Optimized by PM5 Calculation

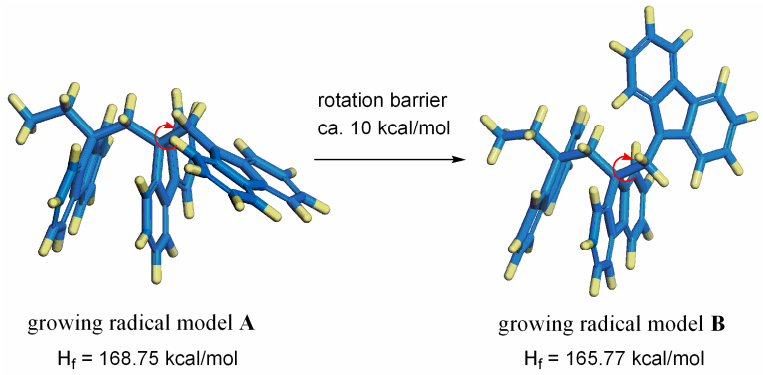

Based on these discussions, defective structures may occur in the mostly π-stacked poly(DBF) prepared by radical polymerization. At the later stages of polymerization where the monomer concentration is lower than at the earlier stages of polymerization, polymer chains with a higher content of conformational defect may be produced at a higher chance.

A similar conformational transition of the growing species might be possible also in anionic polymerization. However, the situation will be different from that of the radical system because of steric effects of counter cation, coordination of solvent molecules to the cation, and aggregation of the growing species. These three factors might disfavor a conformational transition.

2.6 Photophysical Properties

Properties of the polymers and the oligomers were investigated. Absorption and emission spectra are shown along with those of the polymer synthesized by anionic polymerization[2] in Figures 2.8 and 2.9. The quantum yields of the emissions shown in Figure 2.9 are summarized in Table 2.2.

In the absorption spectra (Figure 2.8), the radical polymerization products obtained using AIBN in benzene at 60°C (runs 1 and 10 in Table 2.1) showed remarkable hypochromic effect which is characteristic to a π-stacked structure. However, the magnitude of hypochromicity of the products obtained at $[M]_o$ = 0.08 M was slightly lower compared with that for the anionic polymerization products while that of the polymers obtained at $[M]_o$ = 0.4 M was comparable to that of the anionic polymerization products. This is consistent with the conclusion in the conclusion that the oligomers obtained at $[M]_o$ = 0.08 M have a partially defective conformation.

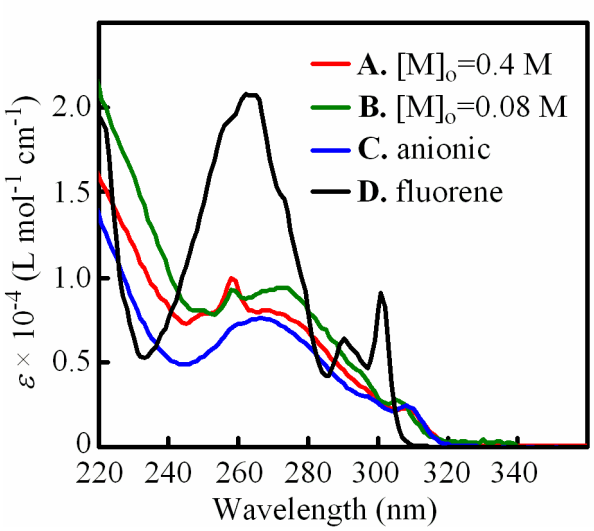

Figure 2.8 Absorption spectra of the radical polymerization products obtained at $[M]_0$ = 0.4 M (run 1 in Table 2.1) (A) and 0.08 M (run 10 in Table 2.1), the polymer having ethyl groups at the chain terminals obtained by anionic polymerization (M_n 1890) (C), and fluorene as model monomeric unit (D) [THF, rt]. The molar extinction coefficients are based on the molar concentration of fluorene moieties in the samples.

In the fluorescence spectra (Figure 2.9), the radical polymerization products obtained at $[M]_o$ = 0.4 M (run 1 in Table 2.1) indicated exclusive intramolecular dimer (excimer) emission (ca. 400 nm) which is characteristic to a π-stacked structure while the products obtained at $[M]_o$ = 0.08 M (run 10 in Table 2.1) indicated both monomer (ca. 305-320 nm) and dimer (excimer) emissions. The monomer emission should have nothing to do with the low *DP*s of the products at $[M]_o$ = 0.08 M and is considered to arise from the conformationally defective parts because a DBF dimer having terminal ethyl groups with a π-stacked structure showed only dimer (excimer) emission.

It is notable that the emission intensity of the products obtained at $[M]_o$ = 0.4 M (run 1 in Table 2.1) was approximately half that of the anionic polymerization product. This may be because the π-stacked structure constructed by radical polymerization is not as regular as that produced by anionic polymerization and have a small amount of defective conformations incorporated in a π-stacked sequence. Such a conformational defect might act as a built-in quenching site. Also, the terminal –CN group originating from AIBN might possibly quench the emission although this possibility has not been investigated in detail.

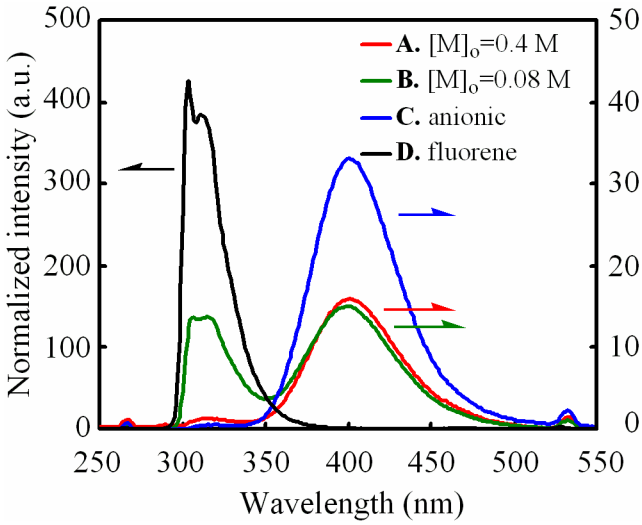

Figure 2.9 Fluorescent spectra of the $CHCl_3$-soluble, radical polymerization products obtained at $[M]_0$ = 0.4 M (run 1 in Table 2.1) (A) and 0.08 M (run 10 in Table 2.1) (B), the anionic polymerization products (M_n 1890) (C), and fluorene as model monomeric unit (D). The intensity was corrected to a constant absorbance at 267 nm [THF, rt, λ_{ex} = 267 nm].

Table 2.2 Fluorescence Quantum Yields (Φ_F) for Spectra in Figure 2.9[a]

spectrum	monomer emission (300–350 nm)	excimer emission (350–500 nm)
A		0.060
B	0.025	0.056
C		0.12
D	0.69	

[a] Determined with reference to 9,10-diphenylanthracene (Φ_F 0.90).

2.7 Solubility

A clear difference between the anionic and radical polymerization products was found in solubility. Although both the radical and anionic products are only partially soluble in solvents, the M_n range of the highest-molecular-weight fractions of $CHCl_3$-soluble part was found to be much higher for the radical polymerization products (run 8 in Table 2.1) than the anionic polymerization products prepared in THF at –78°C using fluorenyllithium (FlLi) at $[M]_o/[I]_o$ = 20,[3] as shown in Figure 2.10. As well as the lower fluorescent efficiency, this also may be explained by minor structural defects in the mostly π-stacked chain prepared by radical polymerization. A slight conformational irregularity may make molecular packing less tight in the formation of the insoluble aggregates.

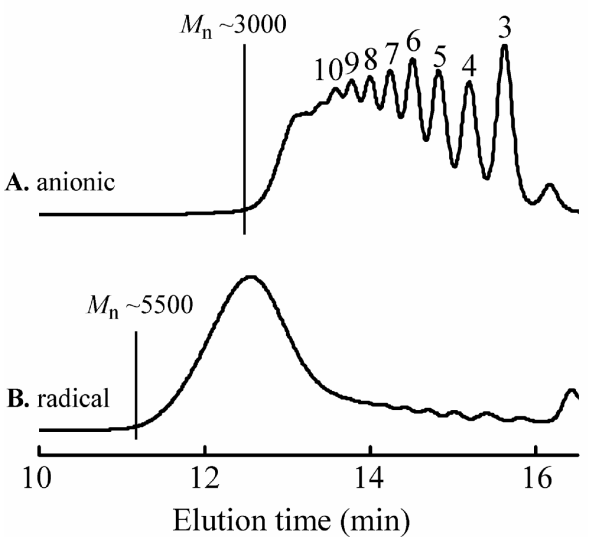

Figure 2.10 SEC curves of the $CHCl_3$-soluble poly(DBF)s obtained by the anionic polymerization using FlLi at $[M]_0/[I]_0 = 10$ in THF (A) and by the radical polymerization in hexane (run 8 in Table 2.1) (B).

2.8 Conclusions

Radical polymerization of DBF was carried out under various conditions, and the structure and properties of the obtained polymers and oligomers were investigated. It was shown that (i) radical polymerization of DBF proceeded through a vinyl addition mode, (ii) the polymers had a mostly π-stacked conformation with a small amount of defective parts, (iii) the polymers showed lower fluorescent efficiency and higher solubility compared with the poly(DBF) synthesized by anionic polymerization possibly due to a small amount of defective conformations, and (iv) a lower monomer concentration and a higher temperature led to defective conformations, which was explained by a proposed reaction mechanism involving two interchangeable conformers of the growing radical with different conformation specificity on monomer addition.

Although regulated and stable π-stacked structures have been realized for several types of polymers other than poly(DBF) and its derivatives, the examples are still limited, and their synthesis generally requires more laborious procedures than simple vinyl polymerization.[16-20] This study opens a way to synthesize a π-stacked polymer by radical polymerization method which is especially facile among various vinyl polymerization techniques. In addition, it is implicated that conformational modification is possible to a certain extent by controlling

reaction conditions (monomer concentration and reaction temperature). This feature may be used to modify not only the solubility discussed here but also other physical properties of π-stacked poly(DBF) such as charge mobility and conductivity.

2.9 Experimental Section

Materials

DBF monomer was synthesized according to the published method.[2,21,22] Anionic polymerization products were available form our recent work.[2] α,α'-Azobisisobutyronitrile (AIBN) was recrystallized from an ethanol solution. Benzoylperoxide (BPO) (Wako) was used as obtained. *N,N*-Dimethylaniline (DMA) was distilled and dried on KOH. $(i\text{PrOCOO})_2$ was kindly provided by NOF Co. (Taketoyo-cho, Chita-gun, Aichi 470-23, Japan). Tetrahydrofuran (THF) (Wako) was refluxed over sodium benzophenone ketyl, distilled and stored on $LiAlH_4$ under N_2 atmosphere, and distilled under vacuum immediately before use. The other solvents were purified by the usual methods, degassed under vacuum and flashed with N_2, and stored under N_2 atmosphere.

Polymerization

The reactions were carried out in a glass ampule sealed with a glass-made three-way stopcock attached to the ampule via a ground joint. The joint was sealed with high-vacuum grease. The ampoule was flame-dried under high vacuum and flashed with N_2 immediately before use. A typical procedure is described for run 1 in Table 2.1. DBF (534 mg, 3.00 mmol) and AIBN (24.6 mg, 0.15 mmol) were placed in a flame-dried ampoule, and the ampoule was evacuated for 5 min at room temperature and flashed with dry N_2 gas. Benzene (6.9 mL) was added using a syringe, and the monomer and the initiator were completely dissolved. The polymerization was initiated by heating the solution at 60°C, and the reaction mixture was cooled at 0°C after 24 h of heating. An aliquot (about 0.1 ml) of the solution part of the reaction mixture was transferred to an NMR sample tube (5 mm ϕ), 0.6 ml of $CDCl_3$ was added, and the resulting diluted solution was subjected to ^{1}H NMR analysis. Comparison of the intensity of the vinyl proton signals of remaining DBF (s, 6.0 ppm) with that of the benzene signal (s, 7.4 ppm) as an internal standard gave a monomer consumption ratio of 54%. After removing the solvents from the rest of the reaction mixture, the residue was separated into $CHCl_3$-soluble and –insoluble parts using a Teflon-made membrane filter (pore size, 0.45 μm). The $CHCl_3$-soluble part was fractionated into the

reaction products (polymers and oligomers) and the remaining monomer with a preparative SEC system. The chromatographically obtained fractions were further purified by reprecipitating in hexane seven times.

Measurements

The ^{1}H NMR spectra were recorded on a JEOL JNM-ECP600NK or a JEOL ECP500 spectrometer (600 and 500 MHz, respectively, for ^{1}H measurement). Analytical scale SEC was carried out using a chromatographic system consisting of a JASCO PU-980 chromatographic pump, a JASCO UV-975 UV detector (254 nm), and a JASCO RI-930 RI detector equipped with two PL-Oligopore columns (30 × 0.72 (i.d.) cm) (Polymer Laboratories) connected in series or on a system consisting of a Hitachi L-7100 pump, an L-7420 UV detector (254 nm), and an L-7490 RI detector equipped with TOSOH TSK gel $G3000H_{HR}$ and $G6000H_{HR}$ columns connected in series (eluent, THF; flow rate, 1.0 mL/min). Preparative SEC separation of oligomers was performed using a JAI LC-908 preparative recycle chromatograph equipped with JAIGEL-1H and JAIGEL-2H columns connected in series. IR spectra were measured with a JASCO FT/IR-420 spectrophotometer using KBr pellet samples. MALDI-mass spectra were taken on a Voyager DE-STR spectrometer equipped with a N_2 laser (337 nm, 3 ns pulse duration, frequency up to 20 Hz) under vacuum (sample chamber pressure 5.5×10^{-7} torr) using the reflector mode (acceleration voltage 20 000 V). The excitation laser power was set to 2000~3000. Samples were prepared by mixing a $CHCl_3$ solution of polymer (concentration 10 mg/mL, 1 μL), a $CHCl_3$ solution of dithranol (concentration 10 mg/mL, 20 μL), and a methanol solution of silver trifluoroacetate (TFA-Ag) (concentration 0.1 mg/mL, 1 μL) and by drying the mixed solution in a sample well on a gold-plated sample slide under air flow. Absorption and emission spectra were measured at room temperature in a 1-cm quartz cell with a JASCO V-550 spectrophotometer and a JASCO FP-777W fluorescence spectrophotometer, respectively. The fluorescence spectrophotometer was calibrated using an aqueous solution of Rhodamine B. Fluorescent quantum yields were determined with reference to 9,10-diphenylanthracene ($\Phi_F = 0.99$).[23] Samples (THF solutions) were degassed by bubbling N_2 gas through for 10 min.

Simulation

Semi-empirical calculations with the PM5[15] wave function were performed using the Cache ver. 5.02 software package (Fujitsu Ltd.). Molecular dynamic simulations were effected using the COMPASS[24] force field implemented in the Discover module of the Material Studio

3.2 (Accelrys) software package under a constant NVT condition in which the numbers of atoms, volume, and thermodynamic temperature were held constant. Berendsen's thermocouple[25] was used for coupling to a thermal bath. The step time was 1 fsec and the decay constant was 0.1 ps.

References

(1) Nakano, T.; Takewaki, K.; Yade, T.; Okamoto, Y. *J. Am. Chem. Soc.* **2001**, *123*, 9182.

(2) Nakano, T.; Yade, T. *J. Am. Chem. Soc.* **2003**, *125*, 15474.

(3) Nakano, T.; Nakagawa, O.; Tsuji, M.; Tanikawa, M.; Yade, T.; Okamoto, Y. *Chem. Commun.* **2004**, 144.

(4) Nakano, T.; Nakagawa, O.; Yade, T.; Okamoto, Y. *Macromolecules* **2003**, *36*, 1433.

(5) (a) Okamoto, Y.; Nakano, T. *Chem. Rev.* **1994**, *94*, 349-372. (b) Green, M. M.; Park, J.-W.; Sato, T.; Teramoto, A.; Lifson, S.; Selinger, R. L. B.; Selinger, J. V. *Angew. Chem., Int. Ed.* **1999**, *38*, 3138. (c) Fujiki, M. *Macromol. Rapid Commun.* **2001**, *22*, 539. (d) Hill, D. J.; Mio, M. J.; Prince, R. B.; Hughes, T. S.; Moore, J. S. *Chem. Rev.* **2001**, *101*, 3893-4012. (e) Nakano, T.; Okamoto, Y. *Chem. Rev.* **2001**, *101*, 4013. (f) Conrnelissen, J. J. L. M.; Rowan, A. E.; Nolte, R. J. M.; Sommerdijk, N. A. J. M. *Chem. Rev.* **2001**, *101*, 4039.

(6) (a) Okamoto, Y.; Habaue, S.; Isobe, Y.; Suito, Y. *Macromol. Symp.* **2003**, *195*, 75. (b) Tsuji, M.; Sakai, R.; Satoh, T.; Kaga, H.; Kakuchi, T.; *Macromolecules* **2002**, *35*, 8255. (c) Miura, Y.; Satoh, T.; Narumi, A.; Nishizawa, O.; Okamoto, Y.; Kakuchi, T. *Macromolecules* **2005**, *38*, 1041. (d) Ray, B.; Isobe, Y.; Morioka, K.; Habaue, S.; Okamoto, Y.; Kamigaito, M.; Sawamoto, M. *Macromolecules* **2003**, *36*, 543. (e) Matsumoto, A.; Tanaka, T.; Tsubouchi, T.; Tashiro, K.; Saragai, S.; Nakamoto, S. *J. Am. Chem. Soc.* **2002**, *124*, 8891.

(7) (a) Nakano, T.; Mori, M.; Okamoto, Y. *Macromolecules* **1993**, *26*, 867. (b) Nakano, T.; Shikisai, Y.; Okamoto, Y. *Polym. J.* **1996**, *28*, 51. (c) Nakano, T.; Mori, M.; Okamoto, Y. *Macromolecules* **1999**, *32*, 2391. (d) Nakano, T.; Tsunematsu, K.; Okamoto, Y. *Chem. Lett.* **2002**, 42.

(8) Nakano, T.; Matsuda, A.; Okamoto, Y. *Polym. J.* **1996**, *28*, 556.

(9) Hoshikawa, N.; Hotta, Y.; Okamoto, Y. *J. Am. Chem. Soc.* **2003**, *125*, 12380.

(10) (a) Evans, A.; George, D. *J. Chem. Soc.* **1961**, 4653. (b) Evans, A. G.; George, D. B. *J.*

Chem. Soc. **1962**, 141. (c) Yuki, H.; Hotta, J.; Okamoto, Y.; Murahashi, S. *Bull. Chem. Soc. Jpn.* **1967**, *40*, 2659. (d) Richards, D. H.; Scilly, N. F. *J. Polym. Sci., Polym. Lett.* **1969**, *7*, 99.

(11) (a) Okamoto, Y.; Mohri, H.; Nakano, T.; Hatada, K. *J. Am. Chem. Soc.* **1989**, *111*, 5952. (b) Okamoto, Y.; Mohri, H.; Nakano, T.; Hatada, K. *Chirality* **1991**, *3*, 277.

(12) (a) Graham, W. D.; Green, J. D.; Pyror, W. A. *J. Org. Chem.* **1979**, *44*, 907. (b) Husain, A.; Hamielec, A. H. *J. Appl. Polym. Sci.* **1978**, *22*, 1207. (c) Olaj, O. F.; Kauffmann, H. F.; Breitenbach, J. W. *Makromol. Chem.* **1976**, *177*, 3065.

(13) Moad, G.; Solomon, D. H. In *The Chemistry of Free Radical Polymerization*; Pergamon: Oxford, 1995; pp 175-183.

(14) Nakano, T.; Matsuda, A.; Okamoto, Y. *Polym. J.* **1996**, *28*, 556.

(15) Stewart, J. J. P. MOPAC2002 software; Fujitsu Limited: Tokyo, Japan, 2001.

(16) Watson, J. D.; Crick, F. H. C. *Nature* (*London*) **1953**, *171*, 737.

(17) Nelson, J. C.; Saven, J. G.; Moore, J. S.; Wolynes, P. G. *Science* **1997**, *277*, 1793.

(18) (a) Lokey, R. S.; Iverson, B. L. *Nature* (*London*) **1995**, *375*, 303. (b) Nguyen, J. Q.; Iverson, B. L. *J. Am. Chem. Soc.* **1999**, *121*, 2639.

(19) (a) Wang, W.; Li, L.-S.; Helms, G.; Zhou, H.-H.; Li, A. D. Q. *J. Am. Chem. Soc.* **2003**, *125*, 1120. (b) Li, A. D. Q.; Wang, W.; Wang, L.-Q. *Chem. -Eur. J.* **2003**, *9*, 4594. (c) Wang, W.; Han, J. J.; Wang, L.-Q.; Li, L.-S.; Shaw, W. J.; Li, A. D. Q. *Nano Lett.* **2003**, *3*, 455.

(20) Morisaki, Y.; Chujo, Y. *Tetrahedron Lett.* **2005**, *46*, 2533.

(21) Greenhow, E. J.; McNeil, D.; White, E. N. *J. Chem. Soc.* **1952**, 986.

(22) More O'Ferrall, R. A.; Slae, S. *J. Chem. Soc., Chem. Commun.* **1969**, 486.

(23) Eaton, D. F. *Pure Appl. Chem.* **1988**, *60*, 1107.

(24) Sun, H. *J. Phys. Chem.* **1998**, *102*, 7338.

(25) Berendsen, H. J. C.; Postma, J. P. M.; van Gunsteren, W. F.; DiNola, A.; Haak, J. R. *J. Chem. Phys.* **1984**, *81*, 3684.

Chapter 3
Charge Transport in Poly(dibenzofulvene)

3.1 Introduction

Conducting polymers are an important class of material required for organic electronics and optoelectronics.[1] While most conducting polymers so far studied have a long electronic conjugation system in the main chain, a few vinyl polymers with no main-chain conjugation indicate intriguing electronic properties as represented by poly(*N*-vinylcarbazole) (poly(NVCz)), which finds practical applications based on its photoconductivity.[2,3] This chapter describes the electronic properties of poly(dibenzofulvene) (poly(DBF)), a vinyl polymer with a characteristic conformation in which the side-chain chromophores are regularly stacked.[4,5] The hole drift mobility measured by a time-of-flight (TOF) method[6] was much higher than the existing photoconductive vinyl polymers, including poly(NVCz), and was comparable to some main-chain conjugated polymers. In addition, cyclic voltammetry measurements indicated that holes may be delocalized over the π-stacked side groups.

3.2 Charge Transfer Interaction

The poly(DBF) was synthesized by the anionic polymerization of dibenzofulvene (DBF) using 9-fluorenyllithium in tetrahydrofuran (THF) at −78 °C at $[DBF]_o/[Li]_o = 5$.[4,5] MeOH-insoluble, THF-soluble part was used for the measurements (M_n = 1070, M_w/M_n = 1.38, SEC using oligo(DBF)s as the standard sample. Poly(DBF) (20 mg) and 2,4,7-trinitrofluorenylidene-9-malononitrile (TNFMN) (1.0 mg) as an acceptor were dissolved in chloroform (1.0 mL), and the solution was cast on an indiumtin oxide (ITO) glass plate and slowly dried under air to afford a thin film (thickness 5 μm). A circular Au electrode (thickness 20 nm, diameter 5 mm) was vacuum deposited onto the 5-μm thick film to produce a sandwich-type cell for the drift mobility measurement.

In order to investigate the interaction between poly(DBF) and the acceptor molecule, absorption spectra were taken in a chloroform solution and in film (Figure 3.1). Both in the solution and in the film, a weak band, probably due to donor–acceptor interaction, appeared around 520 nm in the mixture of poly(DBF) and TNFMN in addition to the bands due to poly(DBF) and TNFMN. These results indicate that TNFMN is an effective electron

accepting dopant toward poly(DBF). In addition, the spectra indicate that pure poly(DBF) absorbs much less than TNFNM and the mixture at 337 nm. This means that N_2 laser irradiation in TOF experiments will mainly excite the acceptor band or the donor–acceptor band to induce charge separation.

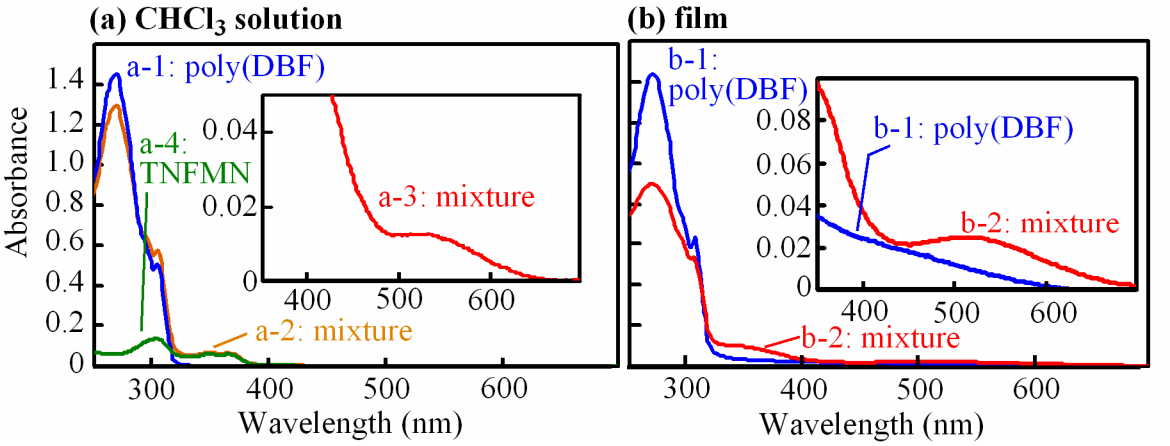

Figure 3.1. Absorption spectra of poly(DBF) in $CHCl_3$ solution (cell length 0.1 mm) (a) and poly(DBF) film (0.5 mm) (b): (a-1) poly(DBF) in $CHCl_3$ ([DBF unit] 1.1×10^{-2} M), (a-2) poly(DBF)–TNFMN mixture in CHCl3 ([DBF unit] 1.1×10^{-2} M, [TNFMN] 2.8×10^{-4} M), (a-3) poly(DBF)–TNFMN mixture in $CHCl_3$ ([DBF unit] 1.1×10^{-1} M, [TNFMN] 2.8×10^{-4} M), (a-4) TNFMN in $CHCl_3$ (2.8×10^{-4} M), (b-1) poly(DBF) film, and (b-2) poly(DBF)–TNFMN film ([DBF unit]/[TNFMN] = 20).

3.3 Time-of-Flight (TOF) Measurements

Charge drift mobility (μ) was estimated by TOF transient photocurrent measurement under vacuum under N_2 pulse laser irradiation (337 nm, pulse duration 3 nsec, 50 μJ). The value of μ was calculated according to $\mu = d/(t_\tau \cdot F)$ ($cm^2V^{-1}s^{-1}$), where d is the film thickness, t_τ is the transit time determined by the TOF experiment, and F is the field strength. By switching polarity in the measurement, it was confirmed that holes mediate the charge drift in the present systems. Figure 3.2 indicates the μ values at different F's and different temperatures. Overall, a higher field strength led to a higher drift mobility; however, a ireversed relationship was observed in the field strength range below 2×10^5 V/cm. In this range, holes may transport in a di.erent path from that predominantly used at the higher field strength,

suggesting that the polymer sample is somewhat heterogeneous in terms of molecular structure and/or intermolecular arrangement. The hole drift mobility was higher at a higher temperature at all field strengths, indicating that the charge drift is thermally activated.

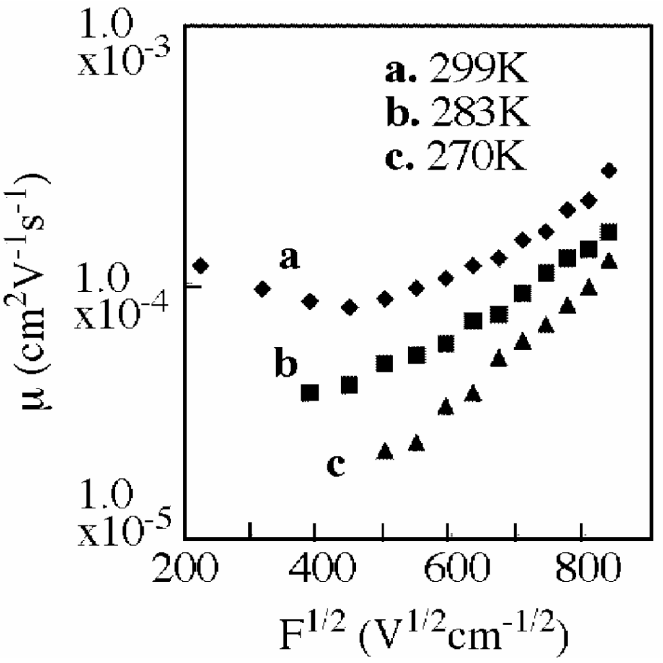

Figure 3.2. Hole drift mobility of poly(DBF) film (4 μm): (a) at 299 K, (b) at 283 K, and (c) at 270 K.

The observed charge drift mobility was as high as 2.7×10^{-4} $cm^2V^{-1}s^{-1}$ at 299K at $F = 7 \times 10^5$ V/cm. This value is higher by the order of 10^3 than those for other side-chain aromatic vinyl polymers including poly(NVCz) and poly(1-vinylpyrene) (10^{-7} $cm^2V^{-1}s^{-1}$ order),[7] and is the highest so far reported for a vinyl polymer although mobility values higher than 10^{-2} $cm^2V^{-1}s^{-1}$ have been reported for some other types of organic polymers.[8] The hole drift mobility is even higher than that of main-chain conjugating poly(p-phenylenevinylene) (1×10^{-5} $cm^2V^{-1}s^{-1}$),[9] is comparable to that of poly(methylphenylsilane) (1×10^{-4} $cm^2V^{-1}s^{-1}$),[10] and is slightly lower than Se (10^{-4} $cm^2V^{-1}s^{-1}$ order),[2] an inorganic semiconductor.

In the film sample, both intramolecular and intermolecular charge transfers may take place, and the observed charge mobility will mainly reflect the slower process. Because the poly(DBF) chains used in this study appear to have disordered intermolecular alignments on the basis of the almost linear field dependences of mobility in the higher field ranges, the

major limiting step of the drift mobility will be the intermolecular charge transfer. This suggests that intramolecular charge transfer may be faster than the bulk mobility characterized by $\mu = 2.7 \times 10^{-4}$ $cm^2V^{-1}s^{-1}$. This idea was supported by cyclic voltammetry measurements of poly(DBF). The oxidation potential for the poly(DBF) measured in a THF solution (0.1 M tetrabutylammonium perchlorate) was 1.49 V (vs Ag/AgCl), which was significantly lower than that for fluorene, a model of monomeric side chain (1.70 V).[5] This indicates that a hole may be readily delocalized over the π-stacked fluorene groups in the side chain, leading to fast intramolecular charge transfer. The ordered π-stacked structure of the poly(DBF) may act as a charge transport pathway.

From the data in Figure 3.2, field-dependent activation energies for the charge transport were calculated to be 0.22 eV at $F = 7.0 \times 10^5$ Vcm^{-1}. This value is much smaller than that of poly(NVCz) (0.4–0.7eV)[2] and is comparable to that of poly(methylphenylsilane) (0.24 eV).[10] For poly(NVCz), locally π-stacked chromophores are trap sites for charge drift,[11,12] and the activation energy corresponds to the thermal hopping-up of charges from the π-stacked trap sites.[2] The smaller activation energies of the poly(DBF) support that the hole transport mechanism in poly(DBF) is completely different from that in poly(NVCz).

3.4 Conclusions

In summary, the charge mobility of poly(DBF) film was found to be as high as some main-chain conjugating polymers. In addition, fast intramolecular charge transport was suggested to take place through the stacked π-electron systems. Charge transport through regularly stacked heteroaromatic systems have been proposed for DNAs where the stacked systems serve as a ‘‘π-way’’[15] although there is controversy as to whether they really conduct.[16] Poly(DBF) may be recognized as a new, synthetic ‘‘π-way’’ molecule. Further studies are under way, to establish the charge transport through single molecule of π-stacked poly(DBF), and to expand the π-stacked molecular design to other versatile synthetic polymers.

References

(1) Strohriegl, P.; Grazulevicius, J. V. In *Handbook of Organic Conductive Molecules and Polymers*; Nalwa, H. S., Ed.; Wiley: New York, 1997; Vol. 1, Chapter 11.

(2) Pearson, J. M.; Stolka, M. *Poly(N-Vinylcarbazole)*; Gordon and Breach: New York, NY,

1981; Chapter 4.

(3) Ellis, J. R. In *Handbook of Conducting Polymers*; Skotheim, T. A. Ed.; Marcel Dekker: New York, 1986; Vol. 1, Chapter 13.

(4) Nakano, T.; Takewaki, K.; Yade, T.; Okamoto, Y. *J. Am. Chem. Soc.* **2001**, *123*, 9182.

(5) Nakano, T.; Yade, T. *J. Am. Chem. Soc.* **2003**, *125*, 15474.

(6) (a) Borsenberger P. M.; Weiss, D. S. *Organic Photoreceptor Systems for Imaging Systems*; Marcel Dekker: New York, 1993. (b) Shirota, Y. *J. Mater. Chem.* **2000**, *10*, 1. (c) P. Strohriegl, *Adv. Mater.* **2002**, *14*, 1439.

(7) Gill, W. *J. Appl. Phys.* **1972**, *43*, 5033 .

(8) (a) Hoofman, R. J. M. O.; de Haas, M. P.; Siebbeles, L. D. A.; Warman, J. M. *Nature* **1998**, *392*, 54. (b) Grozema, F. C.; Siebbeles, L. D. A.; Warman, J. M.; Seki, S.; Tagawa, S.; Scherf, U. *Adv. Mater.* **2002**, *14*, 228 . (c) Grozema, F. C.; van Duijnen, P. T.; Berlin, Y. A.; Ratner, M. A.; Siebbeles, L. D. A. *J. Phys. Chem. A* **2003**, *107*, 5976.

(9) Forero, S.; Nguyen, P. H.; Brütting, W.; Schwoerer, M. *Phys. Chem. Chem. Phys.* **1999**, *1*, 1769.

(10) Kepler, R. G.; Zeigler, J. M.; Kurtz, S. R. *Phys. Rev. B* **1987**,*35*, 281.

(11) Yokoyama, M.; Akiyama, K.; Yamamori, N.; Mikara, H.; Kusabayashi, S. *Polym. J.* **1985**, *17*, 545.

(12) Fujino, M.; Mikawa, H.; Yokoyama M. *Photogr. Sci. Eng.* **1982**, *26*, 84.

(13) (a) Murphy, C. J.; Arkin, M. R.; Jenkins, Y.; Ghatlia, N, D.; Bossman, S. H.; Turro, N. J.; Barton, J. K. *Science* **1993**, *262*, 1025. (b) Okahata, Y.; Kobayashi, T.; Tanaka, K.; Shimomura, M. *J. Am. Chem. Soc.* **1998**, *120*, 6165. (c) Fink, H.-W.; Schönenberger, C. *Nature* **1999**, *398*, 407. (d) Porath, D.; Bezryadin, A.; de Vries, S.; Dekker, C. *Nature* **2000**, *403*, 635

(14) (a) Braun, E.; Eichen, Y.; Sivan, U.; Ben-Yoseph, C. *Nature* **1998**, *391*, 775. (b) Debije, M. G.; Milano, M. T.; Benhard, W. A. *Angew. Chem., Int. Ed.* **1999**, *38*, 2752. (c) Maiya, B. G.; Ramasarma, T. *Curr. Sci.* **2001**, *80*, 1523.

Chapter 4
Synthesis, Structure, and Photophysical and Electrochemical Properties of Poly(2,7-di-*t*-butyldibenzofulvene)

4.1 Introduction

Spatial arrangement of π-electronic groups (chromophores) often has a significant influence on the photoelectronic and photophysical properties of organic materials.[1,2] Conformational control of macromolecules bearing side-chain π-electronic groups is an effective means to realize a regulated, specific chromophore arrangement. In line with this idea, the author synthesized polydibenzofulvene (poly(DBF)) having a π-stacked conformation in which the side-chain fluorene moieties are closely stacked on top of each other and the main-chain carbon-carbon bonds have a slightly twisted all-trans structure as described in Chapters 1 and 2.[3,4] This polymer indicated effective charge transport properties based on the stacked π-electron systems as discussed in Chapter 3.[5]

This chapter deals with the polymerization of 2,7-di-*t*-butyldibenzofulvene (tBu_2DBF)[6] and the structure and properties of the polymerization products. Polymer conformation and properties are often largely altered by introducing a side-chain group. Such cases have been know for helical polymethacrylates: helical sense excess, helix stability, and chiral recognition ability are greatly affected by the structure of the side chain group.[7,8] In this study, two bulky *t*-butyl group were introduced to dibenzofulvene structure at the 2- and 7-positions to examine the side-chain effect on the monomer reactivity and product structure.

4.2 Polymerization

tBu_2DBF was synthesized according to Scheme 4.1A. This monomer was stable in the solid state under air at room temperature, whereas DBF copolymerizes with oxygen under the same condition.[9]

Scheme 4.1 Synthesis and Anionic Polymerization of tBu_2DBF

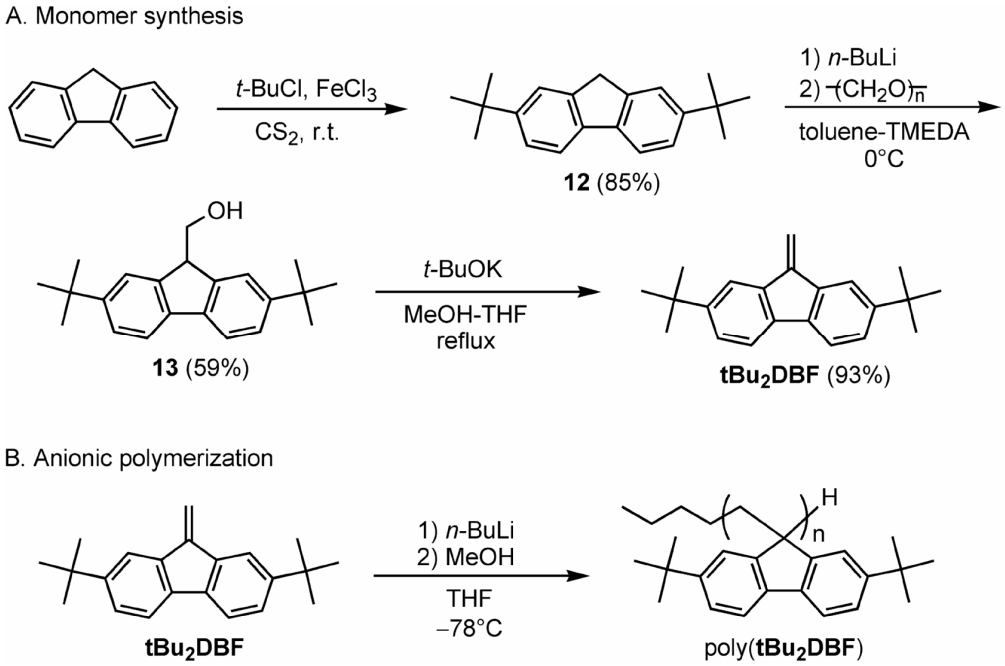

Table 4.1 Polymerization of 2,7-Di-*t*-butyldibenzofulvene (tBu_2DBF) with *n*-BuLi[a]

								THF-soluble part yield[b] (%)		
run	solvent	temp. (°C)	$[tBu_2DBF]_o$ (M)	$[Li]_o$ (M)	$[tBu_2DBF]_o/[Li]_o$	conv.[b] (%)	THF-insoluble part[c] (%)	trimer (n = 3[d])	dimer (n = 2[d])	unimer (n = 1[d])
1	THF	–78	0.20	0.010	20	20	0	17	3	0
2	Toluene	0	0.20	0.010	20	7	0		not determined	
3	THF	–78	0.80	0.040	20	30	27	2	1	0
4	THF	–78	0.20	0.040	5	64	0	58	6	0
5	THF	–78	0.20	0.20	1	>99	0	0	40	60
6	THF	–78	0.040	0.040	1	>99	0	0	45	55

[a] Monomer: 1.4 mmol (run 1,3), 1.6 mmol (run 2), 0.34 mmol (run 4–6); Time, 24 h. [b] Determined by ^{1}H NMR. [c] Determined gravimetrically. [d] See Scheme 4.1B for structure. [e] A mixture of unimer to trimer. The ratio of the three oligomers is not known.

Aiming at the polymerization reaction shown in Scheme 4.1B, tBu_2DBF was polymerized under anionic reaction conditions. The conditions and results of the reactions using *n*-BuLi in THF at –78°C and in toluene at 0°C are summarized in Table 4.1. In the polymerization at $[monomer]_o/[initiator]_o$ = 20 at $[monomer]_o$ = 0.20 M both in THF at –78°C and in toluene at 0°C, only oligomers were obtained at a low conversion (runs 1, 2). On increasing $[monomer]_o$ from 0.20 M to 0.80 M at the same $[monomer]_o/[initiator]_o$ in THF at –78°C (run 3), the monomer conversion was improved and a THF-insoluble fraction was obtained. The

THF-insoluble part is assumed to be a polymer with a higher degree of polymerization (DP) compared with the THF-soluble part. IR spectra supported that the THF-soluble and –insoluble parts have the identical chemical structure. The insolubility may arise from a very rigid polymer structure. These results suggest that the production of only oligomers at low conversion in run 1 and 2 is not due to a side reaction such as quenching of the growing anion but to the sluggish nature of the tBu_2DBF polymerization. This is supported by the fact that the polymerization systems indicated a deep orange color due to the fluorenyl-type growing anion until they were quenched by the addition of methanol containing HCl. tBu_2DBF appears much less reactive than DBF probably because of its bulkiness. Under similar reaction conditions, DBF quantitatively affords a polymer.[3,4] The reactions at $[monomer]_o/[initiator]_o = 5$ and 1 (run 4–6) led to only THF-soluble oligomers in much higher yields than at $[monomer]_o/[initiator]_o = 20$.

The THF-soluble oligmers were found to consist of the three main components in addition to the residual monomer by SEC analyses (Figure 4.1): they were found to be unimer, dimer, and trimer corresponding the oligomer structure in Scheme 4.1B with n = 1, 2, and 3, respectively, by mass spectrometric analysis as discussed in the next section. It is noteworthy that no trimer was detected in the products at $[monomer]_o/[initiator]_o = 1$ where the dimer was the major product and that only a trace amount of tetramer and higher oligomers were detected in the products at $[monomer]_o/[initiator]_o = 2$ and 5 where the trimer was the major product. Along with the fact that monomer was quantitatively consumed at $[monomer]_o/[initiator]_o = 1$ (runs 5, 6), these observations indicate that monomer addition to the unimer anion is faster than that to *n*-BuLi, and that there is a significant energy barrier in the propagation step from the trimer anion to the tetramer anion. Also, it is quite likely that once the tetramer anion is formed upon monomer addition to the trimer anion, it quickly propagates to the THF-insoluble polymer. A similar propagation profile has been reported for asymmetric polymerization of triphenylmethyl methacrylate giving a single-handed helical polymer.[10] The THF-insoluble poly(tBu_2DBF) might possibly have a regulated conformation that could be tightly packed to lead to an insoluble, crystalline material.

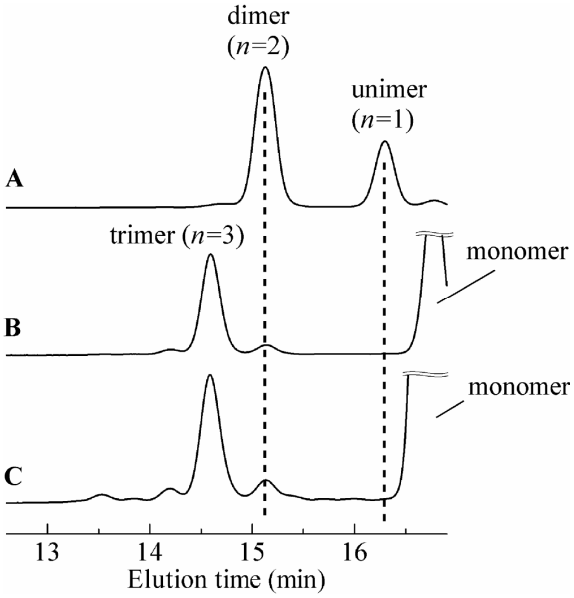

Figure 4.1 SEC curves (UV detection at 254 nm) of the THF-soluble products obtained at $[tBu_2DBF]_0/ [Li]_0$ = 1 (run 5 in Table 4.1, A); 5 (run 4 in Table 4.1, B); and 20 (run 1 in Table 4.1, C).

4.3 Structural Analyses of Oligomers by Mass, 1D NMR, and COSY Spectra

The three major components in the oligomeric products were isolated by preparative SEC and subjected to detailed structural analyses. High-resolution FAB mass analyses confirmed the chemical structure of the oligomers with different DPs: unimer (n = 1), HRMS(FAB) calcd for $C_{26}H_{36}$: 348.2817, found 348.2811; dimer (n = 2), HRMS(FAB) calcd for $C_{48}H_{62}$: 638.4851, found 638.4835; timer (n = 3), HRMS(FAB) calcd for $C_{70}H_{88}$: 928.6886, found 928.6881.

Figure 4.2 shows the NMR spectra of the three oligomers taken in $CDCl_3$. In the spectra shown in Figure 4.2, it is clear that most aromatic proton signals of the trimer are up-field shifted compared with those of the dimer and the unimer, suggesting that the trimer has a π-stacked conformation.

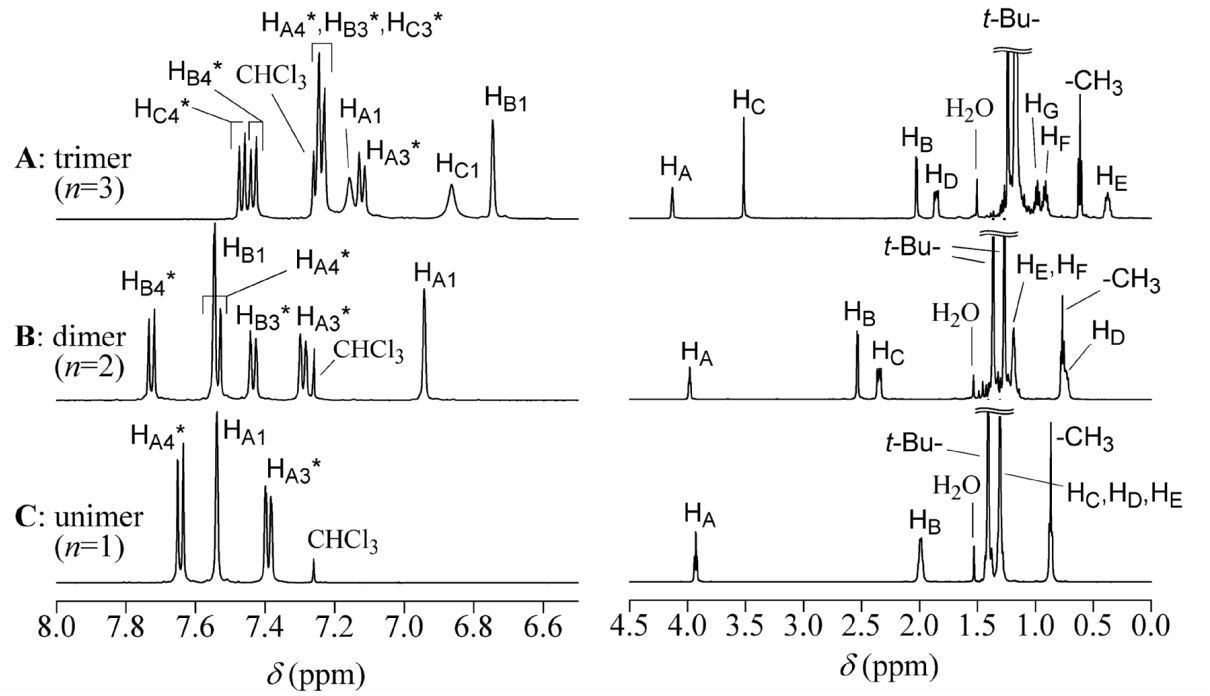

Figure 4.2 ^{1}H NMR spectra of tBu_2DBF trimer (n = 3, A); dimer (n = 2, B); and unimer (n = 1, C) [500 MHz, $CDCl_3$, r.t.]. The assignments of the aromatic protons marked by * are, in part, arbitrary (see text).

Table 4.2. ^{1}H NMR Chemical Shifts (δ, ppm) of the tBu_2DBF Oligomers[a]

proton	unimer (n = 1)	dimer (n = 2)	trimer (n = 3)
H_A	3.93 (t)	3.98 (t)	4.13 (t)
H_B	1.99 (q)	2.35 (d)	2.03 (d)
H_C	1.30 (m)	2.53 (d)	3.52 (d)
H_D	1.30 (m)	0.75 (m)	1.86 (m)
H_E	1.30 (m)	1.19 (m)	0.38 (m)
H_F		1.19 (m)	0.91 (m)
H_G			0.98 (m)
CH_3	0.87 (t)	0.77 (t)	0.62 (t)
t-Bu	1.41 (s)	1.27 (s),	1.18 (s),
		1.26 (s)	1.16 (s)
H_{A1}	7.54 (s)	6.94 (s)	7.16 (s)
H_{B1}		7.55 (s)	6.75 (s)
H_{C1}			6.86 (s)
other	7.64 (d)	7.73 (d)	7.47 (d)
aromatic	7.39 (d)	7.54 (d)	7.43 (d)
protons[b]		7.44 (d)	7.24 (d)[c]
		7.29 (d)	7.12 (d)

[a] See Scheme 4.2 for proton numbering systems. Spectra were recorded in $CDCl_3$ at room temperature (500 MHz). Residual $CHCl_3$ signal (7.26 ppm) was used as an internal reference. [b] Assignments are in part arbitrary. [c] With six-proton intensity.

The peaks were assigned as indicated in Figure 4.2 using the proton numbering systems shown in Scheme 4.2, and the chemical shifts of the signals are summarized in Table 4.2. To achieve accurate $–CH_2–$ peak assignments for the trimer and the dimer, H-H COSY spectra were taken (Figure 4.3). In the COSY spectra of the trimer (Figure 4.3A), the triplet peaks at 0.62 ppm were first assigned to the $–CH_3$ group in the butyl group originating from *n*-BuLi, and the correlation between $–CH_3$ and H_G and that between H_G and H_F were confirmed by the COSY chart. Although no clear correlation was observed between H_F and H_E, the signal in the highest magnetic field, was assigned to be H_E because the $–CH_3$ group of the terminal ethyl group of oligo(DBF)s has been reported to resonate in the highest magnetic field due to the anisotropic effect of the aromatic group.[4] Then, H_D was identified by the correlation with H_E. The terminal methine proton (H_A) was identified based on its single-proton intensity and triplet coupling pattern, and a clear correlation signal was seen between H_A and H_B. Finally, the remaining peak with two-proton intensity at 3.52 ppm showing no clear correlation with any other protons was assigned to be H_C. The assignments of the peaks in the dimer spectra (Figure 4.2B; Figure 4.3B) were completed in a similar way.

For the aromatic protons, the pairs belonging to the same fluorene moiety were identified by the COSY correlations, but the detailed assignments of H_{X3} and H_{X4} (X = A–C) remained arbitrary.

Scheme 4.2 Proton Numbering Systems of tBu_2DBF Oligomers

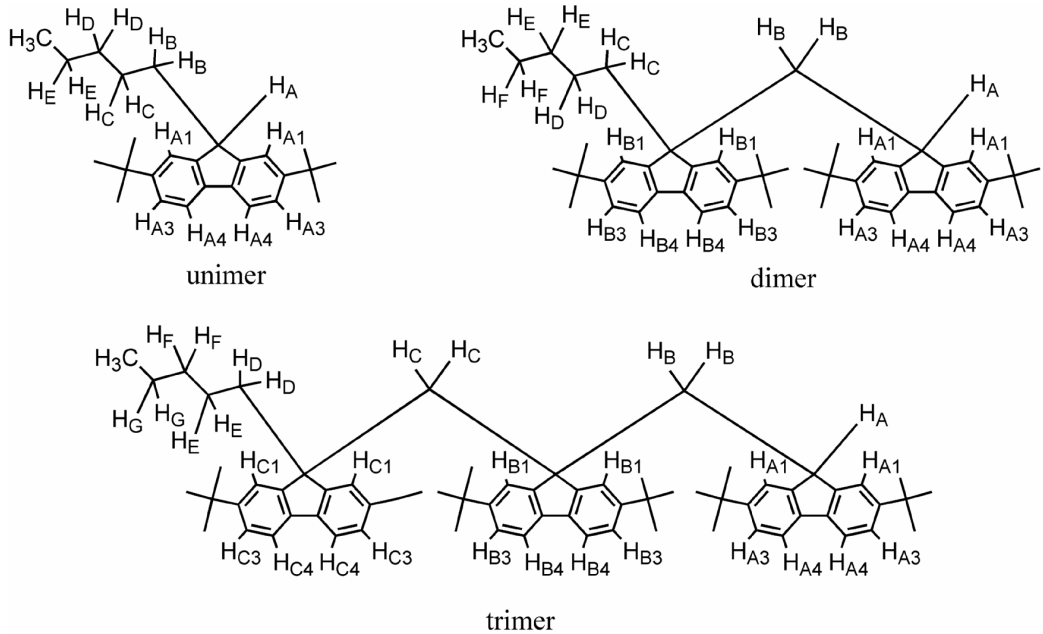

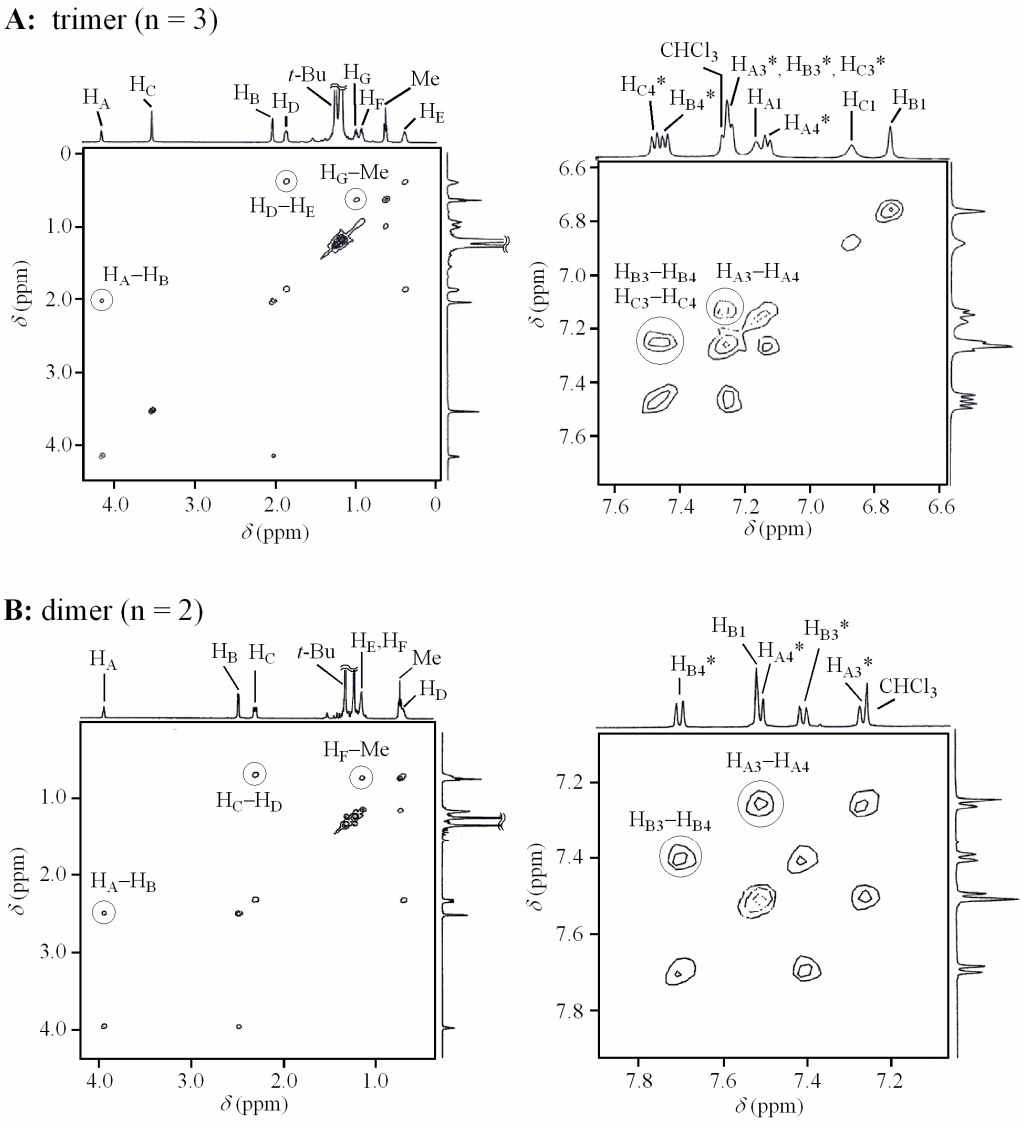

Figure 4.3 H-H COSY spectra of tBu_2DBF trimer (n = 3, A) and dimer (n = 2, B): alkyl (left) and aromatic (right) regions. The assignments of the aromatic protons marked by * are, in part, arbitrary (see text).

4.4 Conformational Analyses of Trimer by NOESY Spectra and Semi-Empirical Calculations

Conformations of the trimer was assessed using the NOESY spectral information (Figure 4.4A) combined with the semi-empirical energy calculation by the PM5 method. In the aromatic region of the trimer spectrum, the signal at 7.16 ppm was identified as H_{A1} because only this signal among the singlet aromatic signals due to H_{A1}–H_{C1} had a clear NOE correlation with H_A (terminal proton) (Figure 4.4A, right). This assignment is reasonable because the distance between the two is fixed to be ca. 3 Å in dependent of conformational variations. Among the remaining two, the one at 6.75 ppm was attributed to H_{B1} because this signal had a NOE correlation with H_B in the same monomeric units. (This assignment was consistent with the most stable conformation found by PM5 calculasions.) With these aromatic peaks assignments, H_A–H_C, H_B–H_C, H_C–H_D, H_A–H_{A1}, H_B–H_{B1}, H_C–H_{A1}, H_C–H_{B1}, and H_C–H_{C1} correlations are evident in Figure 4.4A.

The H_A–H_C and H_C–H_{A1} correlations between the two terminal units would rule out a completely π-stacked conformation with a zigzag main-chain structure such as that of poly- and oligo(DBF)s[4] and suggest a conformation where H_C and the monomeric unit at the termination end (ω-end) are close.

To find a conformation that fits to the NOESY spectra, seven conformers of the trimer were optimized by the semi-empirical PM5 method and their heats of formation were compared. In addition, each was examined if it satisfies the following criterion. Regarding the relation between proton–proton distance and NOE correlation, the author can rely on the results of our detailed structural analyses of DBF oligomers.[4] For a DBF-hexamer having terminal ethyl groups whose conformation has been unambiguously determined to π-stacked as shown in Figure 4.5 (top), both in the solid state and in solution, clear NOE correlations were observed between main-chain methylene protons of the neighboring monomeric units and between the methylene protons and the C1-protons in the closest fluorene unit that are separated by a distance of about 2.4–2.8 Å. In contrast, no NOE correlations were confirmed between main-chain methylenes of the other monomeric units that are separated by a distance of 4.4 Å. Hence, H_C–H_A and H_C–H_{A1} distances (the shorter ones where different distances are available) should be in the range of 2.4–2.8 Å or shorter in a plausible conformation.

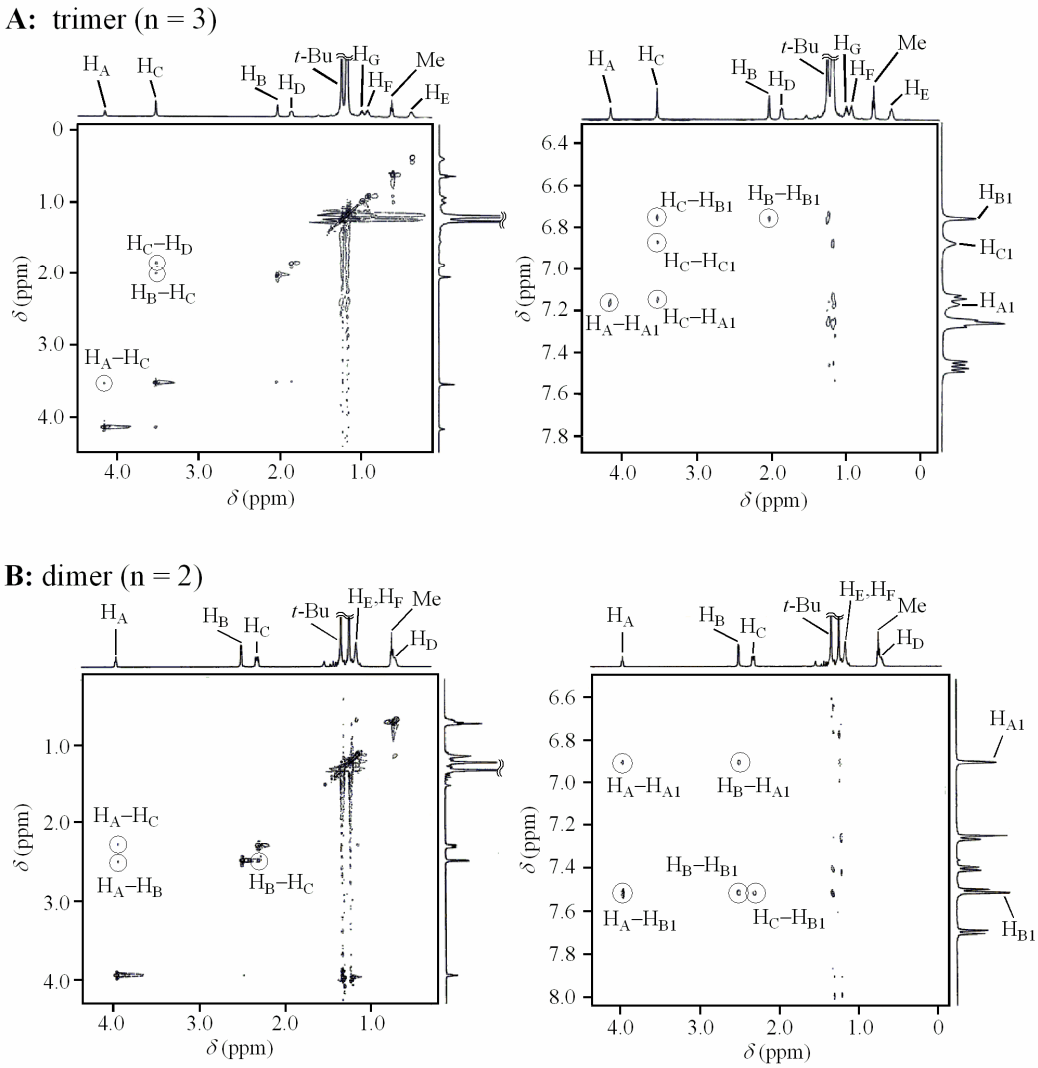

Figure 4.4 NOESY spectra of tBu_2DBF trimer (n = 3, A) and dimer (n = 2, B): alkyl–alkyl (left) and alkyl–aromatic (right) correlation regions.

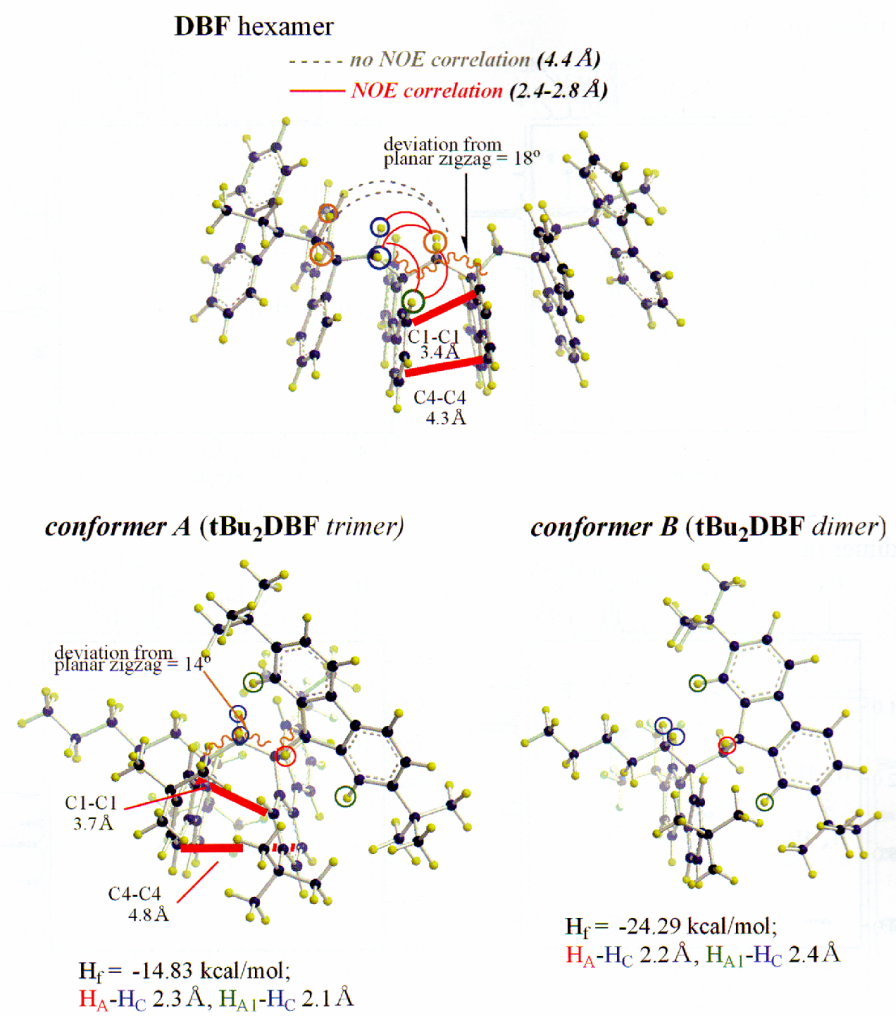

Figure 4.5 Conformation of DBF hexamer obtained by PM5 optimization of the crystal structure with geometrical characteristics (top) and the most plausible conformers of tBu_2DBF trimer (conformer A, bottom left) and dimer (conformer B, bottom right) with heat of formation values (H_f), and H_A–H_C and H_{A1}–H_C distances. For the tBu_2DBF conformers, H_A, H_C, and H_{A1} are marked by red, blue, and green circles, respectively.

The hexamer structure shown in Figure 4.5 (top) was obtained by optimizing the crystal structure by PM5. The fact that the optimized structure was very similar to the original structure suggests that the PM5 method is reliable in the structural analyses of DBF oligomers and their derivatives. Among the seven examined conformers, only conformer A shown in Figure 4.5 (bottom, left) having the lowest heat of formation could indicate both H_C–H_A and H_C–H_{A1} correlations based on the H_C–H_A and H_C–H_{A1} distances. Hence, conformer A is the most plausible conformation of the trimer. In conformer A, the fluorene moieties in the

central and initiation-side monomeric units are stacked on top of each other in a twisted arrangement. This is in line with the up-field shift of the aromatic peaks of the trimer (Figure 4.2A). Conformer A well-explains the tBu_2DBF's polymerization behavior in which there is a significant energy barrier in monomer addition to the trimer anion. The anion site, which is roughly assumed to be in the position of H_A, seems too much crowded to accept the bulky tBu_2DBF monomer.

4.5 Conformational Analyses of Dimer by NOESY Spectra and Semi-Empirical Calculations

Conformation of the dimer was also investigated by NOESY spectra and PM5 calculations. In the aromatic region of the dimer NMR spectra (Figure 4.2B), the signal at 7.55 ppm was attributed to H_{B1} in the initiation-side monomeric unit because H_{A1} in the unimer resonated at almost the same frequency. With this assignment, H_A–H_C, H_A–H_B, H_A–H_{A1}, H_A–H_{B1}, H_B–H_{A1}, H_B–H_{B1}, and H_C–H_{B1} correlations are confirmed in Figure 4.4B. To find a conformation fitting to the NOESY spectra, four conformers of the dimer were optimized by the PM5 method. Among the four, only conformer B shown in Figure 4.5 (bottom, right) with the lowest heat of formation had the H_A–H_C and H_{A1}–H_C distances, which are consistent with the observed NOE correlations, suggesting that conformer B is the most plausible as dimer conformation. The position of H_A in conformer B, similarly to that in conformer A, is too much crowded for the reaction with the bulky tBu_2DBF monomer. The relative spatial arrangment of the two monomeric units in conformer B is very similar to that of the central and termination-side monomeric units in conformer A. This is consistent with the significant chemical shift difference between H_B of the dimer and H_C of the trimer. Although both these protons belong to the monomeric units at the initiation terminal, the two H_B protons of the dimer are rather sandwiched by the two 2,7-di-*t*-butylfluorenyl moieties and may experience shielding effects while the two H_C protons of the trimer are in the positions susceptible to deshielding effects of the nearby aromatic groups. Hence, H_B of the dimer was up-field shifted by more than 1 ppm compared with H_C of the trimer. About the trimer and dimer conformations, it should also be noted that conformer A and conformer B may have a different dynamic characteristics. Evidently, in the ^{1}H NMR spectra of the trimer and dimer shown in Figure 4.2, the signals due to H_{A1} and H_{C1} of the trimer are clearly broader compared with the other aromatic peaks of the trimer (Figure 4.2A) and all the aromatic peaks

of the dimer (Figure 4.2B). This may mean that the trimer conformation is at least partially more confined and less dynamic than the dimer conformation.

4.6 Photophysical Properties of Oligomers

Figure 4.6 shows the absorption and fluorescence spectra of the unimer, the dimer, and the trimer. The molar absorption coefficient (ε) in the absorption spectra has been calculated based on the molar concentration of tBu_2DBF monomeric unit. In the absorption spectra (Figure 4.6A), a clear hypochromic effect and a slight bathochromic shift (red shift) were observed for the trimer and the dimer as compared with the unimer. The hypochromic effect of the trimer can be interpreted in terms of the two stacked monomeric units as in conformer A in Figure 4.5. Although the two fluorene moieties in conformer B of the dimer are not in a π-stacked arrangement, which appears not consistent with the hypochromicity, the dimer may have a relatively flexible conformation, and π-stacked conformations in a dynamic conformational mixture may contribute to the observed hypochromicity. The same consideration may be applicable to the termination-side fluorene moiety of the trimer: the termination-side monomeric units may have a dynamic conformation to a certain extent.

In the fluorescence spectra (Figure 4.6B), all three oligomers indicated mainly a monomer emission band and almost no excimer (intramolecular dimer) emission. This is in contrast to the fact that oligo(DBF)s showed exclusively an excimer emission. In our previous study, even the DBF dimer having hydrogens at the chain terminal, which was revealed *not to* have a stacked conformation as the most stable structure in the ground state, showed a clear excimer emission in addition to a monomer emission.[4]

It is interesting that the tBu_2DBF trimer having the partial π-stacked conformation does not show intramolecular dimer emission. In order to specify the reason for this observation, the most stable conformation of the tBu_2DBF trimer (Figure 4.5, bottom left) was compared with the conformation of DBF hexamer haiving terminal ethyl groups based on the crystal strucuture analysis[4] (Figure 4.5, top). In conformation A of the tBu_2DBF trimer, the stacked di-*t*-butylfluorene units are twisted by a dihedral angle of 14° (the deviation from a completely planar zigzag chain) and the distance between the two units are characterized by the C1–C1 distance of 3.7 Å and the C4–C4 distance of 4.8 Å where C1 and C4 means the carbon at the 1- and 4-positions of fluorene unit (cf. C9 at the 9-position is a part of the main chain). In the structure of DBF hexamer, for the central two fluorene units, the twist angle is

18° and the C1–C1 and C4–C4 distances are 3.4 Å and 4.3 Å, respectively.

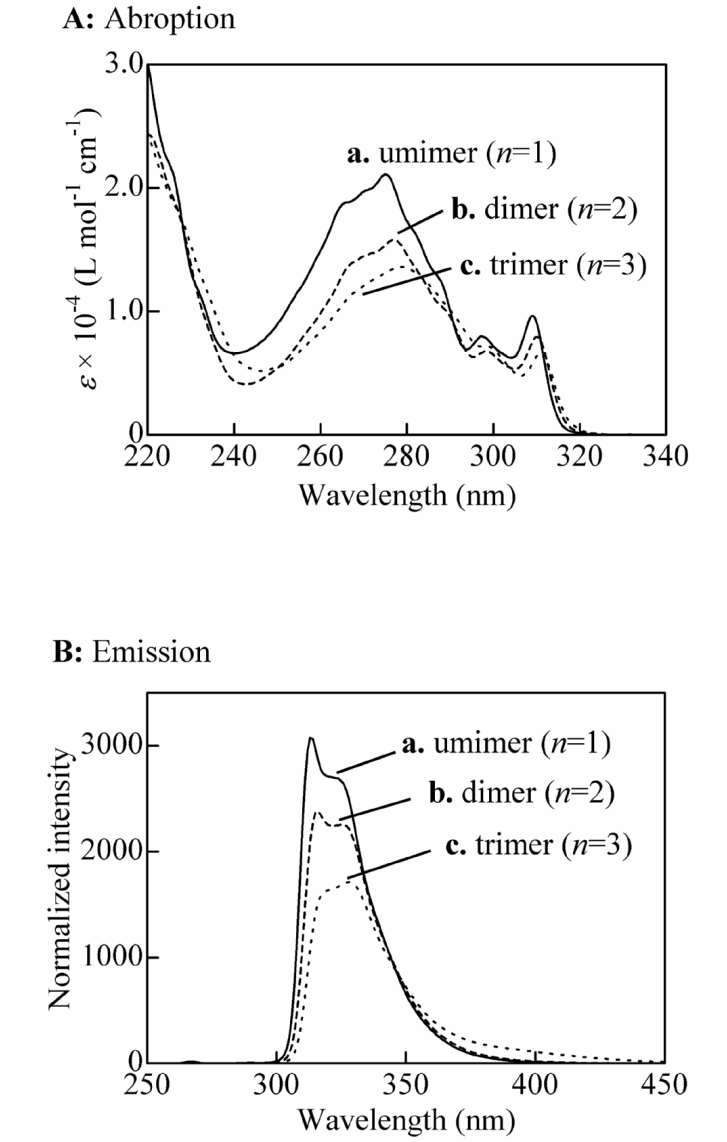

Figure 4.6 Absorption (A) and fluorescent emission (B) spectra of tBu_2DBF trimer (n = 3, c), dimer (n = 2, b), and unimer (n = 1, a) [THF, r.t.]. Molar absorption coefficient (ε) in (A) was calculated with respect the molar concentration of di-t-butylfluorene unit. Excitation wavelength (λ_{ex}) in (B) was 267 nm. Emission intensity in (B) was normalized to a constant absorbance at 267 nm. The arrow in (B) indicates the excimer emission position of poly(DBF).

It is not likely that the minor differences in the π-stacked geometry of the DBF hexamer and tBu_2DBF trimer are responsible for the different emission profiles. The author propose that the stacked fluorene units in the DBF hexamer takes a minor motion upon photoexcitation to form an almost completely face-to-face stack or a closer geometry stack geometry of the two fluorene units than in the ground state to form an excited intramolecuar dimer, while such a local conformational transition is blocked in the tBu_2DBF trimer by the steric repulsion of the bulky *t*-butyl groups. The tBu_2DBF dimer may also not be able to take a very close π-stacked conformation suitable for excimer emission in a conformational dynamics due to steric reasons. In other words, although the reported DBF oligomers appear to have a closely stacked conformation, it might not show an excimer emission if the conformation is frozen, for example, in a solid matrix or at an extremely low temperature. The excited intramolecuar dimer of poly- and oligo(DBF)s may have a slightly different stack geometry than that in the ground state as in the crystal structure and in the solution structure proved by NMR analyses.

The monomer emission band shape of tBu_2DBF trimer was clearly different from that of the dimer and the unimer. This band shape may be inherent to the twisted π-stacked conformation.

4.7 Conclusions

tBu_2DBF, a bulky DBF derivative, was synthesized and polymerized using *n*-BuLi as anionic initiator. tBu_2DBF was found much less reactive in polymerization compared with DBF and mainly gave unimer, dimer, and trimer in most cases, while it led to an insoluble polymer under selected conditions. Conformational analyses of the tBu_2DBF trimer and dimer by means of NOESY NMR spectra and PM5 calculations indicated that the trimer has, in part, a stable π-stacked conformation and the dimer has no stable, π-stacked conformation. The proposed conformations were consistent with the low reactivity of tBu_2DBF. Although the tBu_2DBF oligomers showed clear hypochromicity in absorption spectra indicative of a π-stacked conformation, they showed no or only very weak excimer emission. A local molecular motion of aromatic groups leading to a very close or an almost completely face-to-face stack geometry upon photo irradiation may be necessary to form an excited intramolecular dimer such as that of DBF oligomers. Such a complete π-stacked geometry suitable for excited intramoelcular dimer formation in the excited state is probably impossible

for the tBu_2DBF oligomers due to steric repulsion. The results of the present study indicate that a π-stacked structure, in general, cannot be ruled out because of the absence of intramolecular dimer emission.

Although potential functions of the tBu_2DBF oligomers have not yet been explored, the trimer might be useful as a new material for photophysical and electronic applications based on the partially π-stacked conformation. This study indicated that the trimer can be obtained as the main product under a selected condition (run 4 in Table 4.1) and readily purified by chromatography. This will make it possible to supply the trimer in pure form for functional studies without laborious fractionation processes which are often unavoidable in obtaining uniform oligomer samples.

4.8 Experimental Section

Materials

Fluorene (Wako, >95%), *t*-butyl chloride (Wako, >95%), $FeCl_3$ (Wako, >95%), CS_2 (Wako, >95%), potassium *t*-butoxide (Wako, 85%), $MgSO_4$ (nacalai, 99%), CaH_2 (Nacalai), $LiAlH_4$ (Wako, 80%), methanol (Wako, >99%), $CHCl_3$ (Wako, >98%), CH_2Cl_2 (Wako, >98%), hexane (Wako, >95%), and ethyl acetate (Wako, >99%) were used as obtained. *n*-BuLi (Nacalai, 1.6 M) were used after titration. *N*,*N*,*N*',*N*'-tetramethylethylenediamine (TMEDA) (TCI) were dried over CaH_2, distilled, and stored under N_2 atmosphere. Paraformaldehyde (Wako, >95%) was dried under reduced pressure in the presence of P_5O_2. Tetrahydrofuran (THF) (Wako) was refluxed over sodium benzophenone ketyl, distilled, and stored on $LiAlH_4$ under N_2 atmosphere, and distilled again under vacuum immediately before use. Toluene (Wako) was refluxed over sodium, distilled and stored on sodium under N_2 atmosphere.

2,7-Di-t-butylfluorene[11]

The reactions were carried out under N_2 atmosphere. Fluorene (30.5 g, 184 mmol), $FeCl_3$ (14.8 g, 91 mmol), and CS_2 (300 mL) were mixed to afford a heterogeneous mixture. *t*-Butyl chloride (50 mL, 460 mmol) was added dropwise to the mixture during a 10-min period with vigorous stirring. After the addition, the reaction mixture was stirred at room temperature for 7 hr and was then decomposed by adding H_2O (ca. 300 mL). The mixture was extracted with CH_2Cl_2. The organic layer was washed with saturated aqueous sodium bicarbonate and brine, dried on $MgSO_4$, and concentrated. The crude product was purified by flash silica gel column chromatography with hexane as eluent to afford

2,7-Di-*t*-butylfluorene (**12**) (43.6g, 85%) as a colorless crystalline solid: mp 120.1-120.6°C (lit. mp 120-122°C,[11a] 122°C[11b]).

^{1}H NMR (500 MHz, $CDCl_3$, Me_4Si) δ 7.68 (d, *J*=8.0Hz, 2H), 7.58 (s, 2H), 7.41 (d, *J* =8.0Hz, 2H), 3.88 (s, 2H), 1.40 (s, 18H). ^{13}C NMR (125 MHz, $CHCl_3$) δ 149.42, 143.25, 139.12, 123.76, 121.84, 119.07, 37.08, 34.80, 31.62. IR (KBr) 2959, 2895, 2868, 1473, 1358, 1261, 1163, 817, 716 cm^{-1}. HRMS (EI) calcd for $C_{21}H_{26}$, 278.2034; found 278.2038.

2,7-Di-t-butyl-9-hydroxymethylfluorene

The reactions were carried out under N_2 atmosphere. *n*-BuLi (1.6 M solution in hexane) (68 mL, 110 mmol) was added dropwise to a solution of **12** (10.0 g, 37.0 mmol) in toluene (570 mL) containing TMEDA at 0°C. After stirring the reaction mixture at 0°C for 5 min, paraformaldehyde (3.25 g) suspended in toluene (30 mL) was added. The reaction mixture was stirred at 0°C for 150 min, and H_2O (ca. 10 mL) was then added. The mixture was extracted with ethyl acetate. The organic layer was washed with saturated aqueous sodium bicarbonate and brine, dried on $MgSO_4$, and concentrated. The crude product was purified by flash silica gel column chromatography with a hexane-EtOAc mixture (15/1, v/v) to afford 2,7-di-*t*-butyl-9-hydroxymethylfluorene (**13**) (6.75 g, 59%) as a pale yellow crystalline solid: mp 101.5-103.0°C.

^{1}H NMR (500 MHz, $CDCl_3$, Me_4Si) δ 7.64 (d, *J*=8.0Hz, 2H) , 7.61 (d, *J* =2.0Hz, 2H), 7.34 (dd, *J* =8.0, 2.0Hz, 2H), 4.06 (s, 3H), 1.37 (s, 18H). ^{13}C NMR (125 MHz, $CHCl_3$) δ 149.89, 144.29, 138.93, 124.66, 121.39, 119.26, 65.33, 50.47, 34.87, 31.61. IR (KBr) 3322, 2955, 2866, 1476, 1361, 1259, 1058, 817, 735 cm^{-1}. HRMS (EI) calcd for $C_{22}H_{28}O$, 308.2140; found 308.2138.

2,7-Di-t-butyldibenzofulvene[6] (tBu_2DBF)

Potassium *t*-butoxide (*t*-BuOK; 2.03 g, 18.1 mmol) and **2** (2.04 g, 6.62 mmol) were dissolved in a mixed solvent of methanol (40 mL) and THF (40 mL). The reaction mixture was refluxed for 10 min and then decomposed by adding H_2O (ca. 50 mL). The mixture was extracted with hexane. The organic layer was washed with brine, dried on $MgSO_4$, and concentrated. The crude product was purified by flash silica gel column chromatography with hexane as eluent to afford tBu_2DBF (1.78 g, 93%) as a pale yellow solid: mp 158.6-160.5°C.

^{1}H NMR (500 MHz, $CDCl_3$, Me_4Si) δ 7.74 (d, *J*=2.0Hz, 2H) , 7.56 (d, *J* =8.0Hz, 2H), 7.39 (dd, *J* =8.0, 2.0Hz, 2H), 6.05 (s, 2H), 1.38 (s, 18H). ^{13}C NMR (125 MHz, $CHCl_3$) δ 149.81,

144.02, 138.12, 137.70, 125.97, 119.04, 117.68, 106.47, 34.89, 31.52. IR (KBr) 2959, 1474, 1361, 1253, 1102, 888, 823, 754, 684 cm^{-1}. HRMS (EI) calcd for $C_{22}H_{26}$, 290.2029; found 290.2029.

Polymerization

Polymerization of tBu_2DBF was carried out under dry nitrogen atmosphere in a flame-dried glass ampule equipped with a three-way stop cock. The polymerization was initiated by adding *n*-BuLi to a monomer solution and terminated by adding a small amount of methanol containing aqueous HCl at a prescribed temperature. Insoluble fractions were separated from the mixture with a centrifuge. The solution part was concentrated under reduced pressure, and the products were extracted with chloroform. The organic layer was washed with brine three times and concentrated. The products were fractionated into uniform oligomers by preparative size exclusion chromatography (SEC).

Measurements

^1H NMR spectra were recorded on a JEOL JNM ECP500 spectrometer (500 MHz). Mass spectra were obtained using a JEOL JMS-700 spectrometer. Mass spectra were obtained using a JEOL JMS-700 spectrometer. COSY spectra were taken with a pulse delay of 1.5 s. NOESY spectra were taken with a pulse delay of 1.0 s and a mixing time of 0.5 s. SEC experiments were performed using a chromatographic system consisting of a JASCO PU-980 pump and a JASCO UV-2070 UV detector (254 nm) equipped with two Polymer Laboratories Oligopore columns (0.75 cm (i.d.) × 30 cm, M_w range up to 4500, particle size 6 μm) connected in series (eluent, THF; flow rate, 1.0 ml/min). Preparative-scale SEC was performed using JAI JAIGEL 1H and 2H columns connected in series (eluent, $CHCl_3$). Absorption and fluorescent spectra were measured on a JASCO V-550 spectrometer and a JASCO FP-777 spectrometer, respectively. Oxygen was removed from the sample solution by bubbling N_2 gas through for 10 min immediately before the optical measurements. Infrared (IR) spectra were measured on a JASCO FT/IR-420 spectrometer using a KBr pellet. Conformational calculations were performed using a Cache software package (Fujitsu). Each conformer was fully optimized until the RMS gradient went below 1.00 kcal/(mol Å) or 1.00 kcal/(mol radian).[12]

References

(1) Farchioni, R.; Grosso, G. In *Organic Electronic Materials: Conjugated Polymers and Low Molecular Weight Organic Solids*; Springer-Verlag: Berlin, 2001; Springer Series in Materials Science, Vol. 41.

(2) Guillet, *J. Polymer Photophysics and Photochemistry*; Cambridge University Press: Cambridge, England, 1985.

(3) Nakano, T.; Takewaki, K.; Yade, T.; Okamoto, Y. *J. Am. Chem. Soc.* **2001**, *123*, 9182.

(4) Nakano, T.; Yade, T. *J. Am. Chem. Soc.* **2003**, *125*, 15474.

(5) Nakano, T.; Yade, T.; Yokoyama, M.; Nagayama, N. *Chem. Lett.* **2004**, *33*, 296.

(6) (a) Alberti, A.; Pedulli, G. F.; Leardini, R.; Tundo, A.; Zanardi, G. *Tetrahedron* **1986**, *42*, 2533. (b) Yade, T.; Nakano, T. *Polym. Sci. Part A: Polym. Chem.* **2005**, *44*, 561.

(7) Nakano, T.; Okamoto, Y. *Chem. Rev.* **2001**, 101, 4013.

(8) Nakano, T. *J. Chromatogr. A* **2001**, *906*, 205.

(9) Nakano, T.; Nakagawa, O.; Yade, T.; Okamoto, Y. *Macromolecules* **2003**, *36*, 1433.

(10) (a) Nakano, T.; Okamoto, Y.; Hatada, K. *J. Am. Chem. Soc.* **1992**, *114*, 1318. (b) Okamoto, Y.; Yashima, E.; Nakano, T.; Hatada, K. *Chem. Lett.* **1987**, 759.

(11) (a) Stigers, K. D.; Kourroulis, M. R.; Chung, D. M.; Nowick, J. *J. Org. Chem.* **2000**, *65*, 3858. (b) Buu-Hoi, N. P.; Gagniant, P. *Chem. Ber.* **1944**, *77*, 121.

(12) Stewart, J. J. P. MOPAC2002 software; Fujitsu Limited: Tokyo, Japan, 2001.

General Conclusions

The author clarified the details of the stereostructure of poly(DBF) and found intriguing properties based on the π-stacked structure. Principal findings of this study are summarized as follows:

(1) DBF oligomers and polymers prepared by anionic polymerization were unambiguously established to have a π-stacked structure with the main-chain carbon–carbon bondings being almost all in the *all-trans* conformation not only in the solid state but also in solution. The π-stacked structure led to a remarkable hypochromicity in absorption and exclusive dimer emission and reduced oxidation potential in electrochemical profiles. These results are strongly indicative of poly(DBF)'s ability to delocalize energy and charges through the stacked π-electron systems.

(2) Radical polymerization of DBF was highly conformation-specific (stereospecific), giving a polymer with a π-stacked conformation although the products appeared to have a very small amount of irregular, defective conformation incorporated into the mostly π-stacked chain. This means that the expensive ionic polymerization is not necessary in obtaining π-stacked poly(DBF). In addition, the irregularity of the structure can be controlled to a certain extent, by optimizing the radical polymerization condition.

(3) Charge mobility of poly(DBF) film was much higher than poly(*N*-vinylcarbazole), the semiconducting vinyl polymer once practically used for Xerox and was as high as several main-chain conjugating polymers including a polysilane derivative. These results suggest that a vinyl polymer with relatively short conjugation systems may effectively transport charges when the stereostructure of the chain is properly designed and controlled.

(4) tBu_2DBF was found much less reactive in polymerization compared with DBF and mainly gave oligomers while it led to an insoluble polymer in a low yield under selected conditions. Although the tBu_2DBF oligomers showed clear hypochromicity in absorption spectra indicative of a π-stacked conformation, they showed only weak intramolecular dimer (excimer) emission. These results implicate that a complete π-stacked geometry suitable for excited intramoelcular dimer formation in the excited state is probably impossible for the tBu_2DBF oligomers due to steric repulsion.

DBF has a relatively simple chemical structure based on fluorene and may not look special at a glance. However, it exhibits characteristic polymerization behaviors including the high reactivity and the stereochemical features which have not been known for other simple vinyl monomers such as styrene, vinylfluorenes, or vinylcarbazoles. The π-stacked structure of poly(DBF) is not only unique as a conformation of a vinyl polymer but also has practical importance in the fact that it can mediate charge transport.

π-Stacked structures have not been generally recognized as an important category of structure by polymer chemists so far. Even a DNA duplex is generally classified as helical polymer, not a π-stacked polymer, in the field of structural polymers. This is because there have been only a limited number of π-stacked polymers whose structures were clearly identified and also because their syntheses are not necessarily simple and their practical properties have not been well exploited. However, we now have poly(DBF) which can be readily synthesized and shows intriguing properties as described in this thesis. As the number of reports on the syntheses and properties of its derivatives and analogues increases, π-stacked structure may be gradually regarded as a basic and important structural motif of synthetic polymers.

List of Publications

Papers

1. Synthesis, Structure, and Photophysical and Electrochemical Properties of a π-Stacked Polymer
   Tamaki Nakano and Tohru Yade
   J. Am. Chem. Soc. **2003,** 125, 15474-15484.

2. Charge Transport in a π-Stacked Poly(dibenzofulvene) Film
   Tamaki Nakano, Tohru Yade, Masaaki Yokoyama, and Norio Nagayama
   Chem. Lett. **2004**, *33*, 296-297.

3. Free-Radical Polymerization of Dibenzofulvene Leading to a π-Stacked Polymer: Structure and Properties of the Polymer and Proposed Reaction Mechanism
   Tamaki Nakano, Tohru Yade, Yasuyuki Fukuda, Takashi Yamaguchi, and Shohei Okumura
   Macromolecules **2005**, *38*, 8140-8148.

4. Anionic Polymerization of 2,7-Di-*t*-butyldibenzofulvene: Synthesis, Structure, and Photophysical Properties of the Oligomers with a π-Stacked Conformation
   Tohru Yade and Tamaki Nakano
   J. Polym. Sci., Part A.: Polym. Chem. **2006**, *44*, 561–572.

Other Related Papers

1. Dibenzofulvene, a 1,1-Diphenylethylene Analogue, Gives a π-Stacked Polymer by Anionic, Free-Radical, and Cationic Catalysts
   Tamaki Nakano, Kazuyuki Takewaki, Tohru Yade, and Yosio Okamoto
   J. Am. Chem. Soc. **2001,** *123*, 9182-9183.

2. Solid-State Polymerization of Dibenzofulvene Leading to a Copolymer with Oxygen
   Tamaki Nakano, Osamu Nakagawa, Tohru Yade, and Yoshio Okamoto
   Macromolecules **2003**, *36*, 1433-1435.

3. Revised Interpretation for *N*-Cyclohexylmaleimide Polymerization in the Presence of an Optically Active Cobalt(II) Complex: Polymerization Mediated by Anionic Species Formed through Monomer-Co(II) Complex-O_2 Interaction
Tamaki Nakano, Tohru Yade, and Yoshio Okamoto
Macromolecules **2003,** *36*, 3498-3504.

4. Poly(2,7-di-*n*-pentyldibenzofulvene) Showing Chiroptical Properties in the Solid State Based Purely on a Chiral Conformation
Tamaki Nakano, Osamu Nakagawa, Masashi Tsuji, Mitsuru Tanikawa, Tohru Yade and Yoshio Okamoto
Chem. Commun. **2004**, 144-145.

5. 光学活性コバルト錯体を用いた *N*-シクロヘキシルマレイミドの不斉重合
中野　環, 矢出　亨
高分子論文集, **2004**, *61*, 282-288.

6. 新しいアニオン重合開始剤系の開発：使い勝手の良い精密重合法を目指して
中野　環、矢出　亨、中川　修、辻　雅司
月刊　接着（高分子刊行会） **2004**, *48*, 352-359.

7. Stereospecific Polymerization of 9-Fluorenyl Methacrylate: Tacticity Effects on the Thermal and Photophysical Properties of the Polymers
Hideaki Ishizawa, Tamaki Nakano, Tohru Yade, Masashi Tsuji, Osamu Nakagawa, Takashi Yamaguchi
J. Polym. Sci., Part A.: Polym. Chem. **2004**, *42*, 4656-4665.

8. Synthesis of Fluorenylpotassium Species with Potassium *t*-Butoxide (*t*-BuOK) and Its Use for Anionic Polymerization
Tamaki Nakano, Osamu Nakagawa, Miyuki Tanaka, Tohru Yade, Masashi Tsuji
J. Polym. Sci., Part A.: Polym. Chem. **2005**, *43*, 1150-1154.

Acknowledgments

The present study was conducted at the Graduate School of Materials Science, Nara Institute of Science and Technology (NAIST), from April 2000 to March 2006.

The author is particularly indebted to Associate Professor Dr. Tamaki Nakano for his helpful guidance, numerous fruitful discussions and valuable suggestions, and for his kind comments on this thesis.

The author gratefully acknowledges Professor Dr. Kiyomi Kakiuchi, Research assistant Dr. Ken Tsutsumi, and Research assistant Dr. Tsumoru Morimoto for their encouragement.

The author is indebted to Ms. Yoshiko Nishikawa for mass spectroscopic measurements.

The author acknowledges Professor Dr. Masaaki Yokoyama and Research assistant Dr. Norio Nagayama for TOF transient photocurrent measurements.

The author deeply thanks Dr. Osamu Nakagawa, Dr. Masashi Tsuji, Dr. Hideaki Ishizawa, Dr. Ken-ichi Katsukawa, Dr. Takayuki Yaegashi, Mr. Kazuyuki Takewaki, Mr. Jun-ichi Miyazaki, Mr. Mitsuru Tanikawa, Mr. Kousuke Arai, Mr. Toshio Nishikawa, Mr. Yasuyuki Fukuda, Mr. Takashi Yamaguchi, and Mr. Shohei Okumura for their kind collaborations and helpful advice.

The author wishes to thank all the members of Kakiuchi Laboratory of NAIST for their kind help and encouragement.

Finally, the author wishes to express from the heart to his family, especially to his parents Mr. Yoshizou Yade and Mrs. Machiko Yade for their understanding, encouragement, and financial support.

March 2006

Tohru Yade

Graduate School of Materials Science,
Nara Institute of Science and Technology (NAIST)